Differential modulation of HIV-1 capsid uncoating kinetics revealed by a novel single-particle uncoating assay

Author:
Marquez Badilla, Chantal

Publication Date:
2019

DOI:
https://doi.org/10.26190/unsworks/21201

License:
https://creativecommons.org/licenses/by-nc-nd/3.0/au/
Link to license to see what you are allowed to do with this resource.

Differential modulation of HIV-1 capsid uncoating kinetics revealed by a novel single-particle uncoating assay

Chantal Loretto Márquez Badilla

A thesis in fulfilment of the requirements for the degree of

Doctor of Philosophy

UNSW
SYDNEY

School of Medical Sciences

Faculty of Medicine

October 2018

THE UNIVERSITY OF NEW SOUTH WALES
Thesis/Dissertation Sheet

Surname or Family name: **Márquez Badilla**

First name: **Chantal**   Other name/s: **Loretto**

Abbreviation for degree as given in the University calendar: **PhD**

School: **School of Medical Sciences**   Faculty: **Faculty of Medicine**

Title: Differential modulation of HIV-1 capsid uncoating kinetics revealed by a novel single-particle uncoating assay.

The HIV-1 capsid has been recognised as an attractive antiviral target due to its central role during infection. It acts as a shield to protect the viral genome, facilitates reverse transcription, engages with the nuclear pore complex, and directs integration site targeting. To achieve all of these functions, the capsid disassembles, in a process referred to as uncoating, with temporal and spatial precision. HIV has evolved to exploit a network of host cofactors to regulate capsid stability while the cell has developed restriction factors that recognise the CA lattice to block infection. Despite of that, only few host binders have been identified, and their precise role is not well understood. The fragility of the capsid has so far hindered the development of methods sensitive enough to identify different uncoating behaviours in a high throughput way to allow detailed kinetic studies of how molecules alter capsid stability.

Here, we have developed a single-particle fluorescence microscopy method to follow the real-time uncoating kinetics of authentic HIV capsids *in vitro*. This novel assay allows us to visualise the dynamic interactions of molecules with hundreds of individual capsids and determine their effect on capsid stability. We found that spontaneous uncoating is initiated shortly after the viral membrane is compromised. The opening of the first defect in the lattice is the rate-limiting step of uncoating, which is followed by a rapid, catastrophic collapse. Interestingly, we found that the two phases of uncoating can be modulated differentially. Binding of factors to the $CA_{NTD-CTD}$ hexameric interface, such as PF74 and $CPSF6_p$, accelerate or do not alter capsid opening but strongly stabilise the remaining lattice. In contrast, binding of polyanions to the central capsid pore, such as hexacarboxybenzene and the newly discovered CA-binders IP6 and ATP, strongly delay initiation of uncoating but do not prevent subsequent lattice disassembly. We also determined that CPSF6 binds the HIV-1 capsid with higher affinity than previously reported. This is the first report demonstrating the differential effect on uncoating of capsid binders, and we believe that our novel assay can provide a powerful tool on the development of antiviral drugs.

Signature   Witness   Date

4/10/18

FOR OFFICE USE ONLY   Date of completion of requirements for Award:

Originality Statement

'I hereby declare that this submission is my own work and to the best of my knowledge it contains no materials previously published or written by another person, or substantial proportions of material which have been accepted for the award of any other degree or diploma at UNSW or any other educational institution, except where due acknowledgement is made in the thesis. Any contribution made to the research by others, with whom I have worked at UNSW or elsewhere, is explicitly acknowledged in the thesis. I also declare that the intellectual content of this thesis is the product of my own work, except to the extent that assistance from others in the project's design and conception or in style, presentation and linguistic expression is acknowledged'.

Chantal Loretto Márquez Badilla

Signature: _____

Date: _____04/10/2018_____

Copyright Statement

Chantal Loretto Márquez Badilla

Signature: _____

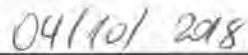Date: _____04/ 10/ 2018_____

Authenticity Statement

'I certify that the Library deposit digital copy is a direct equivalent of the final officially approved version of my thesis. No emendation of content has occurred and if there are any minor variations in formatting, they are the result of the conversion to digital format.'

Chantal Loretto Márquez Badilla

Signature: ⟨Chantal⟩

Date: 04/10/ 2018

Inclusion of Publications Statement

Please indicate whether this thesis contains published material or not.

☐ *This thesis contains no publications, either published or submitted for publication*

☐ *Some of the work described in this thesis has been published and it has been documented in the relevant Chapters with acknowledgement*
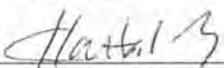
☒ *This thesis has publications (either published or submitted for publication) incorporated into it in lieu of a chapter and the details are presented below*

CANDIDATE'S DECLARATION
I declare that:
- I have complied with the Thesis Examination Procedure
- where I have used a publication in lieu of a Chapter, the listed publication(s) below meet(s) the requirements to be included in the thesis.

Name	Signature	Date (dd/mm/yy)
Chantal Loretto Marquez Badilla	Hatbl	04/10/2018

Postgraduate Coordinator's Declaration
I declare that:
- the information below is accurate
- where listed publication(s) have been used in lieu of Chapter(s), their use complies with the Thesis Examination Procedure
- the minimum requirements for the format of the thesis have been met.

PGC's Name	PGC's Signature	Date (dd/mm/yy)
NICOLE JONES	Njones	8/10/2018

Details of publication:
Full title: Kinetics of HIV-1 capsid uncoating revealed by single-molecule analysis

Authors: Chantal L Márquez, Derrick Lau, James Walsh, Vaibhav Shah, Conall McGuinness, Andrew Wong, Anupriya Aggarwal, Michael W Parker, David A Jacques, Stuart Turville, Till Böcking

Journal or book name: eLife

Date accepted/ published: 2018/6/5

Status	*Published*		*Accepted and In press*		*In progress (submitted)*	
		☒				

The Candidate's Contribution to the Work
Investigation: all experiment except Figures 1.B, 1.D, and Supplement Figure 3; Conceptualisation; Analysis of data; Review and editing of manuscript

Location of the work in the thesis and/or how the work is incorporated in the thesis:
The paper is included in Chapter 3, pages 57 to 83

Primary Supervisor's Declaration

I declare that:

- the information above is accurate
- this has been discussed with the PGC and it is agreed that this publication can be included in this thesis in lieu of a Chapter
- All of the co-authors of the publication have reviewed the above information and have agreed to its veracity by signing a 'Co-Author Authorisation' form.

Supervisor's name	*Supervisor's signature*	*Date (dd/mm/yy)*
TILL BOECKING		04/10/2018

Abstract

The HIV-1 capsid has been recognised as an attractive antiviral target due to its central role during infection. It acts as a shield to protect the viral genome, facilitates reverse transcription, engages with the nuclear pore complex, and directs integration site targeting. To achieve all of these functions, the capsid disassembles, in a process referred to as uncoating, with temporal and spatial precision. HIV has evolved to exploit a network of host cofactors to regulate capsid stability while the cell has developed restriction factors that recognise the CA lattice to block infection. Despite of that, only few host binders have been identified, and their precise role is not well understood. The fragility of the capsid has so far hindered the development of methods sensitive enough to identify different uncoating behaviours in a high throughput way to allow detailed kinetic studies of how molecules alter capsid stability.

Here, we have developed a single-particle fluorescence microscopy method to follow the real-time uncoating kinetics of authentic HIV capsids in vitro. This novel assay allows us to visualise the dynamic interactions of molecules with hundreds of individual capsids and determine their effect on capsid stability. We found that spontaneous uncoating is initiated shortly after the viral membrane is compromised. The opening of the first defect in the lattice is the rate-limiting step of uncoating, which is followed by a rapid, catastrophic collapse. Interestingly, we found that the two phases of uncoating can be modulated differentially. Binding of factors to the $CA_{NTD-CTD}$ hexameric interface, such as PF74 and $CPSF6_p$, accelerate or do not alter capsid opening but strongly stabilise the remaining lattice. In contrast, binding of polyanions to the central capsid pore, such as hexacarboxybenzene and the newly discovered CA-binders IP6 and ATP, strongly delay initiation of uncoating but do not prevent subsequent lattice disassembly. We also determined that CPSF6 binds the HIV-1 capsid with higher affinity than previously reported. This is the first report demonstrating the differential effect on uncoating of capsid binders, and we believe that our novel assay can provide a powerful tool on the development of antiviral drugs.

Acknowledgments

Table of Contents

List of Figures and Tables

Publications and Conference Proceedings

Publications

Chantal L Márquez, Derrick Lau, James Walsh, Vaibhav Shah, Conall McGuinness, Andrew Wong, Anupriya Aggarwal, Michael W Parker, David A Jacques, Stuart Turville and Till Böcking, "Kinetics of HIV-1 capsid uncoating revealed by single-molecule analysis", eLife, June 2018. 10.7554/eLife.34772.

Donna L Mallery, **Chantal L Márquez**, William A McEwan, Claire Dickson, David A Jacques, Madhanagopal Anandapadamanaban, Katsia Bichel, Gregory J Towers, Adolfo Saiardi, Till Böcking, Leo C James, "IP6 is an HIV pocket factor that prevents capsid collapse and promotes DNA synthesis", eLife, May 2018. 10.7554/eLife.35335.

Oral Presentations

Márquez CL., Turville S., Boecking T. "A new platform to visualise the effects of host proteins on HIV-1 capsid uncoating at the single-particle level". Talk presentation delivered at Australian Centre for HIV and Hepatitis Virology Research (ACH2) – Yarra Valley, Australia, June 2018.

Márquez CL., Turville S., Boecking T. "Visualising HIV uncoating – a platform to discover new drugs". Talk presentation delivered at 5th Chilean Graduate Conference in Australia - Sydney, Australia, October 2017.

Márquez CL., Turville S., Boecking T. "A novel fluorescence-based uncoating assay to survey the effects of capsid-binding proteins at the single-particle level". Talk presentation delivered at Retroviruses meeting - Cold Spring Harbour, USA. May 2017.

Márquez CL., Turville S., Boecking T. "Visualising HIV-1 uncoating in virus-like particles at the single particle level". Talk presentation delivered at EMBL Australia Postgraduate Symposium - Adelaide, Australia. November 2016.

Márquez CL., Turville S., Boecking T. "Visualising HIV-1 uncoating in virus-like particles at the single particle level". Talk presentation delivered at 4th Chilean Graduate Conference in Australia – Brisbane, Australia. October 2016.

Márquez CL., Lau D., Turville S., Boecking T. "Visualising HIV-1 uncoating in virus-like particles at the single-particle level". Talk presentation delivered at Australian Centre for HIV and Hepatitis Virology Research (ACH2) - Hunter Valley, Australia. December 2015.

List of Acronyms and Abbreviations

AIDS	Acquired Immune Deficiency Syndrome
(+)ssRNA	Positive-Sense Single-Stranded RNA
2-LTR	2-Long Terminal Repeat
AF568	Alexa-Fluor 568-C5-Maleimide
APOBEC3G	Apolipoprotein B Mrna Editing Enzyme, Catalytic Polypeptide-Like 3G
ATP	Adenosine Triphosphate
bp	Base pair
cART or HAART	Combination Antiretroviral Therapy
CD4+ T cells	CD4 Positive (CD4+) T Lymphocytes
CPSF6	Cleavage and Polyadenylation Specificity Factor 6
CPSF6$_p$	CPSF6$_{313-327}$ or CPSF6 peptide
CsA	Cyclosporine A
CTD	Carboxyl-Terminal Domain
CXCR4	C-C Chemokine Receptor-4
CXCR5	C-C Chemokine Receptor-5
CypA	Cyclophilin A
dNTP	Deoxynucleoside Triphosphate
EC$_{50}$	Effective concentration
EM	Electron Microscopy
Env	Envelope glycoprotein
ER	Endoplasmic reticulum
ESCRT	Endosomal Sorting Complex Required for Transport
gp120	Surface Envelope Glycoprotein
gp41	Transmembrane Envelope Glycoprotein
hCPSF6	Human CPSF6
HIV	Human Immunodeficiency Virus
HIV-1	HIV Type 1
HIV-2	HIV Type 2
HTLV III	T-Lymphotropic Virus III
IFN	Interferon
iGFP	GFP encoded between the MA end CA within Gag
IN	Integrase
IP6	Hexakisphosphate
IPTG	Isopropyl B-D-Thiogalactopyranoside
kb	Kilobase
K$_D$	Dissociation constant
kDa	kilo Dalton
L-domain	Late assembly domain

LTR	Long Terminal Repeats
mCPSF6	Mouse CPSF6
Mellitic acid	Hexacarboxybenzene
MHC	Major Histocompatibility Complex
MLV	Murine Leukemia Virus
Nef	Negative regulatory factor
NES	Nuclear Export Signal
NLS	Nuclear Localisation Signal
NPC	Nuclear Pore Complex
NTD	Amino-Terminal Domain
NUP153	Nucleoporin 153
NUP358	Nucleoporin 358
OI	Opportunistic infection
ORF	Open-Reading Frames
PCA	Protocatechuic Acid
PCD	Protocatechuate-3,4-Dioxygenase
PDMS	Poly-Dimethylsiloxane
PF74	Pf-3450074
PFO	Perfringolysin O
PIC	Pre-integration complex
PR	Protease
R18	Arginine 18
Rev	Regulator of The Expression of The Virion
RNP	Ribonucleoprotein Complex
RRE	Rev-Response Element
RT	Reverse Transcriptase
RTC	Reverse Transcription Complex
TAR	Trans-Activating Response Element
Tat	Transcriptional Trans-Activator
TC	Tetracysteine
TIRF	Total Internal Reflection Fluorescence
TNPO3	Transportin 3
Vif	Viral Infectivity Factor
Vpr	Viral Protein R
Vpu	Viral Protein U
WT	Wild Type

Chapter 1

Literature Review

1. Literature Review

1.1. HIV and AIDS

The acquired immune deficiency syndrome (AIDS) is the final stage of the human immunodeficiency virus (HIV) infection. It is characterised by a severe weakening of the immune system which lead to increased susceptibility to a wide range of opportunistic infections (OIs) such as *Pneumocystis* pneumonia, bacterial enteric infections, candidiasis, and tuberculosis, the leading cause of AIDS-related deaths [1][2]. The earliest known case derives from a blood sample collected in 1959 in the capital of the Democratic Republic of the Congo, where fragments of the HIV-1 genome were found [3]. In 1981 an alarming number of cases were reported in the United States, and three years later, with more than 8000 cases were reported in the US and Europe, the new T-lymphotropic virus III (HTLV III) isolated by Françoise Barré-Sinoussi and colleagues [4] was identified as the causative agent of AIDS [5]. In 1986 the virus was officially re-named as the human immunodeficiency virus (HIV) by the International Committee on the Taxonomy of Viruses [6]. Since then, HIV/AIDS has become a worldwide epidemic causing more than 34 million deaths in addition to almost 37 million people infected by 2016 [7].

Two types of HIV have been identified. HIV type 2 (HIV-2) is less prevalent and it is found principally in western Africa, while HIV type 1 (HIV-1) is the most widespread and pathogenic. Within HIV-1, several groups are recognised: the main group (M), outlier group (O) and non-M/non-O group (N). 10 different subtypes (clade A-K) have been identified within the group M, exposing a high genetic variability of HIV [8].

HIV-1 can be transmitted through mucosal surfaces contact, perinatal route and percutaneous inoculation, however nearly 70% of infections are due heterosexual unprotected sex [9]. Upon transmission, the virus infects primary CD4 positive (CD4+) T lymphocytes [10], but also macrophages, dendritic cells and other cell types [11], [12]. It causes a systemic infection that leads to a progressive death of infected and non-infected CD4+ T cells, resulting in a chronically suppressed immune system.

Antiretroviral therapy is the only treatment available, since preventive HIV-1 vaccines have not been successfully generated yet [13]. Currently, there are almost 40 approved compounds that target different stages of the viral cycle [14]. The combined use of three or more of them, known as combination antiretroviral therapy (cART or HAART),

has been considerably more effective than single drug use and has increased life expectancy by 13 years, converting AIDS from a fatal diagnosis to a chronically managed disease. Despite the success of HAART in suppressing active viral replication and spread, AIDS is still an incurable disease due to HAART-associated toxicities [15], persistence of drug-insensitive latent provirus in viral reservoirs [16] and multi-antiviral resistance variant appearance [17]. HIV-1 has extremely high mutation rates, which increases its probability of evolving resistance against antiretroviral drugs to successfully evade the immune system [18]. It is therefore necessary to develop new therapeutic strategies to control HIV infection.

1.2. Viral structure and life cycle

1.2.1. HIV-1 virion

HIV-1 belongs to the *Lentivirus* genus, within the *Retroviridae* family. Retroviruses are enveloped viruses with a positive-sense single-stranded RNA ((+)ssRNA) genome. To successfully achieve infection, they reverse transcribe their genetic material into DNA by using their own reverse transcriptase (RT) enzyme. The double-stranded viral DNA is then integrated into the host chromosome and the resultant provirus is used as a template for the production of future viral progeny, maintaining a persisting infection within the host [19]. As a lentivirus, HIV-1 is able to efficiently infect dividing cells as well as non-dividing cells. Lentiviruses can import their genome into the host nucleus independently of cell cycle stage [20].

Electron microscopy (EM) images of mature HIV-1 virions revealed that they are roughly spherical with a diameter between 120 to 160 nm [21]. The envelope of a viral particle consists of a lipid bilayer derived from the plasma membrane of the infected cell (**Figure 1.1**). Proteins derived from the host plasma membrane such as HLA-DR, a cell surface receptor from the major histocompatibility complex (MHC) family of proteins, are embedded in the viral envelope [22]. About 14 trimeric envelope glycoprotein (Env) spikes are anchored to the viral membrane. Each spike is composed of three surface envelope glycoprotein (gp120) and three transmembrane envelope glycoprotein (gp41) subunits [23]. The inner leaflet of the viral membrane is associated with an irregular matrix made of MA (p17) proteins [24]. Inside, the conical capsid shell formed by the CA (p24) protein [25] encloses two copies of the (+)ssRNA viral genome [26]. Each copy is covered by multiple molecules of the NC protein (p7), and associates with the viral RT, integrase (IN), and with cellular tRNAs forming the ribonucleoprotein complex (RNP) [27], [28]. The viral proteins P6, Vpr, Nef and Vif are

3

also incorporated into the viral particles, mainly within the viral core [29]–[31] (**Figure 1.1**).
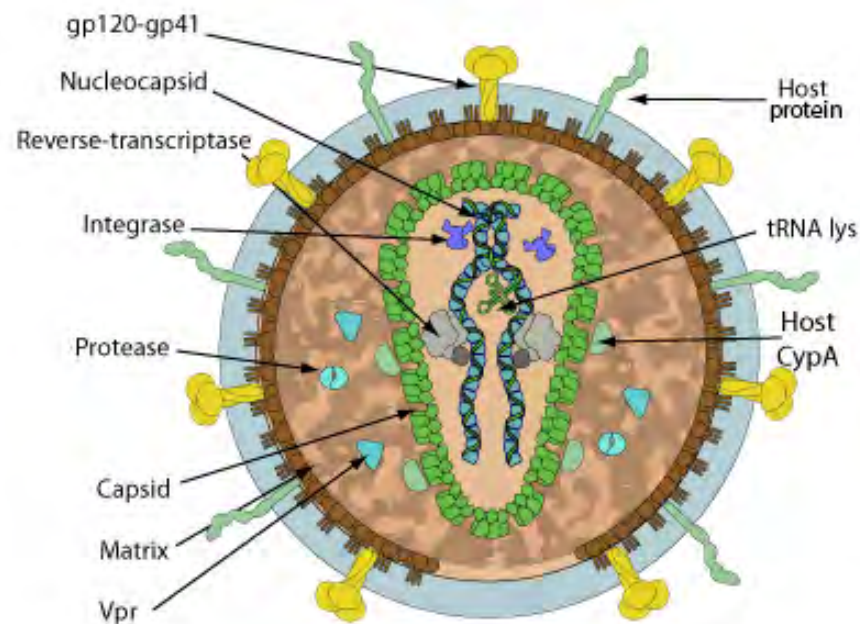
Figure 1.1. Structure of a mature HIV-1 particle. HIV-1 particles are spherical particles with a diameter of ~120 - 160 nm. The outermost layer of a mature virion is composed of a lipid bilayer containing the envelope glycoproteins gp120 and gp41. MA proteins are associated with the inner leaflet of the viral membrane. The viral core on the inside of the particle consists of the viral capsid assembled from CA proteins and the ribonucleoprotein complex (RNP). The RNP consists of two copies of a positive-sense single-stranded RNA covered by NC proteins and associated with the viral integrase (IN), reverse transcriptase (RT) and cellular tRNAs. The viral proteins P6, Vpr, Nef and Vif are also packaged within the viral particles. Illustration modified from ViralZone (www.expasy.org/viralzone, SIB Swiss Institute of Bioinformatics).

1.2.2. HIV-1 genome

The HIV-1 RNA genome is approximately 9.7 kilobases (kb) in length and encodes fifteen viral proteins contained in nine open-reading frames (ORF). These nine genes can be classified in three different groups: structural genes (*gag, pol, env*), regulatory genes (*tat, rev*) and accessory genes (*nef, vif, vpr, vpu*) (**Figure 1.2**) [32].

Structural genes

The *gag* gene produces a 55 kDa polyprotein precursor that is the main component responsible for particle assembly. It comprises four smaller proteins, MA, CA, NC and

p6 (from N-terminus to C-terminus), as well as two spacer peptides, SP1 located between CA and NC, and SP2 located between NC and P6 (**Figure 1.2**). In the immature viral particle, ~5000 Gag precursors assemble in a radial manner [33]. It has been shown that MA mediates binding of Gag with the host cell membrane and is required for incorporating Env into the virions [34], [35]. During assembly, the CA protein drives Gag multimerisation, forming a hexameric lattice [36]. NC protein is involved in packaging the viral RNA into the virion during assembly and facilitating structural rearrangements of the genome to allow reverse transcription, a process that occurs after cell entry [37]. The P6 domain recruits the endosomal sorting complex required for transport (ESCRT) machinery through two late assembly domains (L-domains) facilitating budding and release from the producer cell [38]. During maturation, the individual proteins are cleaved, and the CA molecules rearrange to form the fullerene-like capsid [39].

The *pol* gene gives rise to the viral protease (PR), responsible for proteolytic cleavage after budding of the viral particle, and to reverse transcriptase (RT) and integrase (IN), enzymes involved in the reverse transcription and integration of the viral DNA into the host genome [40], [41] (**Figure 1.2**). During replication, the transcription of *pol* occurs as part of the Gag-Pol precursor (p160) due to a frame shift during translation. This frame shift happens approximately 1 every 20 translations, resulting in a 1:20 stoichiometry Gag:Gag-Pol [42].

The *env* sequence encodes the envelope glycoprotein precursor gp160, which is cleaved into two subunits: the surface domain gp120 that mediates the recognition and attachment to the target receptor and the transmembrane domain gp41, which promotes membrane fusion [43].

Regulatory genes

The *tat* gene encodes the viral transcriptional trans-activator (Tat), responsible for enhancing the efficiency of viral transcription. It binds to the trans-activating response element (TAR), a loop structure found at the 5' end of all HIV-1 mRNAs, and recruits the cyclin T1-CDK9 complex that phosphorylates the RNA polymerase II allowing efficient elongation of the nascent viral RNAs [44].

The regulator of the expression of the virion (Rev) is produced by the *rev* gene and mediates the export of unspliced HIV mRNAs from the nucleus to the cytoplasm by binding to the Rev-response element (RRE) [45].

Accessory genes

The accessory genes *nef, vif, vpr* and *vpu* encode elements that play crucial roles during HIV infection [46]. The negative regulatory factor (Nef) and the viral protein U (Vpu) promote virion infectivity by down regulating several host cellular proteins, such as CD4 and MHC I. The viral infectivity factor (Vif) neutralises the innate antiviral activity of the host factor APOBEC3G (apolipoprotein B mRNA editing enzyme, catalytic polypeptide-like 3G) by poly-ubiquitination and degradation via the proteasome pathway. The viral protein R (Vpr) assists in the nuclear transport of the reverse transcription complex (RTC) during infection in quiescent cells and arrests infected cells in the G2 phase of cell cycle causing apoptosis of the cell [46].
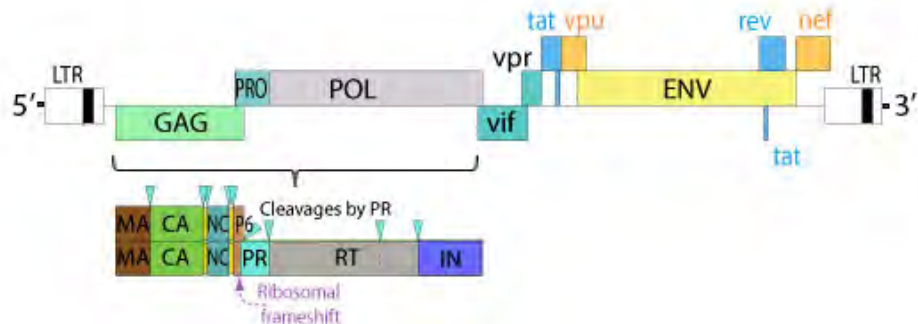
Figure 1.2. HIV-1 genome. The HIV-1 RNA genome is ~9.7 kb, and encodes 9 open reading frames flanked by two long terminal repeats (LTRs) that contain regulatory regions for gene expression. The main structural proteins, Gag and Pol, are synthesised as polyproteins, whereby the Gag-Pol protein precursor is expressed as a result of a ribosomal frame-shift. The polyproteins are subsequently cleaved by viral protease (PR) into subunits. Gag gives rise to MA, CA, sp1, NC, sp2 and p6; and Pol subunits are PR, reverse transcriptase (RT) and integrase (IN). The *env* gene produces gp120 and gp41, and the regulatory (*tat* and *rev*) and accessory genes (*nef, vif, vpr and vpu*) are also codified. Image modified from ViralZone (www.expasy.org/viralzone, SIB Swiss Institute of Bioinformatics).

HIV-1 gene expression is driven by the long terminal repeats (LTR) regions located on both ends of the genome. Each LTR is an almost-identical noncoding region of 640 base pairs (bp), which contain regulatory signals and binding sites for host and viral factors to allow gene expression. Furthermore, the end of the LTRs are used for integration into the host genome. Once integrated, the 5' end LTR functions as promoter to initiate production of mRNA transcript for the entire genome while the 3' end LTR acts in transcription termination and polyadenylation [47], [48].

1.2.3. Replication cycle

The HIV replication cycle is generally divided in two phases, the early stage (pre-integration) and late stage (post-integration). It includes the following steps: binding to the target membrane and fusion (**Figure 1.3A-B**); uncoating and reverse transcription (**Figure 1.3C**); nuclear import and integration (**Figure 1.3D**); viral gene expression (**Figure 1.3E-F**); assembly, budding and maturation (**Figure 1.3G-I**).
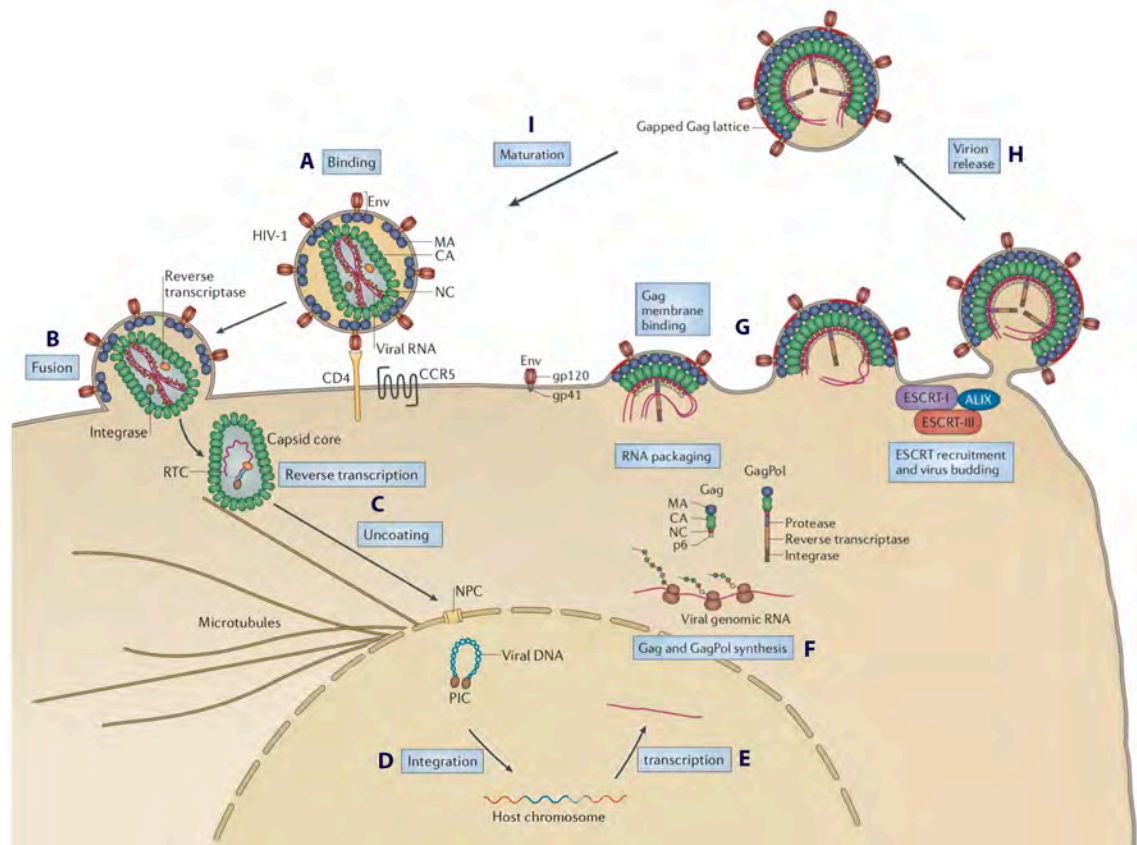
Figure 1.3. HIV-1 replication cycle. **(A)** A mature virion binds to a CD4 receptor and co-receptors (CCR5 orCXCR4) present on the surface of the target cell. **(B)** These interactions promote the fusion of the viral membrane with the cellular membrane and the release of the core into the cytoplasm. **(C)** The RNA genome is then reverse transcribed to yield double-stranded viral DNA, which becomes part of the pre-integration complex (PIC). At some point during these events the capsid core disassembles, in a process known as uncoating. **(D)** The PIC is translocated into the nucleus and the viral genome is integrated into the host genome forming the provirus. **(E-F)** Production of progeny is initiated by transcription and translation of the provirus to yield new viral RNA and proteins. **(G-H)** Viral components are transported across the cytoplasm and assembled at the cellular membrane, where they bud as immature virions. **(I)** The viral protease then cleaves Gag and Gag-Pol precursors leading to a

structural rearrangement that ends with the formation of the fullerene capsid. Figure adapted from [49], [50].

Early stage of HIV infection

The HIV-1 life cycle starts when the virion recognises the target cell and binds to the CD4 receptor through the gp120 glycoprotein (**Figure 1.3A**). This binding promotes a conformational change in gp120, exposing its co-receptor binding site, where either C-C chemokine receptor-5 (CCR5) or CXC chemokine receptor-4 (CXCR4) can bind. Co-receptor binding triggers a conformational change in gp41, resulting in the fusion of the viral with the cell membrane, and the release of the core into the cytoplasm (**Figure 1.3B**) [43]. Even though the conventional model for HIV-1 entry is its direct fusion with the plasma membrane, there is evidence to support the existence of an alternative endocytic pathway for entry. Both pathways may not be mutually exclusive, since HIV-1 infects diverse cell types and uses different modes of viral transmission [51]

Following entry, reverse transcription occurs and the viral capsid disassembles in order to allow nuclear import of the viral dsDNA and establish infection (**Figure 1.3C**). Whether uncoating happens concurrently with reverse transcription is unclear, and different models for this process will be discussed in detail in the following sections. Reverse transcription is initiated upon entry of the capsid into the cytoplasm, leading to the formation of the reverse transcription complex (RTC). During reverse transcription, a linear double-stranded DNA is produced by using the (+)ssRNA genome as template and cellular deoxynucleoside triphosphates (dNTPs) as substrates [52], [53]. The resulting viral dsDNA is associated with IN and various other viral components and host proteins to form the pre-integration complex (PIC) [54]. Genome-containing complexes (RTC/PIC) travel through the cytoplasm to the nucleus, initially using the actin cytoskeleton and then the microtubule network [55]–[58]. Once it reaches the nuclear membrane, the viral PIC is actively translocated through the nuclear pore complex into the nucleus. IN catalyses the integration of the viral genome into a host chromosome, giving rise to the HIV-1 provirus (**Figure 1.3D**) [59]. The location in the host genome where the viral genome integrates is not specific, but weak palindromic sequences within active transcription units are favoured [40], [60]. An alternative outcome to integration is the circularisation of the viral DNA, a process that does not lead to infection [61]. In this case, dissociation of the PIC proteins permits the ligation of the two ends of the viral DNA, forming a 2-long terminal repeats (2-LTR) circle.

Late stage of HIV infection

In order to produce new viral particles, transcription of the provirus is initiated from the 5' LTR by the host RNA polymerase II (**Figure 1.3E**). The first transcripts are fully spliced mRNAs encoding *tat* and *rev.* Early translated Tat and Rev proteins enhance the transcription and translation of singly spliced or unspliced viral sequences to synthetise the rest of the viral components [62]. Translation of the viral genes occurs on free cytoplasmic ribosomes except for the Env precursor, which is translated at the membrane of the endoplasmic reticulum (ER) (**Figure 1.3F**). The membrane-bound gp160 protein is then processed in the Golgi complex where is glycosylated and cleaved into its two subunits, gp120 and gp41, followed by its transportation to the cell membrane [63].

Particle assembly takes place in lipid rafts at the plasma membrane were Gag/Gag-Pol accumulation orchestrates packaging of viral proteins and genomic (+)ssRNA (**Figure 1.3G**) [64]. The MA domain of Gag promotes its targeting to the membrane and assists in Env incorporation via interaction with the cytoplasmic tail of the gp41 subunit. The CA domain mediates Gag multimerisation, forcing a spherical arrangement. The two copies of the RNA that will serve as genome for the virion are encapsidated through interactions with the NC domain of Gag. Other viral proteins are also packaged within the viral particle, including RT, IN and Vpr [25], [65]. Finally, P6 recruits the ESCRT machinery enabling budding of immature viral particles (**Figure 1.3H**). Maturation of these non-infectious virions follows soon after their release and is the result of proteolytic processing of Gag and Pol by the viral protease. Cleavage of the precursors induce dramatic structural rearrangements ending with the assembly of the conical capsid (**Figure 1.3I**) [66]. Viral progeny can now spread and infect other cells.

The HIV-1 replication cycle is a very complex process, which is reflected in the low infectivity rates. It was found that just one particle per 3,500 virions are infectious [67], although a more austere number, 1 in 8 virions, was also reported [68]. Proper formation of the viral capsid has been shown to be critical for infectivity, as only mature viruses are infectious [69].

1.3.　HIV-1 capsid

The term 'capsid' is often used to refer to both the CA (p24) monomer and the fullerene core. In this thesis, 'CA' will be used to describe the monomeric protein while 'capsid' will be used to describe the assembled conical shell.

The HIV-1 CA lattice plays essential roles in both early and late stages of the viral replication cycle (see section 1.3.3). Studies have shown that it acts as a shield to protect the viral genome [70], [71], facilitates reverse transcription [72], engages with the nuclear pore complex [73]–[75], and directs integration site targeting [76]–[78]. Spatiotemporal control of the capsid disassembly is then crucial for the virus, as it has to achieve all of these functions within the cell. To do so, the virus has evolved to exploit a network of supplementary proteins or cofactors to regulate uncoating and evade its detection. On the contrary, the cell has developed restriction factors that recognise the capsid lattice and block infection either promoting premature uncoating or preventing uncoating. Overall, the capsid has evolved as a finely tuned molecular complex that serves as an interaction platform for different proteins but also needs to be optimised for assembly and stability, whereby interfering with these properties can disrupt critical steps in the infection pathway. As such, HIV-1 CA exhibits extreme genetic fragility, whereby many single point mutations are associated with replication deficiency [79].

Due to the importance of the viral capsid during the replication cycle and the genetic fragility of CA, the HIV-1 capsid has been recognised as an attractive antiviral target. The development of compounds targeting the HIV-1 capsid has several advantages: capsid-targeting compounds could stop HIV-1 replication in a large number of steps of the life cycle; they could prevent binding of host molecules required for infection; the probability of the virus to give rise to mutations that confer resistance to the drug are very low as it has to maintain a delicate balance in the functions of the capsid.

Despite the central role of the capsid in the HIV-1 life cycle, only few host capsid-binding proteins have been identified and the precise mechanisms of how they modulate infection are not clear. Understanding capsid-binding host factors is therefore particularly necessary, but the lack of rapid and sensitive methods to screen for capsid-binding molecules and test their effect on uncoating has prevented progress in this matter.

1.3.1. CA monomer

The HIV-1 CA is a 24 kDa protein with two independently folded domains linked by a 5-residue flexible peptide (**Figure 1.4A**) [80]–[83]. The amino-terminal domain (CA$_{NTD,}$ residues 1–145) is made up of 7 α-helices (H1-H7) and an amino-terminal β-hairpin, forming an arrowhead shape. Between the helices 4 and 5, an extended loop forms a hydrophobic motif (residues 85-93) that binds the host protein cyclophilin A (CypA),

known as the CypA-binding loop [84], [85]. The carboxyl-terminal domain (CA$_{CTD}$, residues 150–221) has a more globular geometry. It contains 4 α-helices (H8-H11) and a short single-turn 3_{10} helix at the N-terminal end [86]. In helix 8, there is a highly conserved 20 residue long motif known as the major homology region (MHR), which has been shown to be critical for particle assembly [87]. In solution, HIV- 1 CA dimerises with a dissociation constant (K$_D$) of 18 µM and the dimerisation interface is highly dependent on the residues Trp[184] and Met[185] from H9 helix of the CA$_{CTD}$ [86].
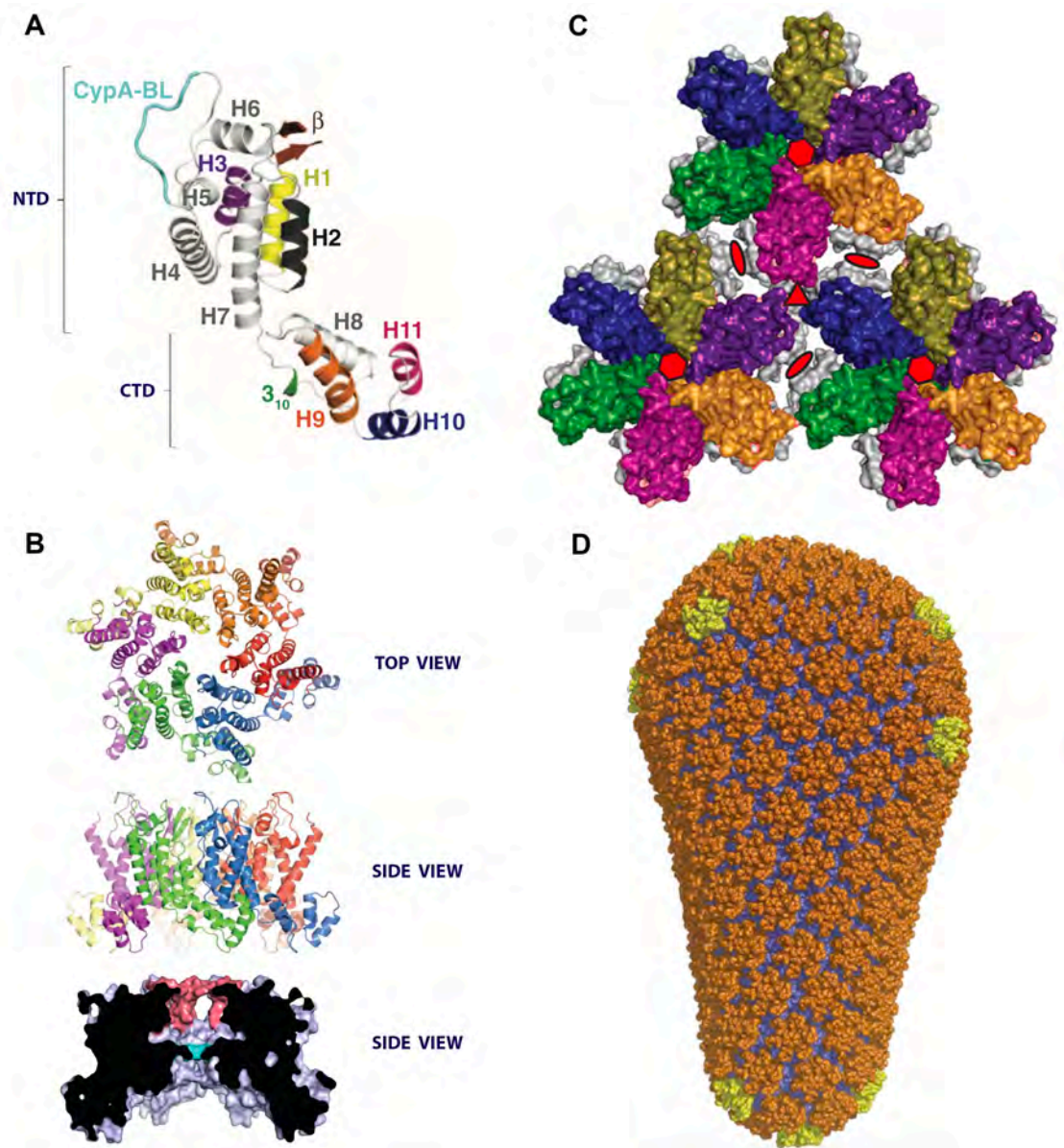
Figure 1.4. HIV-1 CA, hexamer and assembled capsid. (A) HIV-1 contains 11 α helices (H1-H11) arranged into an amino-terminal domain (NTD) and a carboxyl-terminal domain (CTD). The cyclophilin-A binding loop (CypA-BL) in CA$_{NTD}$ is coloured in cyan and the helices highlighted in purple, yellow and black are involved in the intermolecular interactions, which contribute to the formation of hexameric and

pentameric rings. The helices H9 (orange), H10 (dark blue) and H11 (fuchsia) in CA$_{CTD}$ engage in interactions that hold together different hexamers and pentamers to assemble a larger structure. **(B)** Top and side view of a CA hexamer, including a cross-section that shows the cavity above the R18 ring (cyan) with the β-hairpin (pink) in an open conformation. **(C)** Arrangement of hexamers within the HIV-1 capsid lattice. The 2-fold, 3-fold, and 6-fold symmetry axes are indicated by red ellipses, triangles, and hexagons, respectively. **(D)** 3D representation of a mature capsid core, showing the spatial configuration of the hexamers (orange) and pentamers (yellow). The twelve CA pentamers are present at the ends of the structure creating the distinctive fullerene shape. Figures adapted from [88]–[90].

When the HIV-1 CA is compared with CAs from other retroviruses, minimal sequence conservation is observed (~20%), except for the MHR in CA$_{CTD}$. However, the tertiary structure of CA is highly conserved among retroviruses [91]. This conservation suggests that the CA structure has crucial characteristics as a building block to construct the capsid shell.

1.3.2. Capsid structure

Assembled HIV-1 capsids have a cone/fullerene shape, with sizes ranging 100-200 nm in length and 45-60 nm in width (**Figure 1.4D**) [21], [92]. It is composed of CA organised in ~250 hexamers and exactly 12 pentamers [21], [33]. The distribution of the pentamers, seven located at the base and five at the tip, induces high curvature allowing the closure of the capsid shell [92], [93].

Within the assembled pentamers and hexamers, each CA$_{NTD}$ is located to the centre of the ring structure, oriented to the outer surface of the capsid (**Figure 1.4B**). The NTD-NTD interface is formed by intermolecular interactions between the H1 and H3 from one CA with the H2 of the adjacent CA. This forms an 18-helix bundle at the centre, a structure that obeys a 6-fold rotational symmetry [81]. The interactions between the NTDs are the main interactions that stabilise the pentameric/hexameric subunit although the interface formed between CA$_{NTD}$-CA$_{CTD}$ from contiguous monomers is also involved in maintaining the intra-subunit structure [89], [94]. This NTD-CTD interface, which involves helices 4, 7, 8 and 11 serves as a binding pocket to diverse host factors such as nucleoporin 153 (NUP153) and the cleavage and polyadenylation specificity factor 6 (CPSF6) [75], [95]–[97]. The small compounds PF74 and BI-2 also target the same binding interface [96], [98].

The six CTDs are positioned to the ring's edge and oriented towards the interior of the capsid shell. Neighbouring hexamers/pentamers in the capsid lattice are held together by CTD-CTD contacts (**Figure 1.4C**). This interface is stabilised by hydrophobic interactions between H9 of two CAs from different hexamers forming the dimer interface (2-fold axis) [81], [86]. Residues from H10 and H11 have also been shown to be involved in the interconnection of hexameric subunits by the formation of a three-helix bundle at the 3-fold interface formed between hexamers [92], [99]. The intrinsic flexibility of this region, especially of the H9 helix, is probably essential to allow the curvature needed for the assembly of a closed core.

In 2016 Jacques *et al*. described a new feature of the CA hexamer [72]. A cavity of about 25 Å deep and 3,240 Å^3 in volume exist at the centre of the hexamer (**Figure 1.4B, bottom side view**). On the outer surface, the β-hairpins act as a cap that can open and close depending on pH. Low pH causes the β-hairpins to open while high pH triggers a closed conformation. At the bottom of the chamber there is a highly positively charged pore formed by a ring of six arginine residues (R18). This R18 pore can also adopt multiple conformations with a maximum diameter of 8 Å [72].

What drives CA proteins to join together and create a fully closed core with exactly 12 pentamers is not clear. The position of the pentamers allows different geometries to be formed: tubular capsids arise when 6 pentamers are located at each end of the cylindrical tube, or spherical capsids are formed if pentamers are evenly distributed in the lattice [100], [101]. Indeed, different capsid forms such as cylinders and pleomorphic shapes can be found in HIV-1 virions, as well as many unclosed cones or multiple small capsids [21], [25], [102], [103].

Around ~5000 copies of the Gag polyprotein are packaged into the viral particles, but the HIV-1 capsid comprises just 1000-1500 copies of CA. This means that more than half of the CA proteins contained within the virion do not form part of the main lattice [33]. The role of the free CA is not well understood, but it has been speculated that the high protein concentration inside the virus may assist in maintaining the capsid organisation. Efforts to isolate HIV-1 cores from virus preparation have shown that they are extremely unstable, with just ~15% of the input CA recovered as assembled lattice [104], [105]. Furthermore, CA complexes can be assembled *in vitro* but high ionic strength or crowding agents are needed to stabilise them [106]–[108]. The stability of the HIV-1 capsid within the virion not only depends on itself, but also relies on the interaction with other viral components. For example, it has been shown that Vif [30]

and the viral integrase [109] are essential for optimal stability of the viral core. Overall, the high degree of polymorphism, poor assembly fidelity and intrinsic core instability has made the HIV capsid a technically challenging entity to study.

1.3.3. Roles of CA/ Capsid during infection

The HIV-1 capsid orchestrates several steps of the viral cycle. Here, different roles of CA in the early phase of infection are described.

1.3.3.1. Protection of viral genome and immune evasion

The most recognisable role of the capsid is the protection of the viral RNA and proteins within the cytoplasm of the infected cell. The capsid shell is assembled upon maturation of the virus, encapsidating the genetic material inside. In early years, it was thought that its only role was to ensure the correct delivery of the genome into the target cell. This idea was based on analysis of the RTC components, where CA was not found [52], [54]. However, latest evidences revealed new roles of CA in HIV-1 infectivity, including immune evasion.

Typically, an innate antiviral response is triggered in cells following viral entry in order to create a hostile environment for the infectious agent. In that situation, the cell recognises the viral nucleic acids and then induces an interferon (IFN) response to activate the immune system to fight the pathogen. Surprisingly, HIV-1 infection of lymphocytes and macrophages does not induce antiviral IFN responses, even though the high error rate of the viral RT produces high amounts of non-productive dsDNA that should trigger the host sensors [110]. Studies have shown that evasion of the immune system recognition is accomplished by the viral capsid [70], [71]. HIV-1 bearing the CA mutations N74D and P90A cannot replicate in primary human monocyte-derived macrophages because these cells activate the innate response [71]. Interestingly, these mutants are impaired for CA interaction with the host proteins CPSF6 and CypA, respectively, suggesting that the capsid utilises host factors to hide from the immune sensors. Capsids with increased affinity for CypA also fail to prevent detection by immune sensor [70], implying that binding per se is insufficient, but the interaction has to be functional.

1.3.3.2. Reverse transcription

Conversion of the viral ssRNA into dsDNA is a key step in HIV-1 infection. This reverse transcription reaction is a complex process requiring different catalytic activities that are carried out by RT, and includes strand transfer events [111]. It is generally accepted

that reverse transcription is initiated in the closed capsid, which served as a reaction compartment that maintains association of RT with the viral genetic material. Whether reverse transcription is also completed inside the closed capsid or after the capsid has started to disassemble is not clear, as there is evidence supporting both alternatives. It has been shown that reverse transcription can take place within the closed capsid [112], as long as it is supplied with dNTPs. The recently discovered electropositive pore at the centre of the CA hexamers supports the binding of nucleotides with high affinity [72]. This pore was shown to be essential in an in vitro reverse transcription assay, suggesting that the virus could use it for nucleotide recruitment to regulate reverse transcription inside the host cell. Nevertheless, several host proteins have been identified to be critical for efficient completion of reverse transcription within the cell. This observation suggests that capsid must open, or at least be permeable, to host cofactors in order to allow their interaction with the RTC [113].

Regardless of whether the capsid uncoats during or after the formation of the viral dsDNA, optimal stability of the core has been shown to be crucial for efficient reverse transcription. Mutations that either reduce or increase its stability impair reverse transcription [105], [114], and induction of premature uncoating with PF74 [115] or TRIM5α also decreases RT activity [116]. Conversely, reverse transcription has been shown to influence capsid stability. Inhibition of reverse transcription with drugs or mutations in RT results in increased stability of the viral core [117], [118]. A recent paper proposed that viral DNA mechanically triggers initiation of capsid disassembly [119], whereby conversion of the flexible ssRNA into a rigid dsDNA molecule provides the pressure to initiate capsid uncoating. Although the precise timing of uncoating and reverse transcription is still not well understood, it is apparent that there is a tight relationship between these processes.

1.3.3.3.   Transport towards the nucleus

The trafficking of the viral genetic material towards the nucleus utilises the microtubule network. Several studies have linked the HIV capsid with the movement through the cytoplasm, more specifically by interaction with dynein [55], [57]. Disruption of the microtubule-mediated transport or depletion of the microtubule motors such as dynein or kinesin-1 delays uncoating [57], [58], supporting the role of CA in the transport towards the nucleus.

1.3.4. Nuclear entry and integration

One of the characteristics of lentiviruses is that they can efficiently infect non-dividing cells because they actively translocate their genome into the host nucleus [20]. The ability to enter the nucleus via the nuclear pore complex is dependent on the capsid. Chimeric viruses in which HIV-1 CA is replaced with the corresponding sequence from murine leukemia virus (MLV) are unable to infect nondividing cells [120]. The same result is obtained with viruses containing mutated CA [121]. Additionally, HIV-1 CA plays an important role in viral integration and site integration targeting [40]. CA T54A/N57A mutant viruses efficiently translocate their PIC into the nucleus but fail to integrate [121], while a virus with a CA P90A substitution favoured integration into regions with an increased density of transcription units compared to WT CA [77] .

The mechanism by which the capsid regulates nuclear entry and integration is unclear, mainly because the spatiotemporal control of uncoating remains poorly understood. There is a wide variety of diverging observations of where uncoating occurs. Some of them postulate a very early disassembly while others propose capsid disassembly at the nuclear membrane [50]. However, it is now widely accepted that in order to control nuclear transport and integration, a significant level of CA remains associated with the PIC [122], [123]. Furthermore, it has been shown that HIV-1 CA interacts with cellular transport machinery to regulate nuclear entry and integration. Several host factors have been identified in genetic screens that are involved in active transport of the PIC across the nuclear membrane and in viral integration [124]. CypA, CPSF6, NUP358, NUP153 and transportin 3 (TNPO3) area among these potential modulators [125], [126] and their specific functions related to capsid will be discussed in the section 1.4.2.2.

Collectively, these data suggest that the HIV-1 capsid plays important roles in several steps of the viral life cycle.

1.4.   Uncoating

Uncoating is described as the disintegration or disassembly of the viral capsid [127]. Even though it has been studied for almost 30 years [128], there are still many unresolved questions regarding the precise moment, location and mechanism of uncoating. Understanding the HIV capsid disassembly has been incredibly hard due to numerous reasons: the wide range of roles in which the capsid involved, the high rate of unproductive entry events [67], the interplay between cofactors and restriction factors, its cell-type dependence [129], the heterogeneity of the HIV population [102],

and its intrinsic fragility [105]. Additionally, the apparently conflicting evidence that suggest different modes of uncoating has made its study even more challenging.

For long time the leading model of uncoating proposed that the disassembly of the viral capsid take place shortly after its release into the cytosol, i.e. close to the plasma membrane. This model was based on results from early work when more sensitive technologies to detect capsid inside the cell, such as fluorescence microscopy, were limited. The main evidence that supported the early uncoating model are electron microscopy images of infection events where no intact cores beneath the fusion site could be found, suggesting that cores must disintegrate shortly after entry [128]. Moreover, a biochemical study found that CA was no longer associated with the reverse transcription complex (RTC) at 1 hour post-infection. This short period, compared with the 8-12 hours that the complex spent in the cytosol before translocation, suggested that the capsid disassembles very early in the viral life cycle [52]. However, several recent observations contradict this model, such as the need for CA to allow infection of nondividing cells and viral genome integration [40], [121]. Additionally, it has been widely shown that premature disassembly of the viral core leads to aborted infection. For example, viruses bearing CA mutations that produce intrinsically more unstable capsids compared to wild type (WT) CA, such as P38A, inhibit infection in almost 100% [105]. The same result was obtained when destabilisation factors, like the host restriction factor TRIM5α, were used [116]. In summary, these observations suggest that rapid uncoating does not support successful infection.

Recent research results have led to a general agreement that capsid disassembly occurs after release of the core into the cytoplasm and before nuclear import, yet is still not clear whether it is a gradual process in the cytoplasm or a discrete event at the NPC (**Figure 1.5**) [50].

The significant sensitivity of reverse transcription to changes in intrinsic core stability [105], [114], the binding of host cell factors to the RTC within the cytoplasm [113], and the detection of dissociated CA in the cytoplasm of the infected cells support the cytoplasmic uncoating model (**Figure 1.5A**). Hulme *et al.* showed that assembled CA steadily decreases during the first 4 hours after infection, with an uncoating half-life of 39-85 min post-infection by using a fluorescence *in situ* hybridisation approach and cyclosporine A (CsA)-washout assay, [118], [130]. A similar result was obtained using a dye that stains viral RNA only after uncoating is initiated [131]. In this study, an initial

increase of the dye signal was observed at 30-45 minutes post-infection indicating opening of the capsid within this period of time. The initial signal increase was then followed by a gradual signal loss over time, which was interpreted as the release of RNA into the cytoplasm due to a more advanced dissociation of the CA lattice [131]. A novel live-cell imaging approach that follows HIV-1 viral particles that lead to successful infection gave a median capsid opening time of 30 minutes, and revealed that loss of the majority of CA occurs in the cytoplasm [132].
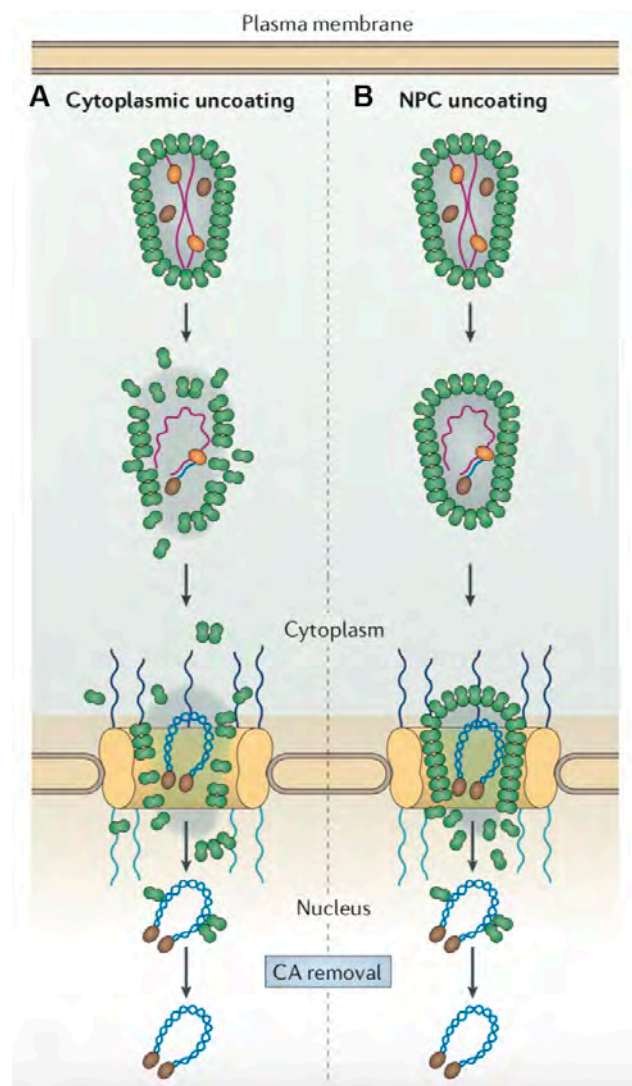
Figure 1.5. Models of viral uncoating. (A) In the cytoplasmic uncoating model uncoating occurs gradually in the cytoplasm but some amount of CA remains associated with the reverse transcription complex (RTC) until it reaches the nucleus. **(B)** The NPC uncoating model proposes that the core remains intact until it reaches the nuclear pore complex (NPC) were it disassembles. Some CA remains associated with the viral DNA after entry into the nucleus but is lost upon integration. Illustration adapted from [50].

Even though the cytoplasmic uncoating model is compatible with available data, it is still unclear how the virus can lose a large portion of CA from the capsid and still hide its dsDNA from host DNA sensors [70]. A model where the capsid remains intact during its transport towards the nucleus but disassembles once it reaches the nuclear pore complex support that observation (**Figure 1.5B**). Furthermore, several other findings support this uncoating at the NPC model. Fluorescent immunostaining approaches have found high levels of CA at the nuclear membrane and even inside the nucleus, implying that an assembled viral core reaches the nuclear pore complex [133], [134]. The CA-binding cell factor NUP153, which is involved in nuclear import of the RTC, binds with higher affinity to hexamers than non-assembled CA in an interface that is lost after disassembly. This suggests that an assembled CA surface is needed at the nuclear pore for this factor to bind [96]. Additionally, a recent research that track particles that lead to successful infection revealed that the capsid is required for docking into the nuclear pore and that the disassembly of most of the CA lattice occurs at the nuclear envelope [135], [136]. Despite all of these observations that support uncoating at the nuclear pore, the need for binding of host proteins to the RTC/PIC before nuclear translocation, as well as the impaired integration observed with PICs that contain elevated levels of CA [123] challenge this model.

Regardless of whether the capsid disassembles gradually in the cytoplasm or at the nuclear pore, it is still controversial at what extent CA remains associated with the PIC during and after nuclear translocation. CA has been detected within the nucleus of infected cells [137]. The diameter of the nuclear pore complex (NPC) allows translocation of cargos with a width of up to ~39 nm [138], while the fullerene cone is about 45-60 nm in width [21], [92]. This size constraint for import has led to the view that a substantial amount of CA must dissociate from the PIC before it can translocate through the NPC. However, recent data suggest that the NPC to be a flexible and dynamic gate [139]. This model allows re-evaluation of the need to shed most of the capsid before nuclear entry.

1.4.1. Known factors that affect uncoating

Irrespective of where uncoating takes place, it has been shown that uncoating is influenced by different factors such as CA mutations and binding of host cell proteins, small molecules or antiviral drugs.

1.4.1.1. CA mutations

Much of our knowledge of HIV-1 uncoating is derived from studies of CA mutations that disturb capsid stability and its functionality. It is important though to differentiate between mutations that directly alter capsid stability from others that indirectly have an effect due to altered interactions with host factors that facilitate or restrict uncoating.

Numerous CA studies have demonstrated that point mutations in CA can increase or reduce the inherent stability of the viral capsid [79], [105], [114], [140]. Examples of this extreme fragility are the single residue substitutions P38A and E45A. Both amino acids are located in the CA_{NTD}, forming part of the H2 helix. Even though both mutations lead to the production of viral particles with conical capsids at levels comparable to WT CA, they reduce infectivity by ~30-fold relative to WT virus. While CA P38A yields capsids with reduced stability, the CA E45A mutation generates hyperstable lattices that disassemble more slowly than WT capsids [105], [114]. In addition, these mutations alter reverse transcription kinetics, whereby reverse transcription is faster with CA P38A than for virus with WT CA, and slower with CA E45A. These opposite effects on reverse transcription kinetics reflect the effect of capsid stability on this process during infection [105]. Another difference between these mutants is their ability to infect nondividing cells. Viruses containing the CA P38A mutation do not discriminate between stages of the cell cycle for infection, but virus containing CA E45A displays just 18% infectivity in nondividing cells relative to dividing cells [121]. An important finding is the relationship between these mutants and PF74, a small drug that inhibits infection. Even though the binding of PF74 to capsids assembled with CA E45A and CA P38A was maintained or even increased, respectively, the CA E45A substitution gave resistance to the drug while P38A was even more sensitive than WT, showing an increased inhibition of infection [115]. To further investigate these differences, a study selected for second-site suppressor mutations, T216I for P38A and R132T for E45A, that were able to restore infectivity of these mutants up to 40% of WT [141]. Despite the higher levels of infectivity obtained, the double mutants CA P38A/T216I and CA E45A/R132T exhibited similar core yields and disassembly levels compared to the respective single mutants, indicating that the second mutations did not restore normal capsid stability *in vitro*. Still, the CA R132T mutation relieved the cell-cycle dependence imposed by the CA E45A mutation as well as restoring sensitivity to PF74 [141]. Taken together, the data suggest that the structure of CA is exceptionally delicate and that a balance is needed to have an optimal stability of the viral capsid. Interestingly, the E45A CA substitution is also insensitive to the inhibitory effect of CPSF6-358 and to depletion of TNPO3 and NUP153, even when the E45 residue is not part of their

binding surface [142], [143]. For more information about the role of these host proteins please refer to the next section.

Some CA substitutions have been found to disrupt the binding of host proteins to the viral capsid. The CA G89V and CA P90A mutations exhibit marked defects on binding of cyclophilin A (CypA). These residues are part of the proline-rich region located on CA, which serves as CypA binding domain. Virions containing these mutations do not incorporate CypA and are unable to replicate [144]. In addition to CypA, HIV-1 CA P90A mutant was found to be insensitive to NUP153 and NUP358 depletion, and to promote integration in regions with a higher density of transcription units compared to WT [77], [145]. The P90 residue does not localise with the binding region for these proteins, suggesting that its effect is not necessarily by a defect in direct binding, but rather implies a potential connection between CypA and nuclear import proteins.

The HIV-1 CA N74D mutant was described to prevent binding of CPSF6. Experiments using *in vitro* CA assemblies bearing the N74D mutation exhibited a severe decrease in CPSF6 binding [143], [146], [147]. The reduced affinity was also shown by isothermal titration calorimetry (ITC), where there was practically no binding of CPSF6 peptide to the HIV-1 CA N74D N-terminal domain (K_D of 5.3 mM against 362 μM to WT CA) [95]. This mutation gives resistance to the restriction imposed by expression of cytoplasmic CPSF6 and to depletion of NUP153 and NUP358 [143]. However, CA N74D binding to the C-terminal domain of NUP153 is still observed [75]. Binding of PF74 is also just slightly decreased by the mutation, even though it binds to the same binding surface than CPSF6 [95]. The CA N74D substitution was shown to delay capsid disassembly, increasing the uncoating half-life by 30% [130], although another study indicated that N74D does not change the intrinsic stability of CA assemblies [108]. Intriguingly, the CA N74D mutant has also been reported to alter CypA dependence and impair macrophage infection [148]. CypA was found to bind 70% less *in vitro* to CA tubes assembled from CA N74D than from WT CA, and N74D HIV-1 infectivity is reduced in CypA depleted HeLa cells [148].

The CA A105T, N57A and K70A substitutions have also been shown to disrupt binding of capsid binders [95], [142]. CA A105T disrupts the interaction between CA and CPSF6, and is resistant to the inhibitory effects of CPSF6-358 and to TNPO3 depletion [142]. The HIV-1 CA N57A and K70A mutations abolish PF74 binding completely, reduce affinity to CPSF6 peptide and lose the dependency on TNPO3 and NUP358 [95].

1.4.1.2. Host cell factors

Several host cell factors have been identified to interact with the viral capsid and to modulate its stability [149]. Some of the binders, called cofactors, are part of the cell machinery hijacked by the virus to control uncoating, while others are restriction factors that recognise the capsid lattice and reroute the capsid into degradative pathways as a defence mechanism from the host cell to block infection. Despite the key role of the capsid in the HIV-1 replication cycle, very few capsid-binders have been identified (**Figure 1.6**). Host factors known to interact with the capsid are described in the following sections.
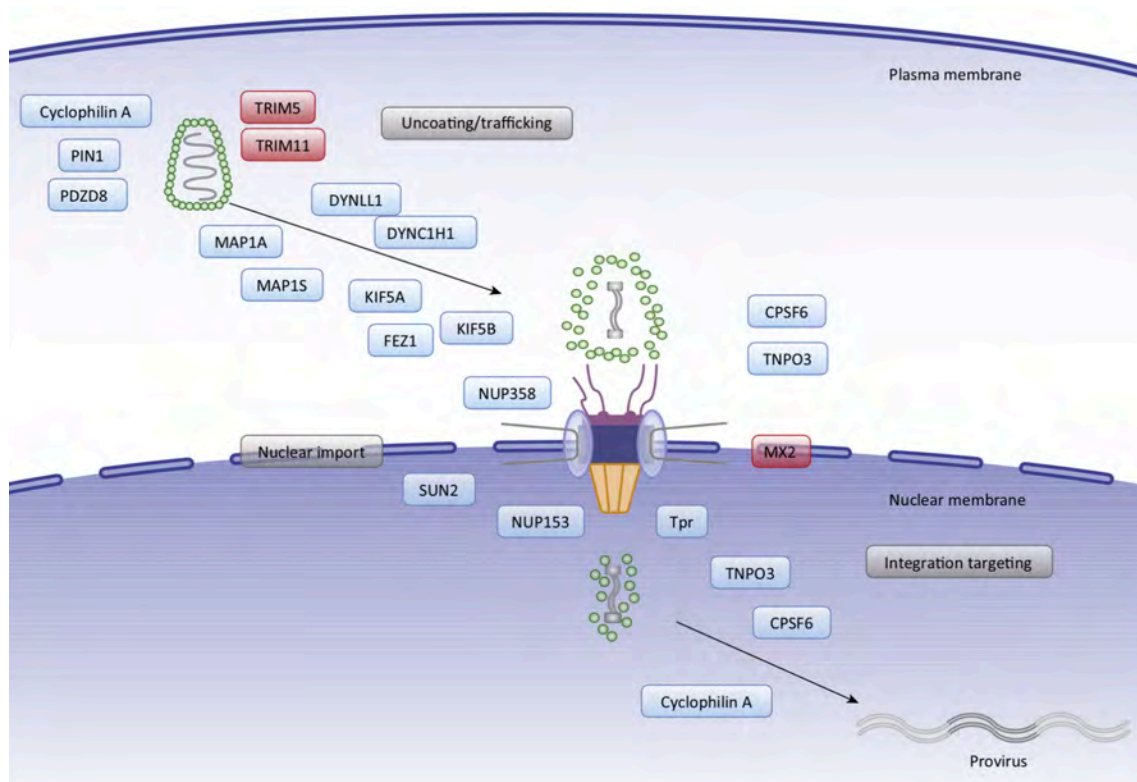
Figure 1.6. Capsid-dependent host cell factors involved in HIV-1 entry. During the transport of the viral capsid towards the nucleus, several host cell factors directly interact with the CA lattice and either promote (cofactors shown in blue) or restrict (restriction factor shown in red) HIV-1 infection. Cyclophilin A (CypA) is thought to bind the viral core very soon after release into the cytoplasm and remains bound to the capsid until arrival at the nucleus. HIV-1 nuclear entry is mediated by interaction with the nucleoporins NUP153 and NUP358 and import receptors CPSF6 and TNPO3. The positioning of the different factors in the figure does not necessarily reflect the location or timing of the virus–host interaction. Image adapted from [149].

1.4.1.2.1. Cyclophilin A

Cyclophilin A (CypA) is a cytosolic proline isomerase that catalyses cis-trans isomerisation of proline peptide bonds. It regulates various biological processes in mammalian cells including intracellular signalling, protein folding, transcription, inflammation and apoptosis [150]. Even though it is one of the most studied capsid binding proteins, its role in HIV infection remains unclear. Around 200 CypA molecules are incorporated into the HIV-1 virion during assembly and prevention of its inclusion reduces infectivity by 50 to 100-fold [151]. Although it has been shown that packaged CypA is key for viral replication, other studies suggest that the CypA present in the target cell plays a more important role in the HIV life cycle [152], [153].

CypA binds to monomeric and hexameric CA with a similar dissociation constant (K_D) of 12-16 µM [154], [155]. The proline-rich loop in the CA_{NTD} is the main binding site for CypA [154], [156]. This CypA-binding loop is very flexible and protrudes to the outer surface of the assembled capsid [92] which allows the binding of CypA without the need of substantial rearrangement of the capsid lattice (**Figure 1.4A**). CA residues A88, G89 and P90 are key for the CypA interaction, and become buried in the CypA active site upon binding. The interface between CA and the canonical binding site of CypA is stabilised by several van der Waals interactions as well as hydrogen bonds [85]. A recent cryoEM structure of CypA associated with CA tubular assemblies revealed that CypA molecules bind preferentially to high curvature regions within the lattice and that steric hindrance limit the binding of CypA to a 1:2 CypA:CA ratio. Further, single CypA molecules appeared to interact with two CA proteins at the same time, bridging the dimer interface between neighbouring hexamers. In this binding mode, each CA CypA-binding loop interacts with different CypA regions, one with the canonical binding site and the other with a new non-canonical binding site on the opposite side of the CypA molecule [157]. This new binding interface in CypA might strengthen its binding to the CA lattice through avidity. CypA binding to CA can be prevented by the use of the competitive inhibitor cyclosporine A (CsA), which binds to CypA [158], [159], or by mutations in the CypA binding loop on CA, specially CA residues G89 and P90 [154] (reviewed in section 1.4.2.1).

The precise role of CypA for HIV infection is still an open question. CypA-binding deficient viruses are unable to replicate in primary human monocyte-derived macrophages because they trigger an antiviral state, suggesting that CypA is used by HIV-1 to cloak its replication in primary human macrophages [71]. An early publication revealed that reduced incorporation of CypA into budding virions does not affect viral

assembly, budding or maturation of the particles but interrupt reverse transcription. The reduced infectivity could not be overcome by the binding of CypA present on the target cell during infection [151]. This defect was not associated with a change in capsid stability, as WT and CypA-depleted virions exhibited same levels of core recovery, suggesting that CypA was not modulating capsid stability [151]. In contrast, several other studies have shown CypA to modulate uncoating. There is evidence to suggest that CypA stabilises isolated cores and assists in the *in vitro* assembly of CA-NC complexes, but other studies indicate that CypA binding promotes capsid destabilisation [160]–[163]. A recent study found that different CypA concentrations cause different effects on core stability [157]. This observation could help explain the contradictory results obtained using different cell types [129], [153]. Indeed, intracellular concentration of CypA can be quite dissimilar in different cell types, making the comparison of results from different studies very challenging. In general, it is considered that intracellular concentrations of CypA are typically around 20 μM [158], but CypA levels in HeLa cells have been found to be 3-fold higher than in Jurkat cells [161].

How exactly CypA modulates uncoating is still unclear. It has been proposed that CypA regulates uncoating in a concentration manner by a direct effect on the capsid structure. At low concentrations, as inside the virion, CypA stabilises the CA lattice. Its release into the cytoplasm allows more CypA molecules to bind, increasing the stability of the core but binding saturation promotes the lattice to collapse due to steric hindrance between CypA bound to adjacent hexamers starting the uncoating process [157]. Another theory proposes that CypA catalyses the isomerization of the G89-P90 bond in CA, changing the conformation of the CypA-binding loop and destabilising the capsid structure [164]. De Laco *et al.* studied the effect of CypA depletion in 27 different cell lines and found that HIV-1 reverse transcription was diminished equally in all of them, but restriction at the level of nuclear entry was differently affected. He postulated that these differences are due to an unknown restriction factor that requires CypA binding to CA, and that this factor is expressed differently in the different cell lines [165]. Similarly, another study indicated that viruses, which are unable to bind CypA, integrate their viral genome in regions with higher density of transcription units. This altered pattern was due to a defective interaction of CA with other host factors such as NUP153 and NUP358, implying that the CypA interaction dictates the use of other CA-binding factors for nuclear entry [77], [145]. CypA has also been shown to modulate the activity of TNPO3 [160], strengthening the idea that the CypA role in HIV-

1 infection is to the regulate the binding of other host factors to CA rather than to directly control the capsid stability itself.

1.4.1.2.2. NUP358

Nucleoporin 358 (NUP358), also called RanBP2, is the largest nuclear pore protein out of the ~30 that make up the nuclear pore complex (NPC). It is the main component of the eight NPC filaments that are projected to the cytoplasmic face and it functions in several processes such as cell cycle control and nuclear import and export [166]. NUP358 contains a cyclophilin domain-like moiety in its CTD [167]. Several studies have demonstrated using either recombinant CA_{NTD} or CA-NC *in vitro* assemblies that CA binds directly to this Cyp domain [77], [133], [167], [168]. Lin *et al.* found that NUP358-Cyp domain binds to CA with extremely low affinity (K_D > 200 µM) [167], in contrast to the 94 µM found by Bichel *et al.* or the 16 µM found by Schaller *et al.* [77]. In the last case, the dissociation constant for the NUP358-CypA/CA interaction was twice of the one obtained with CypA protein (7 µM). They also found that NUP358-Cyp interaction with CA was not inhibited by CsA suggesting that NUP358 and CypA do not form identical interactions with CA. The crystal structure of the complex revealed that the CA P90 residue is key for NUP358-CypA binding, in the same way that it is for CypA binding [168].

Depletion of NUP358 reduces HIV infectivity [133], [169], [170]. Production of 2-LTR is diminished, and integration of the viral genome decrease by 12-fold [133], [170]. All these observations suggest that NUP358 is a cofactor required for HIV-1 infection, but how specifically it is used is still unclear. By using fluorescent immunostaining and cellular fractionation, it was shown that during infection CA localises less with the nuclear membrane in NUP358-depleted cells than in control cells. This indicates that NUP358 mediates the docking of HIV-1 cores on NPC cytoplasmic filaments [133]. Contrarily, another study revealed that HIV-1 infection promotes relocalisation of NUP358 to the cytoplasm and that NUP358-depletion promotes higher localisation of CA at the nuclear membrane [74]. Interestingly, CA N74D or CA P90A HIV-1 mutants were shown to be insensitive to NUP358 depletion in HeLa cells; infectivity and nuclear import were similar in NUP358-depleted and control cells, and relocalisation of NUP358 to the cytoplasm was not promoted. These results suggest that CA P90A and CA N74D use a NUP358 independent route to enter the nucleus. However, when tested in human monocyte derived macrophages (MDM), replication of N74D or P90A CA HIV-1 was seriously diminished, and NUP358 proteins were located within the nuclear compartment [74]. The different results obtained with different cell types that

express proteins differently, reveal the importance of cofactors for HIV-1 infection, especially for nuclear translocation. CA N74D and P90A mutations are known to disrupt interactions with CPSF6 and CypA, respectively, so the authors tested whether NUP358 was still re-localised to the cytoplasm in CPSF6 or CypA-depleted cells. CPSF6 but not CypA depletion, prevented the redistribution of NUP358 to the cytoplasm [74].

NUP358 also influences the selection of chromosomal sites for HIV-1 integration, reducing integration frequency in gene-dense regions [76]. Taken together, all the observations suggest CA can interact with different NPC proteins and that differential interaction may direct transport through different nuclear import pathways with different effects on integration.

The mechanism by which NUP358 influences uncoating is unknown. Using fluorescent immunostaining it was shown that NUP358-depletion delays uncoating [74]. Additionally, NUP358 was shown to catalyse a more rapid isomerisation of the G89-P90 peptide bond from cis to trans conformation than CypA, which has been proposed to destabilise the CA lattice [168]. A plausible possibility is that NUP358 cytoplasmic filaments facilitate recruitment of viral cores to the vicinity of NPC. This interaction stimulates uncoating by accelerating CA isomerisation and at the same time facilitates interaction of the PIC with the nuclear transport machinery.

1.4.1.2.3. NUP153

Nucleoporin 153 (NUP153) is another component of the NPC, forming part of the nuclear ring [171]. It anchors to the nuclear side of the NPC through its NTD, while its flexible ~220 nm long CTD can potentially reach through the nuclear basket towards the cytoplasmic side. The C-terminal domain contains 29 Phe/Gly (FG)-repeats that are natively unfolded and allows NUP153 to play several roles in nuclear translocation [169], [172], [173].

Depletion of NUP153 reduces HIV-1 infectivity [77], [133], [143], [174]. Further characterisation revealed that 2-LTR circle production is reduced and integration is decreased by 6-fold [133]. NUP153 binds directly to CA, which is mediated by the NUP153 FG motifs, as revealed with mutagenesis experiments. The complex between the C-terminal domain of NUP153 (NUP153C) and CANTD has an estimated KD of 28 μM [75] while binding of NUP153-FG peptide binds to hexameric CA with a KD of 49 μM[155], but does not bind to monomeric CA [97]. A different group also tested the FG-

peptide and determined a KD of 3300 µM for binding to CANTD, and 484 µM for binding to CA hexamers [96]. Even though different dissociation constants have been obtained, it is clear that there is a tighter binding to assembled CA than to monomeric CA.

The crystal structure of NUP153-FG peptide in complex with CA hexamers revealed that the binding site corresponds to a hydrophobic pocket involving helices 2, 3, 4 and 7 from the CANTD and helices 8 and 9 of the adjacent CACTD (Figure 1.7A) [97]. Strikingly, the same binding interface is used by the small molecule PF74 and the host protein CPSF6 (sections 1.4.2.2.5 and 1.4.2.3.1). Indeed, competition experiments for HIV-1 CA binding showed a dose-dependent reduction of NUP153 binding to CA when PF74 was present. This effect was not observed with N74D CA, a mutation that abolishes PF74 binding but not the interaction with NUP153. Similarly, CPSF6 binding to CA is reduced in the presence of NUP153 [75], [97].

The stronger binding of NUP153-FG peptide to the assembled CA lattice supports the idea that the viral core must reach the nuclear pore in a largely intact state [96], and that NUP153 promotes nuclear import of the PICs. NUP153 has been shown to interact with chromatin and plays a direct role in HIV-1 integration. NUP153 depletion causes a significant reduction in the tendency of viral DNA to integrate into gene-dense transcriptionally active regions of chromosomes, although this effect is in less in magnitude when compared with TNPO3 or NUP358 depletion [174].

1.4.1.2.4.   TNPO3

Transportin 3 (TNPO3), also known as Tnp3 or TRN-SR2, is a member of the importin-β family of proteins. It shuttles between the cytoplasm and the nucleus to assist with nuclear import. It usually interacts with cellular serine/arginine-rich proteins (SR proteins) that are involved in the splicing of mRNA, trafficking them through the nuclear pore [175].

Depletion of TNPO3 has been shown to inhibit HIV-1 infectivity [77], [134], [160], [176], [177]. Furthermore, it reduces 2-LTR circle formation, inhibits nuclear translocation, and alters the selection of chromosomal sites for integration, reducing integration frequency in gene-dense regions [76], [142], [178]. TNPO3 was first identified as a cofactor for HIV import to the nucleus by using pull-down experiments with HIV integrase (IN) [178], but later reports demonstrated that TNPO3 binds directly to HIV-1 CA in its soluble form [134] and to CA-NC *in vitro* assemblies [176]. Shah *et al.* showed

that incubation of purified HIV-1 cores with recombinant TNPO3 promoted accelerated uncoating *in vitro* [160]. Zhou *et al.* observed by immunofluorescence an accumulation of CA levels in the nucleus of TNPO3-depleted cells compared to control cells where most of the CA signal was localised in the cytoplasm [134]. Based on these results, the authors proposed that high levels of CA accompany the PIC into the nucleus, followed by TNPO3-mediated export of CA to the cytoplasm.

Several CA mutations confer resistance to TNPO3 depletion, such as N57A, A105T, N74D, E45A and T107N [134], [142], [143], [160]. These mutations do not necessarily alter the CA binding surface for TNPO3, which is unknown, but could disrupt CA interactions with other host factors that may work in conjunction with TNPO3. Indeed, pull down experiments with CA N74D demonstrated normal binding to TNPO3 even though the same substitution confer resistance to its depletion [134]. Furthermore, Shah *et al.* showed that addition of CypA into the *in vitro* uncoating assay with TNPO3 reduced its disassembly effect as well as CsA treatment enhanced HIV infection in TNPO3-depleted cells, suggesting a link between TNPO3 and CypA [160]. Another research suggests that the TNPO3 influence on HIV infection is due to direct interaction with CPSF6 instead of binding directly CA (see next section) [142], [179].

1.4.1.2.5. CPSF6

The cleavage and polyadenylation specificity factor-6 (CPSF6) is a 68 kDa protein, which is part of the mammalian cleavage factor I (CF Im). It is required for processing of the mRNA precursors in the nucleus prior to their export to the cytoplasm where they are used for protein synthesis [180]. It contains a serine/arginine-rich (RS) domain in its CTD, thus it is a possible partner of TNPO3. It localises primarily to the nucleus but can dynamically shuttles between the nucleus and the cytoplasm in a transcription-dependent manner [181]. Deletion of the RS domain relocates CPSF6 to the cytoplasm.

Lee *et al.* identified CPSF6 as a capsid binder from a mouse cDNA expression library in 2010. The protein identified in that study was a truncated form, mCPSF6-358, that lacked the C-terminal RS-domain required for nuclear localisation [143]. When expressed in cells, the variant is enriched in the cytoplasm, in contrast to the endogenous protein that is mainly nuclear. Depletion of the cellular CPSF6 gives normal HIV-1 infection, suggesting that it does not act as a cofactor for infection [143], [147]. However, expression of the truncated form inhibits infection [95], [142], [143], [147]. Restriction is not due to altered synthesis or reverse transcription, but

accumulation of 2-LTRs is reduced, which suggested that HIV-1 PICs were unable to enter the nucleus. mCPSF6-358 was shown to bind CA directly via its phenylalanine-glycine (FG) motif, and its binding is reduced by the CA N74D mutation. Also, infection with CA N74D HIV-1 virus was normal in cells expressing mCPSF6-358, which indicates that the CA residue N74 is key for CPSF6 binding [142], [143], [147]. The restriction of HIV-1 infection by mCPSF6-358 was shown to be due to its mislocalisation to the cytoplasm. mCPSF6-358 fused to a nuclear localisation signal (mCPSF6-358-NLS) was localised only in the nucleus and did not restrict HIV-1 infectivity. Moreover, full-length CPSF6 tagged with a nuclear export signal (mCPSF6-NES) localised in the cytoplasm and inhibits HIV-1 infection [142].

Different mutations revealed a very tight correlation in the behaviour of CA with TNPO3 depletion and CPSF6 suggesting a common mechanism of action for HIV-1 infection [142]. Since CPSF6 has an RS-domain and TNPO3 imports RS proteins, TNPO3 may serve as an import factor for CPSF6, and TNPO3 depletion may cause endogenous CPSF6 to accumulate in the cytoplasm. Indeed, it has been shown that TNPO3 binds CPSF6, and that disrupting this interaction leads to inhibition of HIV infection [179]. De Laco *et al.* observed by immunofluorescence that endogenous CPSF6 is aberrantly detectable in the cytosol when TNPO3 is depleted [142]. Furthermore, they showed that HIV-1 infection in cells simultaneously depleted for TNPO3 and CPSF6 was normal. These results are consistent with the view that CPSF6 acts as a restriction factor for HIV-1 infection when it is in the cytoplasm and that the role of TNPO3 is to relocate CPSF6 to the nucleus, thus avoiding restriction. Contrary to these observations, a parallel study found that CPSF6 subcellular distribution does not change upon depletion of TNPO3, and the authors suggested that the effect of CPSF6 on viral replication occurs inside the nucleus [147].

How CPSF6 binding in the cytoplasm restricts HIV infection is not clear. Recovery of viral cores from infected cells expressing mCPSF6-358 or depleted of TNPO3 was higher than in control cells [142]. Incubation of *in vitro* CA-NC assemblies with recombinant CPSF6 (first 321 residues) also stabilises the complexes in a concentration manner [108]. This suggests that inhibition of HIV-1 replication might be due a hyperstabilisation of the CA core, delaying transit of the PIC to the nucleus. In contrast, binding of endogenous full-length CPSF6 from control cells and TNPO3-depleted to CA-NC complexes was similar, although capsid recovery from infected cells expressing CPSF6-NES is 10-fold higher, supporting the idea that cytoplasmic CPSF6 increases the stability of HIV-1 capsids [147]. A noteworthy report studied the

human CPSF6 instead of mouse CPSF6. The main difference between them is that the mouse CPSF6 (mCPSF6-358) has several extra residues encoded by exon 6 (residues 232 to 268) that the human form (hCPSF6-375) does not have as a result of splicing. Both forms inhibit infection and localise to the cytoplasm but hCPSF6-375 promotes destabilisation of cores and inhibits viral cDNA synthesis, while mCPSF6-358 stabilises cores and does not affect synthesis or accumulation of early or late reverse transcription products but interferes with the nuclear entry of the PIC [182].

Recently recombinant mCPSF6-358 was produced using a mammalian expression system with albumin as a secretion signal [183]. The authors showed that the protein purifies as dimers and higher-order oligomers. These species bind to *in vitro* assembled CA tubes and physically break them into small fragments but without dissociation into soluble proteins. Binding to CA hexamers was not observed, suggesting that the assembled CA lattice is needed for CPSF6 interaction. Using fluorescently tagged mCSPF6-358 they observed that upon HIV-1 infection the protein formed higher-order complexes in the cytoplasm of the infected cell. Fluorescent punctae are observed as early as 10 minutes post infection and their number increases after 30 min. CPSF6-358 assembly was avoided with addition of PF74 or when N74D CA HIV was used, but was increased when CsA was used. This suggests that CypA might shield the capsid lattice in the cytoplasm. The CPSF6 signal often colocalised with IN signal, suggesting that it is formed around the viral capsid, although both signal generally separate from each other after 3 minutes of interaction [183]. Even though this work is a breakthrough in the study of CPSF6, it is puzzling that many CPSF6 punctae in the cell do not colocalise with IN.

Besides being involved in capsid stability, CA-CPSF6 binding directs HIV-1 integration. Depletion of CPSF6 or the deletion of the CA binding domain of CPSF6, revealed decreased proviral integration into transcriptionally active genes [78], [184].

CPSF6 residues 313–327 constitute the minimal binding epitope for interaction with CA [146]. Binding affinity experiments have yielded different K_D values for the interaction of CPSF6 peptide (CPSF6$_{313–327}$ or CPSF6$_p$) with CA. Price *et al.* determined a K_D of 362 µM for binding of CPSF6$_p$ to CA$_{NTD}$, half of the value determined by Saito *et al.* (730 µM) [95], [185]. Bhattacharya *et al.* obtained a K_D of 1170 µM for binding of CPSF6$_p$ to CA$_{NTD}$, 436 µM for binding of CPSF6$_p$ to full-length CA and 80-100 µM for binding of CPSF6$_p$ to CA hexamers [96]. Zhou *et al.* calculated a much lower K_D value for binding

of CPSF6$_p$ to hexamers, 50 µM [155], similar to the value obtained by Lad *et al.*(17 µM for binding of CPSF6$_p$ to hexameric CA) [186]. In all cases, CPSF6$_p$ was found to bind more tightly to assembled than unassembled CA. The crystal structures of CPSF6$_{313-327}$ in complex with HIV-1 CA$_{NTD}$ and CA hexamers have been solved [95]–[97]. The structure of the complex with CA N-terminal domain revealed that CPSF6$_{313-327}$ lies in a binding pocket formed between helices 3, 4 and 5. The interaction is stabilised by intra- and intermolecular hydrogen bonds. The N- and C- ends of the CPSF6$_{313-327}$ project out of the binding site, suggesting that the peptide protrudes from the full-length CPSF6 structure, allowing its binding to the CA interface [95]. The conformation of the CPSF6 peptide in the CA hexamer revealed that the bound CPSF6$_p$ sits is in close proximity to the CTD of the adjacent CA (**Figure 1.7B**). In this structure, the H8 and H9 of the neighbouring CA$_{CTD}$ flank the peptide from the bottom side, with the flexible linker between the two helices making contacts with the peptide. CA K182 may form a hydrogen bond with the G318 of the CPSF6$_p$, while Q179 interacts with P317 and G319 [96]. NUP153 and PF74 bind to the same NT interface and it has been shown to compete for CPSF6 binding (**Figure 1.7**).
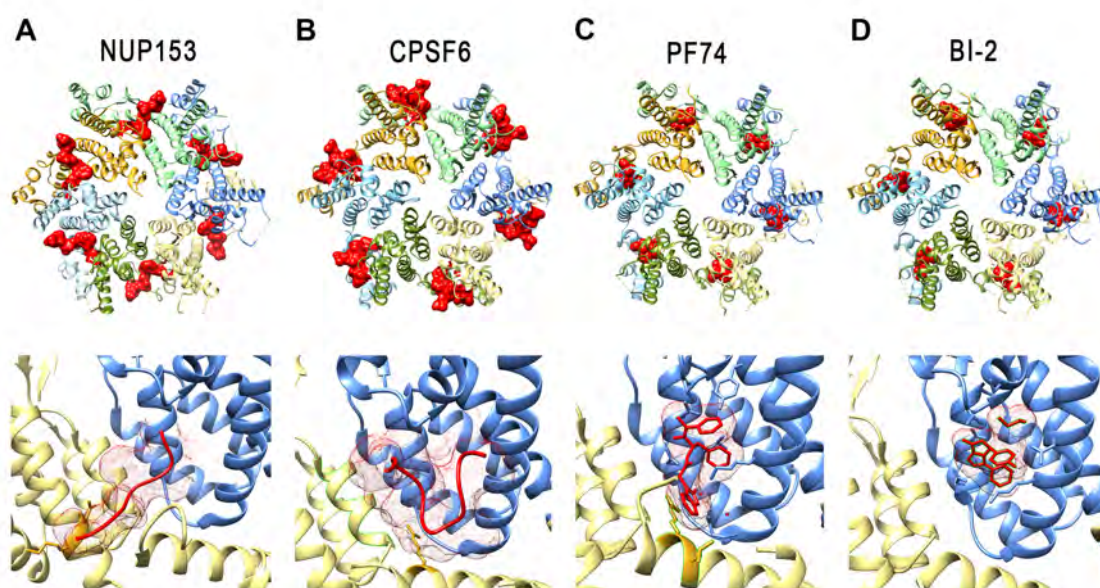
Figure 1.7. Structure of NUP153-FG peptide, CPSF6$_{313-327}$, PF74, and BI-2 in complex with HIV-1 CA hexamers. Top view (top) and close up (bottom) of a crystal structure of HIV-1 CA hexamer in complex with **(A)** NUP153-FG peptide, **(B)** CPSF6$_{313-327}$, **(C)** PF74, and **(D)** BI-2. Peptides and drugs (shown in red) interact with the NTD-CTD surface between adjacent CA subunits within the hexamer (shown in different colours). Images were generated from PDB 4U0A (CPSF6), 4U0C (NUP153), 4U0E (PF74), and 4U0F (BI-2) using Chimera.

Intriguingly, the CA E45A substitution was found to be resistant to mCPSF6-568 expression, while G89V/A92E or P90A/A92E displayed a greater sensitivity to it. As observed for the other host factors, it seems that CPSF6-358 restriction can be modulated by the binding (or lack of binding) of other host factors to the capsid, or by the appropriate assembly of the CA lattice.

Even though there is structural information of the interaction between the CA hexamer and CPSF6 peptide, the mechanism by which CPSF6-358 restricts HIV-1 infection is not fully understood. A better understanding will require both a fully assembled HIV-1 capsid and purified full-length CPSF6-358 protein, which has been a challenge to obtain.

1.4.1.2.6. Nucleotides

Deoxynucleoside triphosphates (dNTPs) are used by RT as substrates to synthesise viral DNA. A recent paper proposed that reverse transcription can occur in the closed core [72]. This proposal is based on the discovery of an electropositive pore at the centre of the CA hexamers. dNTPs bind to this positively charged channel with very high affinities (6-40 nM). Binding and unbinding kinetics are very rapid, suggesting that nucleotides are recruited efficiently by the capsid and imported into the capsid as substrates for reverse transcription. This interaction can be prevented by the addition of the small polyanionic compounds such as hexacarboxybenzene (mellitic acid), which compete with dNTPs for binding to the electropositive pore (**Figure 1.8**).
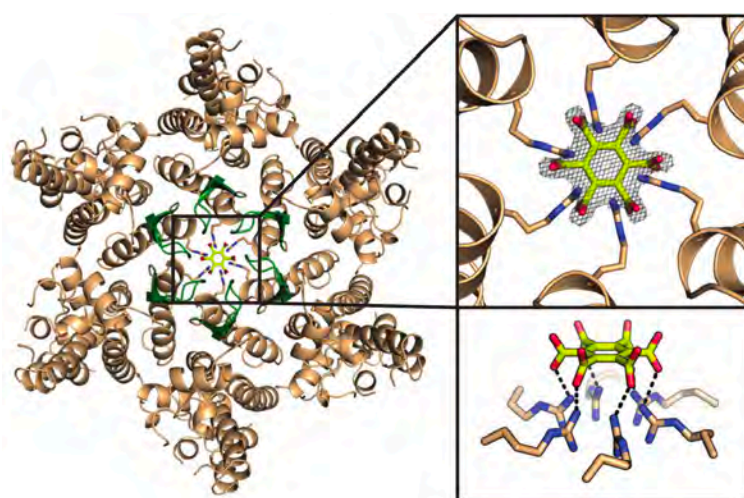
Figure 1.8. Crystal structure of CA hexamer in complex with hexacarboxybenzene. The R18 electropositive pore at the centre of the CA hexamer coordinates the polyanionic molecule. Reproduced from [72].

Binding of dNTPs or hexacarboxybenzene with CA hexamers increases hexamer stability, and the stabilising effect is less pronounced with tetra- or tricarboxybenzene molecules [72]. This result suggests that binding of negatively charged molecules to the R18 pore can modulate the capsid stability. Strikingly, dNTPs are not the only polyanion molecules in the cell. Adenosine triphosphate (ATP) is typically present with >100-fold in excess to dNTPs and could be potential competitor for dNTP. Similarly, inositol hexakisphosphate (IP6), also known as phytic acid, is a strongly negatively-charged metabolite abundantly present (~35-50 µM) in cells [187], [188]. IP6 has been shown to interact with immature capsid lattice and catalyse its *in vitro* assembly [189], but its effect on the mature capsid lattice had been unknown until recently.

1.4.1.3.   Antiviral drugs

A large number of small chemical compounds and peptide inhibitors that target HIV-1 CA have been developed [190]. This review focuses on PF74 and BI-2.

1.4.1.3.1.   PF74

PF-3450074 or PF74 is the most studied chemical compound that binds to HIV-1 CA. It was identified in 2010 by Blair and colleagues as a potent inhibitor of infection, showing a half maximal effective concentration (EC_{50}) of 0.57 µM [98].

The inhibitory activity of PF74 is concentration-dependant, exhibiting a triphasic curve [97], [160], [191]. HIV-1 infectivity is ~90% reduced when ~1.5 µM or lower concentrations of PF74 are used. In the range of ~1.5-5 µM inhibition remains unchanged. HIV infectivity decreases steadily again when cells are incubated with higher PF74 concentration, yielding almost complete inhibition at 10-30 µM. At the same time, high but not low concentrations of PF74 reduce the production of viral cDNA [97], [98], [115], [192]. RT inhibition is reversible when <30 µM PF74 is used and then washed out, but reversibility is not observed with higher concentrations [97]. This observation suggests that low and high doses of PF74 inhibit HIV-1 infection in different ways, probably by competing for host factors binding at low concentrations and by causing irreversible changes to the capsid structure at high concentrations.

The crystal structure of PF74 in complex with CA_{NTD} showed that it occupies a pocket in between the helices 4, 5 and 7. The binding is mediated by hydrophobic interactions between the R1 and R2 aromatic moieties of the compound with CA_{NTD} residues while the R3 moiety protrudes from the NTD [98]. The subsequent crystal structure of the drug in complex with CA hexamers revealed that the R3 interacts with the R173 and

L172 residues from the neighbouring CA_{CTD}, demonstrating that the principal surface for binding is the assembled capsid and not the monomeric CA (**Figure 1.7C**) [96], [97]. This observation is reflected by the different binding affinities obtained with monomeric or assembled CA. PF74 binds to isolated CA_{NTD} and full-length CA with similar dissociation constants in the range between 1.3 - 4.3 µM [96]–[98], [186]. The K_D to disulfide-stabilised CA pentamers or hexamers CA is >10-fold lower, ranging from 0.02 to 0.26 µM depending on the method used to determine affinity [96], [97], [186]. As mentioned before, this binding pocket is shared with the host proteins CPSF6 and NUP153 [95]–[97].

The influence of PF74 on viral uncoating has been investigated with several methods, giving seemingly contradictory results. On one side, PF74 decreases the stability of authentic viral cores. This conclusion is based on the observation that PF74 reduces the amount of core-associated CA recovered from isolated viral particles or from the cytoplasm of infected cells [115], [192]. Moreover, PF74 accelerates the *in vitro* disassembly of isolated cores [115], [160]. When tested in infected cells, it allows access of ribosomes to the viral genome more readily, indicating that shedding of CA from PICs is higher than in untreated cells [193]. However, with a different approach it was shown to modestly delay capsid uncoating during infection [136]. On the other side, it significantly increases the stability of *in vitro* CA assemblies. It promotes higher rates of CA multimerisation [98], and improves the stability of HIV-1 CA-NC complexes in a concentration dependent manner [96], [108], [192].

Other studies support an effect of PF74 not only in uncoating, but also in later steps of the viral replication cycle. HIV-1 is susceptible to PF74 restriction even when is added twelve hours post-infection, presumably long after capsid uncoating and reverse transcription has occurred [137], [191]. Live-cell imaging approaches have shown that PF74 (both 2 and 10 µM) block nuclear entry of PICs, disrupting its nuclear envelope docking [135]. Furthermore, PF74 (1.4 µM) retargets HIV-1 integration site distribution, significantly decreasing integration within genes and gene-dense regions [191]. Is not clear yet how PF74 modulates all these steps, but a possible explanation is that PF74 binding to CA disturbs the binding or activity of host factors that have been implicated in late steps of viral infection, such as CPSF6 or NUP153.

PF74 competes with CPSF6 and disrupts its binding to HIV-1 CA-NC assemblies [75], [147]. During infection, CPSF6 depletion significantly reduces the potency of PF74 at

low concentrations but not at high doses. The same result was observed when CPSF6 binding to CA was prevented via the CA K182A mutation, which abolishes CPSF6 binding but not PF74 binding [191]. These findings reveal not only that PF74 restrict CPSF6 binding to CA, but also that CPSF6 contributes to the unique dose-response of the small antiviral drug. A comparable outcome is obtained with NUP153, NUP358 and TNPO3. PF74 competes for NUP153 binding to CA in a dose-dependent manner [75]. PF74-mediated inhibition of HIV-1 infection at low concentrations is less drastic in NUP153-, NUP358- and TNPO3-depleted cells [75], [160], [191]. At high PF74 concentrations, the level if inhibition of infection is comparable in control and TNPO3-depleted cells [160]. When incubated with isolated cores, TNPO3 and PF74 exhibit a synergistic interaction, promoting an accelerated CA disassembly than observed when the two factors are used separately [160]. Surprisingly, a similar result is achieved with CypA. Its binding to HIV-1 CA enhances the antiviral activity of PF74 [115]. In presence of CsA, CypA-depleted cells or CA P90A subtitution, the inhibitory effect of PF74 at low concentrations is lower than in control conditions, but similar when a concentration of 5 µM or more is used [191]. Taken together the studies indicate that CypA, CPSF6, NUP153, NUP358 and TNPO3 interactions are required for the triphasic dose-response curve for PF74.

Several CA substitutions, such as Q67H, K70R, T107N and L111I, confer reduction in susceptibility to the drug due to loss of binding [98], [115]. CA E45A exhibit reduced sensitivity to PF74 inhibition even though it binds to similar levels as wild type [115], [137], [141]. The N74D substitution was shown to decrease PF74 binding by just 2-fold [95]. Some reports found that the PF74 inhibitory effect for CA N74D is as strong as with WT CA [137], while other found a 7-fold decrease in sensitivity [160].

1.4.1.3.2. BI-2

Another antiviral compound that targets the HIV-1 capsid is BI-2 [194]. It inhibits HIV-1 infection at a step after reverse transcription but prior nuclear import. BI-2 targets CA and interacts with the same binding pocket as PF74, CPSF6 and NUP153 (**Figure 1.7D**). However, unlike PF74 that interact with two neighbouring CA subunits in the hexamer, BI-2 interacts only with a monomeric CA_{NTD} unit [97]. Indeed, BI-2 binding affinity to CA hexamers is just 2-fold higher than with monomers (1.2 µM and 3 µM respectively) [97], [194]. In a similar way to PF74, BI-2 destabilises HIV-1 cores but increases the stability of *in vitro*-assembled CA complexes [108], [192], although its activity is less potent.

As expected, BI-2 also prevents binding of CPSF6 and NUP153 to the HIV capsid [97], [192]. In contrast to PF74, BI-2 does not affect the production of early or late RT products at any concentration [137], [194]. The need for a higher concentration to match the same level of restriction obtained with PF74 is a consequence of its weaker binding to CA. When their inhibition activities are normalised to their respective affinities, the block in infection is the same for PF74 and BI-2 [97].

1.4.2. Current methods to study capsid stability

Understanding the HIV-1 capsid disassembly process has been a challenging task. Several *in vivo* and *in vitro* approaches have been employed, but none of them can resolve different uncoating steps of individual capsids. The intrinsic instability of HIV capsids complicates its isolation to perform biochemical assays. Its genetic sensitivity obstructs experimental manipulation, such as the addition of fluorescent labels. Furthermore, the high variability and low infectivity rate hinders the understanding of genuine uncoating because it is hard to distinguish between particles that will lead to successful infection from impaired particles that will produce an abortive one. Despite all of these obstacles, several experimental approaches have been used to measure uncoating.

1.4.2.1. *In vitro* CA assemblies

The use of *in vitro* CA assemblies has been key to identify CA mutations that increase or decrease the CA lattice intrinsic stability, as well as to evaluate the influence of cellular factors, chemical compounds or macromolecular crowding on CA stability [100], [105]–[108], [147], [157], [192], [195], [196]. Two different assays are generally used, (1) and assay to measure the rate of CA multimerisation and (2) an assay to measure the stability of CA assemblies.

In vitro CA multimerisation assay

HIV CA spontaneously oligomerises in presence of high salt, causing changes in optical density [106]. The kinetics of CA multimerisation can be detected easily by measuring the sample absorbance. This assay allows testing the effect of proteins or compounds on the rate of formation of higher order CA multimers. Some examples of compounds tested with this method are PF74 [98] or E45A substitution [197].

Stability of *in vitro* assembled CA

Recombinant CA can be assembled *in vitro* to form tubes made of CA hexamers [106], [195]. Spheres or cone-shaped assemblies are also observed, and can be enriched by

introducing CA mutations that stabilise pentameric arrangements or when the CA protein is incubated with RNA [100], [106], [198]. Efficient formation of CA tubes requires high protein concentration and salt. Those requirements can be reduced when CA-NC protein is used [100], [195]. CA-NC tubes have been widely used to investigate the structure of the HIV-1 capsid [162], to detect direct binding of proteins to CA assemblies [176], and to study the effect of CA-binding proteins on lattice stability [108], [192]. Typically, assembled CA-NC complexes are incubated with the factor to be tested and then the sample is centrifuged through a sucrose cushion to separate assembled and soluble protein. The degree of CA-NC disassembly is determined by the amount of soluble and assembled protein compared to the input.

Even though the CA-NC tubes are a suitable model to study the viral capsid, they do not fully recapitulate the fullerene-shaped capsid structure. This became evident with the conflicting results obtained with PF74 and BI-2, where they were shown to stabilise CA-NC tubes but destabilise isolated viral cores.

1.4.2.2.   Isolated viral cores

Purification of viral cores has been used extensively over the past years. HIV-1 cores can be purified from virions to perform biochemical or genetic studies, or recovered from infected cells to measure the level of disassembly under different conditions (fate of capsid assay).

In vitro stability of isolated viral cores

To isolate viral cores, virions are subjected to ultracentrifugation through a sucrose density gradient containing a mild detergent layer to remove the viral membrane. As a result, intact cores and free CA are separated into different fractions, which can be detected by Western blot or ELISA [29], [104], [105]. Notably, only a low proportion of the input (~16 % of total CA) is recovered in the fraction corresponding to assembled cores.

The relative amounts of CA present as assembled cores and as soluble CA is used as a measure to assess the intrinsic stability of the viral cores under different conditions, for example to compare CA mutants or viral particles produced in cells with or without expression of a specific factor [105].

Furthermore, the isolated cores can be used to analyse the influence of capsid binders on their stability *in vitro*. To do so, purified capsids are incubated in the presence of the

molecule to be tested for various times, and then the sample is pelleted by ultracentrifugation. The amount of released CA (supernatant) from the large assemblies (pellet) is quantified to determine the extent of capsid disassembly [104], [105]. Isolated WT cores are usually stable at 4-25°C, showing only 20-30% disassembly in two hours. Incubation at 37°C induces disassembly at higher rates (20-50% in 30 min; 75% in two hours). Addition of proteins or small compounds can change the rate of disassembly.

Despite the important insights into capsid stability this approach has provided, it is considered a bulk assay that does not resolve the high heterogeneity of capsids observed in the viral population. In particular, the isolation method is likely to enrich for highly stable capsid architectures.

Fate of HIV capsid

The fate of capsid assay measures the stability of the HIV-1 capsid during infection. After virus entry, cells are lysed and the cytosolic fraction is layered onto a sucrose cushion for ultracentrifugation. Assembled CA present in the pellet and soluble CA in the supernatant is then detected by Western blot [116], [199]. The effect of cellular factors on capsid stability can be assessed by comparing the amount of CA in both fractions from cells that express or lack the desired protein. Like the previous approach, this assay measures the ensemble properties of cores.

1.4.2.3. CsA-washout

The cyclosporine A washout (CsA-washout) assay is based on the ability of the CA restriction factor TRIM-cyclophilin A (TRIM-CypA) to inhibit HIV-1 infection. Restriction is abolished with the addition of cyclosporine A (CsA), that binds to TRIM-CypA and competes with its binding to CA [118], [200], [201]. To monitor uncoating, cells expressing TRIM-CypA are infected with a GFP reporter virus in presence of CsA. In this condition, CsA is bound to TRIM-CypA preventing its inhibitory effect, so that capsids can disassemble normally and infection can proceed. CsA washout at different time points of infection will release TRIM-CypA, allowing it to bind to still intact cores and restrict infection, while cores that have already undergo uncoating are no longer susceptible to TRIM-CypA inhibition. Infectivity for each time point is determined by flow cytometry giving an estimate of the uncoating half-life [118], [201]. Unlike the previous assays, CsA-washout just measures the viruses that can successfully infect the cell, giving a more precise understanding of uncoating. However, the mechanism of TRIM-Cyp-mediated restriction is not completely clear, which is a weakness of the

method that needs to be considered when interpreting the results. TRIM-CypA restriction can be disturbed by the competition of other host factors present in the cell, giving some artefacts in the uncoating measurement.

1.4.2.4. Fluorescence imaging

The recent progress in live cell imaging thanks to the improvements in microscopy techniques as well as fluorescent probes, has allowed to visualisation HIV-1 uncoating at the level of individual viral particles within the spatial context of the cell. Several strategies have been used to fluorescently tag different components of the virion, as direct labelling of CA may have a detrimental impact on capsid stability or interactions.

Membrane staining is usually used to discriminate between virions that have been non-specifically endocytosed from those that have productively fused their membrane with the host cell [118], [202]. Fluorescent tagged Vpr and integrase have been utilised to indirectly detect uncoating as they remain associated with the viral RTC after capsid disassembly [55], [73], [118], [137], [203]. In a similar way, RNA detection has been used to determine capsid disassembly. Ma *et al.* labelled the viral RNA with a ($[Ru(phen)_2(dppz)]^{2+}$) complex during viral assembly to follow it during infection [204]. Xu *et al*. incorporated the modified nucleoside 5-ethynyl uridine (EU) that can be detected by ligation with an azide-containing fluorescent dye. However, the detection is done after fixation of the cell, limiting its use [131]. In a different approach, Da Silva Santos *et al*. used RNA translation as a reporter of capsid opening. In this approach, a packaging sequence derived from HIV-1 together with the firefly luciferase open reading frame (called EU-repRNA) is incorporated into HIV-1 virions. When the capsid structure is compromised, ribosomes have access to the viral RNA and can translate the luciferase sequence, which is detected via generation of luminescence. If the capsid is stabilised or destabilised, the level of luciferase produced will be altered accordingly [193]. This approach can be useful to assess proteins or molecules that can alter the capsid stability in general, but lacks the sensitivity to follow uncoating of individual virions.

Direct detection of CA has been attempted in diverse ways. Immunofluorescence labelling of CA has been very useful to detect the localisation of the viral capsid under different conditions. However, cells need to be fixed giving a limited information of the disassembly process [122], [137], [202]. Real-time imaging has been achieved by labelling CA with smalls tag, such as the tetracysteine (TC) tag. The TC tag is introduced within the CA protein and then is labelled with a fluorescent FlAsH or

ReAsH dyes, although a mix of WT CA and modified CA needs to be used to produce replication competent virions [132], [204]–[206]. CA has been also followed *in vivo* by the use of CypA fused to a tetrameric fluorescent protein (CypA-DsRed) that is incorporated in sub-stoichiometric amounts into budding virions. CypA-DsRed binds tightly and irreversibly to the capsid lattice, allowing its visualisation as it travels through the cytoplasm of the infected cell [135], [136]. Nevertheless, the binding of an oligomeric CypA to the capsid lattice might perturb its normal disassembly. As an alternative that avoids perturbing the intrinsic capsid stability, GFP has been used as a fluid phase marker. In this case, GFP is expressed as part of the Gag polyprotein between the MA and CA sequences flanked by proteolytic cleavage sites (Gag-iGFP) [207], [208]. The GFP molecules are released by proteolysis during maturation, where a fraction is incorporated inside the viral core [102], [209]. The Gag-iGFP viruses exhibit a slight attenuation in infection relative to WT, but infectivity can be recovered without reducing the GFP signal intensity excessively when it is co-expressed with the plasmid lacking the GFP sequence [208]. By using this approach, Mamede *et al.* observed that indeed a subset of the GFP gets trapped within the intact viral capsid, and determined a median capsid rupture of ~30 minutes in the context of productive infection [132].

1.5. Research proposal and aims

The development of new antiviral drugs that target HIV-1 capsid require a molecular understanding of how the virus regulates uncoating. It is generally accepted that HIV has evolved to exploit a network of host cofactors that interact with the capsid to regulate its stability. At the same time the cell has evolved restriction factors that recognise the CA lattice to block infection. However, only few host capsid-binders have been identified so far, and their precise roles in capsid stability are not well understood.

Most of the current methods to study HIV capsid stability, such as *in vitro* uncoating of isolated cores, the fate of capsid assay or CsA washout assay rely on observing the average behaviour of large numbers of viral cores, which obscures the observation of intermediates in the uncoating process. Fluorescence microscopy methods can resolve the uncoating of individual capsids in the cytoplasm, but complementary *in vitro* methods that allow high throughput measurements and detailed kinetic studies under defined conditions are still missing.

<u>Research Aim</u>

The overall aim of this thesis is to develop a single-particle fluorescence microscopy method to follow the real-time uncoating kinetics of authentic HIV capsids *in vitro* and to visualise the effects of host proteins and molecules on capsid stability. This imaging assay will allow us to follow the uncoating kinetics of hundreds of individual HIV capsids in a single experiment, resolving intermediates in the disassembly pathway that are otherwise averaged out in traditional assays. With this new method, we will study how host proteins and small molecules influence capsid disassembly. Furthermore, we will use this approach as a platform to study the kinetics of protein binding to authentic HIV capsids at the single-particle level. This thesis is divided into three results chapters followed by a general conclusion.

Chapter 3 describes the development of the single-particle fluorescence microscopy methods to follow the real-time uncoating kinetics of authentic HIV capsids *in vitro*. The assays utilise immobilised viral particles that are permeabilised on the coverslip using the pore-former protein perfringolysin O (PFO) and are designed to detect the following molecular processes:

- Capsid opening detection. The precise moment at which the capsid develops its first defect is detected by the release of a solution phase marker (GFP).

- Dynamic interactions of proteins with authentic cores. Permeabilised viral particles containing intact capsids are used as a platform to quantify the binding of labelled proteins or molecules at the single-particle level. As an example, the interaction of fluorescently labelled CypA with the capsid will be assessed.

- Visualisation of lattice disassembly. Labelled CypA is used to "paint" the CA lattice to determine the integrity of the capsid lattice over time.

The capsid opening and lattice disassembly assays will be used to study the intrinsic stability of capsids assembled from WT CA and CA E45A (a mutant known to yield hyperstable capsids), and to determine the effect of cell lysate on capsid stability.

The aim of **Chapter 4** is to study how molecules and proteins that bind to the interface formed between CA_{NTD}-CA_{CTD} of neighbouring subunits in the CA hexamer affect the stability of the capsid. Capsid opening and lattice disassembly kinetics will be measured in the presence of the known antiviral drugs PF74 and BI-2. Additionally, the host binding protein CPSF6 will be studied by using its minimal binding peptide ($CPSF6_p$) to determine its binding to the capsid. Binding competition with PF74 and effect on capsid uncoating will be also determined.

The aim of **Chapter 5** is to study how polyanionic molecules that bind to the highly positively charged pore formed by the ring of six arginines at the centre of the hexamer affect the stability of the capsid. Capsid opening and lattice disassembly kinetics will be measured in the presence of hexacarboxybenzene as well as the cytosolic compounds inositol hexakisphosphate (IP6) and ATP.

Chapter 6 will summarise the main conclusions and future directions for the research.

Chapter 2

Materials and Methods

2. Materials and Methods

2.1. HIV-1 viral particles

2.1.1. Culture of HEK-293T cell line

The adherent HEK-293T cell line was cultured in DMEM supplemented with 10% v/v fetal calf serum (DMEM, Gibco) in plastic tissue culture flasks (Corning), and maintained at 37°C with 5% CO_2 in a humidified environment. Cells were passaged when they approached 90% confluency by removing the culture medium, washing the monolayer with PBS and incubating with 1x trypsin-EDTA (Thermo Fisher Scientific) for 5 min at 37°C. Cells were then resuspended in new culture media and 20% of the total volume was re-seeded in a new flask.

2.1.2. Plasmid constructs

2.1.2.1. pNL4.3-iGFP-ΔEnv

The pNL4.3-iGFP-ΔEnv [207], [208] construct has the pNL4.3 HIV-1 provirus as backbone with two modifications which upon transfection will generate non-infectious viral particles loaded with the enhanced green fluorescent protein (eGFP). The alterations are:

- A stop codon was introduced at the start of the Env gene to block the expression of the envelope protein (gp160), preventing the docking and fusion of the virus with the target cell.

- The eGFP gene flanked by protease cleavage motifs was inserted between the coding sequences for MA and CA within the Gag open reading frame (ORF). In this way, monomeric eGFP molecules will be released inside the viral particle during the maturation process; this design has previously been referred to as internal GFP (iGFP).

The construct was generated by a member of Stuart Turville's group as described previously [208]. For propagation, a small aliquot from a glycerol master stock containing frozen Stbl2 Escherichia coli (Invitrogen) transformed with the plasmid was inoculated into 150 mL of LB media containing 100 µg/mL ampicillin for antibiotic selection. The culture was incubated overnight at 30°C to minimise recombination of the retrovirus sequence, and the plasmid DNA was extracted using a HiSpeed Plasmid Maxi Kit (QIAGEN) according to the manufacturer's instructions.

2.1.2.2.   pNL4.3-iGFP-E45A-ΔEnv

The CA E45A substitution was introduced to the pNL4.3-iGFP-ΔEnv by subcloning a fragment encoding that mutation from another plasmid using the Xba-SbfI restriction sites (**Figure 2.1**).
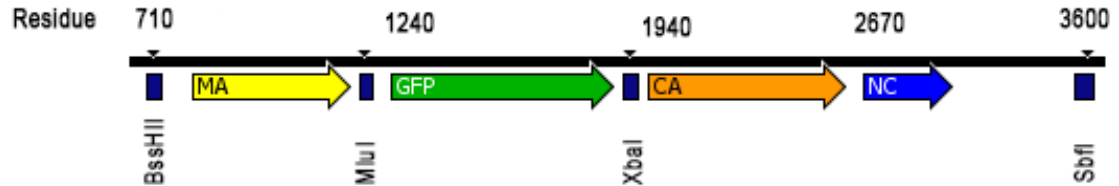
Figure 2.1. Gag region of the pNL4.3-iGFP-ΔEnv sequence map with restriction sites.

The ligation reaction mixture (pNL4.3-iGFP-E45A-ΔEnv) was transformed into MAX Efficiency Stbl2 Competent E. coli (Life Technologies) according to the manufacturer's instructions. Transformed bacteria were streaked on LB agar plates containing 100 µg/mL ampicillin for antibiotic selection and incubated overnight at 30°C. Individual colonies were inoculated in 5 mL of LB media with antibiotic selection, grown over night at 30°C and DNA was extracted using a miniprep kit (QIAPREP) following the manufacturer's instructions. A clone containing the desired mutation was identified by DNA sequencing (Ramaciotti Centre for Genomics facility, UNSW Sydney, Australia) using the primers P5 (5'-GGAGCCACCCCACAAGATTTAAATACCATG-3') and P6 (5'-TATCCACGCTTTATAGATGGCTCCTACTGG-3'). The plasmid pNL4.3-iGFP-E45A-ΔEnv was then propagated as detailed above (**see 2.1.2.1**)

2.1.2.3.   psPAX2

The second-generation lentiviral packaging plasmid psPAX2 (Cat# 11348, from Didier Trono) encoding the Gag, Pol, Rev, and Tat genes was obtained through the NIH AIDS Reagent Program, Division of AIDS, NIAID, NIH. The plasmid was propagated as described above (**see 2.1.2.1**)

2.1.3. Production of HIV-1 viral particles

HIV-1 viral particles used in this thesis were generated by transfecting HEK-293T cells using polyethylenimine (PEI Max) reagent (Polysciences, 9002-98-6) with the plasmid combinations shown in **Table 1**.

Table 1. Plasmid combination used to generate WT and CA E45A HIV-1 viral particles.

Viral particle name	Plasmid 1	Plasmid 2
WT Viral particles	pNL4.3-iGFP-ΔEnv (6.6 µg)	psPAX2 (3.3 µg)
CA E45A Viral particles	pNL4.3-iGFP-E45A-ΔEnv (10 µg)	n/a

The DNA solution for transfection was prepared by mixing 10 µg of the corresponding plasmids with 60 µl of 1 mg/mL PEI max solution in a final volume of 500 µl of 0.9% w/v sodium chloride (Sigma-Aldrich). The mixture was incubated for 30 min at room temperature to allow formation of DNA-PEI complexes and then added to a suspension of 7×10^6 HEK-293T cells in 1 mL of culture media. After 5 minutes, the mixture was homogeneously added drop by drop to a 10 cm^2 culture dish (BD Biosciences) containing 6.5 mL of culture media, and incubated at 37°C with 5% CO_2. The virus-containing supernatant was collected 48 h post transfection and centrifuged (2100 x g, 10 min, 4°C) to remove cellular debris.

2.1.4. Biotinylation of HIV-1 viral particles

To allow immobilization of the viral particles on the coverslip surface for imaging, the viral membrane proteins were biotinylated with EZ-LinkTM Sulfo-NHS-LC-LC-Biotin (Thermo Scientific, 21338). 1 mg of biotinylation reagent was added to 7 mL of virus-containing medium and the mixture was incubated for at least 90 minutes at 4°C with rotation.

2.1.5. Purification of HIV-1 viral particles by size exclusion

Biotinylated viral particles were then separated from proteins contained in the culture medium and from free biotin by size exclusion chromatography using a HiPrep 16/60 Sephacryl S-500 HR column (GE Healthcare). The column was washed with 2 column volumes (CV) of de-gassed distilled water to replace the storage solution (20% ethanol) and then equilibrated with 2 CV of HBS pH 7.5 (50 mM HEPES, 100 mM NaCl). The sample containing biotinylated viral particles was loaded onto the column using a 50-mL loop and 1 mL fractions were collected until a total of 1.5 CV was reached. The elution of viral particles and other components was monitored by absorption at 280 nm and the fractions containing viral particles were collected (corresponding to the first peak (void) eluting from the column), combined stored at 4°C for use within 7 days.

2.2.   Perfringolysin O (PFO)

Recombinant cysteine-less (C459A) N-terminal His-tagged Perfringolysin O (PFO) was generously supplied by Sara Lawrence and Michael Parker (University of Melbourne). The protein stock solution (3 mg/mL [54 µM] in 20 mM Tris pH 8, 20 mM NaCl) was stored in aliquots at -80°C. When required, an aliquot was thawed by submerging it in a water bath at 37°C for 10 seconds followed by a short spin in a table top centrifuge. Once thawed, protein was kept at room temperature for use within several weeks.

2.3.   Small Molecules

Small molecules binders were obtained from different sources:

- PF74 (PF-3450074, SML0835, Sigma Aldrich) was dissolved at a concentration of 10 mM in DMSO (Invitrogen), stored in aliquots at -80°C. Once thawed, the aliquot was kept at room temperature for use within several weeks. PF74 was used at final concentrations of 0.1-10 µM in HBS pH 7.

- BI-2 (Z1982491200, Enamine) was dissolved in DMSO at a concentration of 10 mM, and stored in aliquots at -80°C. Once thawed, the aliquot was kept at room temperature for use within several weeks. BI-2 was used at a final concentration of 50 µM in HBS pH 7.

- IP6 (Inositol hexaphosphate, P8810-10G, Sigma Aldrich) was dissolved in 50 mM HEPES buffer pH 7 at a concentration of 10 mM. The stock solution was stored at 4°C. IP6 was used at final concentrations of 1-100 µM in HBS pH 7.

- Hexacarboxybenzene (Mellitic acid, M2705-1G, Sigma Aldrich) was dissolved at a concentration of 200 mM in 50 mM HEPES buffer pH 7. The stock solution was stored at 4°C. Hexacarboxybenzene was used at final concentrations of 10-1000 µM in HBS pH 7.

- ATP was dissolved at a concentration of 100 mM in distilled water, adjusted to pH 6.5, stored in aliquots at -40°C. The solution was thawed on the day of use and the remainder was discarded. ATP was used at a final concentration of 1000 µM in HBS pH 7.

- Cyclosporine A (CsA) (#9973, Cell Signaling Technology) was dissolved in 100% ethanol to a concentration of 50 mM and stored at -40°C. CsA was used at final concentration of 10 µM in HBS pH 7.

2.4. Cyclophilin A protein

Recombinant cyclophilin A (CypA) used in this thesis was purified by Vaibhav Shah and Derrick Lau, and labelling with fluorescent probes was carried by Derrick Lau and Amir Mousapasandi.

2.4.1. Expression and purification of CypA

Human CypA was expressed using a pET expression vector in BL21 (DE3) *E. coli* cells were grown in LB medium at 37°C. Protein expression was induced for 3 hours by addition of isopropyl β-D-thiogalactopyranoside (IPTG) to a final concentration of 1 mM. Bacterial cells were collected by centrifugation, resuspended in cold (4°C) lysis buffer (25 mM HEPES, pH 7.6, 1 mM DTT, 0.02% NaN3, supplemented with "Complete" protease inhibitor and 1 mg/mL lysozyme) and lysed by sonication on ice. The lysate was clarified by centrifugation (29000 x g, 30 min, 4°C) and the supernatant was passed through a syringe filter (0.22 µm) and further purified by subtractive anion exchange chromatography using a 10 mL HiTrap Q HP column (GE Healthcare Life Science, 17-1154-01) equilibrated with a buffer containing 25 mM HEPES, pH 7.6, 1 mM DTT, 0.02% NaN3. CypA fractions (eluted in the flowthrough) were collected and adjusted to a pH of 5.8 with 1% v/v acetic acid. Aggregates were removed by centrifugation (29000 x g, 1 h, 4 °C) and the supernatant containing the soluble proteins was applied to a cation exchange chromatography column (5 mL HiTrap SP HP, GE Healthcare Life Science, 17115201) equilibrated with a buffer containing 25 mM sodium phosphate pH 5.8, 1 mM DTT and 0.02% NaN3 for further purification. CypA was eluted with a NaCl linear gradient (0 to 1 M) over 20 CV. Fractions containing purified CypA were dialysed against CypA storage buffer (25 mM MOPS, pH 6.6, 1 mM DTT, 0.02% NaN3), concentrated using an Amicon-15 Ultra centrifugal filtration device (10k MWCO, Merck, UFC901024) to a final concentration of 300 µM, aliquoted and frozen in liquid nitrogen for storage at -80 °C. The yield was approximately 3 mg/g of cell mass.

2.4.2. Labelling of CypA

Purified CypA was labelled with Alexa-Fluor 568-C5-maleimide (Thermo Fisher Scientific, A10254) at the Cys-51 residue. The reaction was carried out using a 4-fold molar excess of dye in PBS (pH 7.4, 0.1 mM TCEP) for 10 minutes at room

temperature, followed by quenching of the unconjugated dye by addition of 1 M DTT to a final concentration of 17 mM. Removal of unconjugated dye was achieved using Zeba desalting spin columns (Thermo Fisher Scientific, 89883) equilibrated with AF568-CypA storage buffer (50 mM Tris, pH 7.9, 20% v/v glycerol, 1 mM DTT). Labelled AF568-CypA was aliquoted, frozen in liquid nitrogen and stored at -40°C.

2.5. CPSF6 peptide and labelling

The peptides $CPSF6_{313-327}$ ($CPSF6_p$, PVLFPGQPFGQPPLG) and $CPSF6_{313-327}$ with an extra cysteine at the C-terminal ($CPSF6_p$-Cys) were synthetized by GenScript. Peptides were dissolved in water at a concentration of 2.5 mM, aliquoted and stored at -40°C.

$CPSF6_p$-Cys was labelled with Alexa-Fluor 568-C5-maleimide (A10254, Thermo Fisher Scientific) using an equimolar ratio in HEPES buffer pH 8. Labelling was verified by thin layer chromatography (TLC). No conjugated dye was observed on TLC. $CPSF6_p$-Cys-AF568 solution was aliquoted and stored at -40°C.

2.6. HeLa cell lysate

HeLa cell lysate was prepared by Derrick Lau as follows: HeLa cells were washed with PBS, resuspended in lysis buffer (10 mM Tris-HCl pH 8, 10 mM KCl, 1.5 mM MgCl2, protease inhibitor and phosphatase inhibitor), and incubated for 15 minutes at 4°C. Lysis was achieved by passing the cell suspension through a 30.5 g needle (130 strokes with cooling the sample on ice for 2 minutes at every 10th stroke). Cell lysis was verified by staining a sample of the lysate with trypan blue (added to a final concentration 0.2% w/v). The lysate was centrifuged (18000 x g, 30 min, 4°C) to remove cell debris and protein levels in the supernatant were estimated from the absorbance at 280 nm. Lysate was frozen in liquid nitrogen and stored at -40°C.

2.7. TIRFM

2.7.1. Microscope set up

Images were collected on a TIRF microscope built by Philip Nicovich and James Walsh based on an ASI-RAMM frame (Applied Scientific Instrumentation) with a Nikon 100× CFI Apochromat TIRF (1.49 NA) oil immersion objective. Lasers were incorporated using the NicoLase system [210]. Images were captured on two Andor iXon 888 EMCCD cameras (Andor Technology Ltd) and 300 mm tube lenses were used to give a field of view of 88.68 μm × 88.68 μm.

2.7.2. Microfluidic flow cells set up

Poly-dimethylsiloxane (PDMS) microfluidic devices were prepared by standard protocols for soft lithography using the Sylgard184 silicone elastomer kit (Dow Corning).

Two different master moulds were used for fabrication of microfluidic flow cells depending on the experiment performed (**Figure 2.2**). For core opening and binding experiments, the device contained five straight channels of 0.8 mm width, 0.06 mm height, and 10 mm length (**Figure 2.2A**). For dissociation experiments requiring rapid solution exchange, the channel design contained one inlet and two outlets (**Figure 2.2B**). In this design images were acquired in the part of the main channel behind the restriction (0.2 mm wide section). Solutions were pre-loaded into the part of the channel in front of the restriction by passing it through the side outlet, and then drawn through the main channel by passing it through the outlet at the end of the main channel.
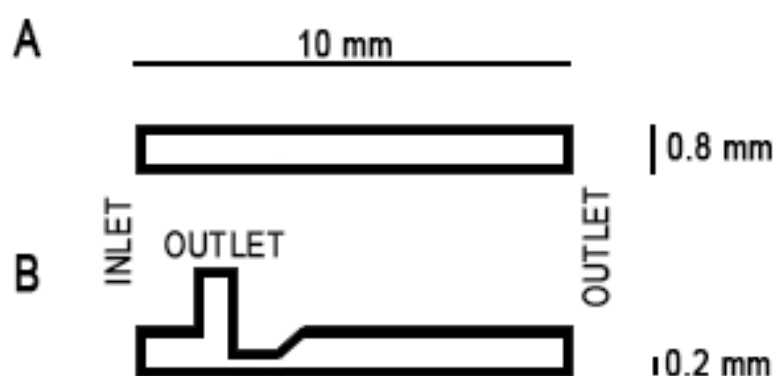
Figure 2.2. Schematic representation of the microfluidic channels. Two different channels were used for imaging. Capsid opening and protein binding was done by using channel shown in (**A**) while dissociation kinetics experiments were done using channel shown in (**B**).

The transparent polymer mixture (elastomer/curing agent ratio 10:1 w/v) was poured onto the master, degassed in a vacuum desiccator for 20 min and allowed to cure at 70°C overnight. Cured PDMS devices were then removed from the mould and holes for inlets and outlets were created with a Harris Uni-Core 1.0 mm punch. The device was then cleaned by immersion in water, isopropyl alcohol (100%) and water (10 min each step).

Round glass coverslips (25 mm diameter, Karl Hecht GmbH&Co KG) were cleaned by sonication in absolute ethanol for 30 minutes followed by sonication in 1 M NaOH for 30 min, and finally rinsed 3 times with ultrapure water and dried.

PDMS devices and coverslips were exposed to plasma inside a plasma cleaner for 3 min (PDC-32G, Harrick Plasma). The PDMS device was then immediately mounted on the coverslip. Assembled microfluidic flow cells were heated in an oven at 70°C for at least 15 minutes to improve bonding between the glass and the PDMS.

2.7.3. Capture of viral particles onto the flow cell surface

To allow specific binding of the viral particles inside the flow cell and prevent nonspecific adsorption of proteins or other molecules, the glass surface was modified with a PLL-g-PEG-biotin monolayer followed by a layer of streptavidin for capture of the biotinylated viral particles.

The assembled microfluidic device was mounted in a magnetic chamber (Chamlide chamber, Live Cell Instrument) and 1 mg/mL solution of biotin-poly-L-lysine-g-poly-ethylene glycol (PLL-g-PEG-biotin, PLL(20)-g[3.5]-PEG(2)/PEG(3.4)-biotin(20%) , SuSoS AG) was injected into the flow channels with a micropipette for 30 minutes incubation at room temperature. Inlet and outlet tubing were connected to the PDMS device. The channels were rinsed by drawing water through the tubing with a syringe and dried by drawing air through the tubing. The channels were then incubated for 15 minutes with a solution of 0.2 mg/mL streptavidin (SNN1001, Life Technologies Australia) in blocking buffer (20 mM Tris pH 7.5, 2 mM EDTA, 50 mM NaCl, 0.03% NaN3, 0.025% Tween 20, 0.2 mg/mL BSA) and rinsed with HBS pH 7.5. The microfluidic device was mounted on the microscope stage and a syringe pump was connected to the outlet tubing. The syringe pump was operated in "withdraw" mode to pull solutions through the channels. Biotinylated viral particles in HBS pH 7.5 were flowed through the channel at a flow rate of 25 µL/min until a density of ~1000 viral particles per field of view was obtained (typically 30-100 µL). Unbound viral particles were washed out with 50-100 µL of HBS pH 7.5 at a rate of 65 µL/min.

2.7.4. Core opening assay

Core opening assays were performed by injection of 30 µL of HBS pH 7 containing PFO (200 nM) and the protein or molecules to be tested, at a flow rate of 65 µL/min.

TIRF images were acquired with excitation from a 488 nm laser with 20 ms exposure time and ~200 nm penetration depth. For "short" experiments, two different acquisition regimes were used to image over 30 minutes: (1) 900 frames were acquired with a frequency of 1 frame per second for the first 800 frames and then 100 frames at 1 frame every 10 seconds; (2) 600 frames were imaged with a frequency of 1 frame every 3 seconds. For "long" experiments, a total of 880 frames were acquired with a frequency of 1 frame every 6 seconds, for a total acquisition time of 88 minutes.

2.7.5. Lattice disassembly assay

Lattice disassembly assays were carried out with HBS pH 7 containing an oxygen quenching system (2 mM trolox, 2.5 mM protocatechuic acid (PCA) and 0.25 U/mL protocatechuate-3,4-dioxygenase (PCD)) to reduce photobleaching during the dual colour experiments.

To initiate the assay, HBS (30 µl) containing 200 nM PFO, 1 µM AF568-CypA and the molecule to be tested was injected into the flow channel. TIRF images were acquired sequentially with 488 nm and 561 nm lasers (20 ms exposure time each, ~200 nm penetration depth). Most of the experiments were obtained with a frequency of 1 frame/s for a total of 800 frames (13.3 min). Long lattice disassembly assays were imaged for a total of 880 frames with a frequency of 1 frame every 6 seconds, for a total time of 88 minutes.

2.7.6. CA binder-capsid interaction assay

Binding of fluorescent CA-binding molecules to the capsid was imaged using sequential acquisition (488 nm and 561 nm lasers, 20 ms exposure time each, 1 frame/s) after flowing \HBS pH 7 (30 µl) supplemented with the PCA/PCD oxygen quenching system and containing PFO (200 nM) and different concentrations of AF568-CypA (0.1 - 20 µM) or $CPSF6_p$-Cys-AF568 (0.1 - 50 µM) into the flow channel. Binding experiments with concentrations above 1 µM were carried out with a mixture of unlabelled and labelled binder, whereby the concentration of the labelled molecule was kept at 1 µM.

Dissociation experiments were carried out by exchanging the solution using the rapid exchange solution PDMS device. 100 µl of imaging buffer was injected at a rate of 60 µl/min while images were acquired using excitation with the 561 nm laser (20 ms exposure time, 5 frame/s).

2.7.7. Single Molecule Photobleaching

Single molecule photobleaching was carried out for every repetition of the lattice disassembly and/or CA binder-capsid interaction assay.

A clean coverslip (previously described in section 2.8.2) was mounted in a magnetic chamber and passivated by incubation with 0.02 mg/mL BSA for 2 minutes followed by washing with HBS. A solution of 10 nM of AF568-CypA or CPSF6$_p$-Cys-AF568 in HBS pH 7 was added to the coverslip and incubated in the dark at room temperature for 3 to 5 min. Unbound molecules were removed by washing with HBS and the sample was mounted on the microscope stage for imaging. Usually, four different field of views were acquired with a 561 nm laser with exposure times of 200 and 400 ms until most of the single molecules were photobleached (~150 frames).

2.7.8. Image analysis

Images were analysed with a software written in MATLAB (The MathWorks, Inc.) adapted from previous work [211].

First, images in the time series were aligned by cross-correlation to the first frame to correct for x/y-drift. Then, GFP-loaded viral particles, which appear as diffraction limited objects, were detected as local maxima in the first frame and their positions determined by Gaussian fitting. Overlapping particles were excluded from analysis. Next, fluorescence traces were calculated by integrating the fluorescence intensity in a 7×7 pixel region for each channel. The fluorescence intensity for each object was corrected for background fluorescence determined from pixels in the vicinity of the object. Fluorescence traces were then fitted with step traces to identify the presence and time of steps corresponding to permeabilisation and capsid opening. Traces were sorted into five classes on the basis of the following criteria: (1) loss of entire GFP signal in one step; (2) loss of GFP intensity in one large (permeabilisation) and one small (capsid opening) step; (3) loss of the majority of the GFP signal in one step with residual GFP signal persisting for the rest of the experiment; (4) no permeabilisation; (5) uninterpretable traces. Pre-assignment to classes was done automatically but all traces were verified by visual inspection and re-assigned if necessary. Traces with very low GFP levels were excluded from analysis.

For the core opening assay, capsid opening times were calculated for traces in class 2 as the time difference between permeabilisation and capsid opening. Capsid opening times were plotted as a survival curve of intact cores and capsid opening half-life was

estimated by fitting of the survival curve with a bi-exponential decay function, whereby the reported half-life corresponds to that of the majority of capsids.

For CA binder-capsid interaction assays, AF568-CypA or CPSF6$_p$-Cys-AF568 binding traces from classes 2 and 3 were aligned at the time of membrane permeabilisation and plotted as a heatmap. For each concentration, the median binding trace was calculated and the number of bound fluorescent molecules at equilibrium was determined from the ratio of the binder fluorescence intensity associated with the capsid to the fluorescence intensity of a single fluorescent binder molecule obtained from single molecule photobleaching experiments. Dissociation constant (K_D) was obtained by fitting the median number of bound molecules at equilibrium as a function of the molecule concentration with the following equation: $N(eq) = [binder] \times N(max) / ([binder] + K_D)$, where $N(eq)$ is the number of molecules bound at equilibrium for a given binder concentration, $[binder]$ is the concentration of the binder, $N(max)$ is the number of molecules bound at saturation and K_D is the dissociation constant.

For lattice disassembly assays, median disassembly kinetics were obtained. Individual binding traces from class 1 were aligned at the time of membrane permeabilisation while traces from class 3 were aligned at the time of core opening.

Chapter 3

Kinetics of HIV-1 capsid uncoating revealed by single-molecule analysis

3. Kinetics of HIV-1 capsid uncoating revealed by single-molecule analysis

3.1. Introduction

The HIV capsid has emerged as an attractive therapeutic target due to its multiple roles in the replication cycle and its genetic fragility. To develop capsid-targeting antiviral compounds, it is necessary to (1) understand how uncoating is regulated, including the precise role of host factors in capsid disassembly and their interaction dynamics, and (2) have a high throughput method with which the effect of different molecules on capsid stability can be determined.

To contribute in this matter, in this chapter we describe a new single-particle fluorescence microscopy method to follow in real-time the uncoating of authentic HIV capsids *in vitro*. The assay enables us to measure the two processes involved in capsid uncoating, (1) the opening of the first defect in the capsid sand (2) the disassembly of the lattice thereafter. Furthermore, we can utilise this assay to study how different molecules and proteins modulate these two phases of uncoating and the dynamic interactions of them with the viral capsid.

The content of this chapter was published in the following peer-reviewed journal:

The paper includes the following work undertaken as part of this PhD thesis:
1. Development of the imaging assay
2. Description of the uncoating kinetics of WT CA viral particles.
3. Effects of capsid-binding factors (CypA, BI-2, PF74, and hexacarboxybenzene) or of cell lysate on capsid opening and lattice disassembly.
4. Effect of the CA E45A mutation on capsid opening. The effect of the CA E45A substitution on the kinetics of lattice disassembly is included in section 8.1 of this thesis as additional information to the paper.

Kinetics of HIV-1 capsid uncoating revealed by single-molecule analysis

Chantal L Márquez[1,2], Derrick Lau[1,2], James Walsh[1,2], Vaibhav Shah[1,2], Conall McGuinness[1,2], Andrew Wong[3], Anupriya Aggarwal[3], Michael W Parker[4,5], David A Jacques[1], Stuart Turville[3], Till Böcking[1,2]*

[1]EMBL Australia Node in Single Molecule Science, School of Medical Sciences, UNSW, Sydney, Australia; [2]ARC Centre of Excellence in Advanced Molecular Imaging, UNSW, Sydney, Australia; [3]The Kirby Institute, Sydney, Australia; [4]Australian Cancer Research Foundation Rational Drug Discovery Centre, St. Vincent's Institute of Medical Research, Melbourne, Australia; [5]Department of Biochemistry and Molecular Biology, Bio21 Molecular Science and Biotechnology Institute, University of Melbourne, Melbourne, Australia

Abstract Uncoating of the metastable HIV-1 capsid is a tightly regulated disassembly process required for release of the viral cDNA prior to nuclear import. To understand the intrinsic capsid disassembly pathway and how it can be modulated, we have developed a single-particle fluorescence microscopy method to follow the real-time uncoating kinetics of authentic HIV capsids in vitro immediately after permeabilizing the viral membrane. Opening of the first defect in the lattice is the rate-limiting step of uncoating, which is followed by rapid, catastrophic collapse. The capsid-binding inhibitor PF74 accelerates capsid opening but stabilizes the remaining lattice. In contrast, binding of a polyanion to a conserved arginine cluster in the lattice strongly delays initiation of uncoating but does not prevent subsequent lattice disassembly. Our observations suggest that different stages of uncoating can be controlled independently with the interplay between different capsid-binding regulators likely to determine the overall uncoating kinetics.
DOI: https://doi.org/10.7554/eLife.34772.001

*For correspondence:
till.boecking@unsw.edu.au

Introduction

HIV is an enveloped virus that carries its RNA genome and associated viral proteins within a protein shell called the capsid (*Welker et al., 2000*). Upon engagement of CD4 and the chemokine receptor CCR5 or CXCR4, the viral membrane fuses with the plasma membrane of the host, depositing the viral core (defined here as the capsid and its contents) in the cytoplasm (*Blumenthal et al., 2012*). In order to establish infection, the virus must reverse transcribe its single stranded RNA genome into double stranded DNA, traverse the cytoplasm and cross the nuclear membrane, after which it integrates into the host chromosome (*Bukrinsky, 2004*). We now know that the capsid plays a key role in these processes and is critical for successful infection. It not only acts as a shield to protect the viral genomic material from pattern recognition and degradation (*Lahaye et al., 2013*; *Rasaiyaah et al., 2013*), but is also thought to facilitate reverse transcription (*Jacques et al., 2016*), engage with the nuclear pore complex (*Burdick et al., 2017*; *Dharan et al., 2016*; *Matreyek et al., 2013*), and direct integration site targeting (*Ocwieja et al., 2011*; *Schaller et al., 2011*; *Sowd et al., 2016*). In order to achieve many of these proposed functions, the capsid must interact with host proteins and small metabolites, as well as disassemble to release the viral DNA at the appropriate place and time (*Campbell and Hope, 2015*). The nature of this 'uncoating' process and how it is influenced by host co-factors remains a key unanswered question in HIV biology.

eLife digest Viruses need to enter their host's cells in order to replicate their genetic material and produce more copies of the virus. A protein shell called a capsid protects the virus during this journey. But the structure of the capsid presents a mystery. How can this protein shell be strong enough to remain intact as it enters a host cell, and yet quickly open up to release the viral genome after replication?

Unlike the capsids of many other viruses, those of HIV have irregular structures that rapidly fall apart once removed from the virus. This has thwarted attempts to study intact HIV capsids in order to understand how they work. However, we do know that HIV hijacks a range of molecules produced by the invaded host cell. Dissecting their effects on the capsid is key to understanding how the capsid disassembles.

Márquez et al. have now developed a method that can visualize individual HIV capsids – and how they disassemble – in real time using single-molecule microscopy. This revealed that capsids differ widely in their stability. The shell remains closed for a variable period of time and then collapses catastrophically as soon as it loses its first subunit.

Using the new technique, Márquez et al. also found that a small molecule drug called PF74 causes the capsid to crack open rapidly, but the remaining shell is then stabilized against further disassembly. These observations reconcile seemingly contradictory observations made by different research groups about how this drug affects the stability of the capsid.

The method developed by Márquez et al. enables researchers to measure how molecules produced by host cells interact with the viral capsid, a structure that is fundamental for the virus to establish an infection. It could also be used to test the effects of antiviral drugs that have been designed to target the capsid. The new technique has already been instrumental in related research by Mallery et al., which identifies a molecule found in host cells that stabilizes the capsid of HIV.
DOI: https://doi.org/10.7554/eLife.34772.002

The HIV capsid comprises 1000–1500 copies of a single viral protein, CA, corresponding to less than half of the total CA released by proteolytic processing of the Gag polyprotein during maturation (*Briggs et al., 2004*). CA is a two-domain protein, which can form both hexameric and pentameric assemblies. The conical capsid is a fullerene structure, which incorporates 12 pentamers into the otherwise hexameric lattice, a geometric constraint that must be satisfied in order to achieve capsid closure (*Li et al., 2000*; *Pornillos et al., 2011*). However, there is no such constraint on the number of hexamers nor the positions of pentamers and, as such, HIV capsids are polymorphic. Typically, capsids have a conical shape with an average length of 119 nm and an average width of 61 nm (*Briggs et al., 2003*). In addition, a large fraction of viral particles contain 'defective' capsids, which do not have closed surfaces (*Frank et al., 2015*; *Mattei et al., 2016*; *Yu et al., 2013*). This high degree of polymorphism and poor fidelity of assembly mean that the HIV capsid is a technically challenging entity to study, especially when compared to the more regular icosahedral viruses, many of which can even be crystallized.

Current biochemical methods used to study HIV capsid stability include an in vitro uncoating assay for the release of CA from isolated capsids (*Ambrose and Aiken, 2014*; *Shah and Aiken, 2011*), the fate of capsid assay (*Stremlau et al., 2006*; *Yang et al., 2014*) and the cyclosporin A washout assay (*Hulme et al., 2011*). These assays measure uncoating in bulk, that is rely on observing the average behavior of large numbers of viral cores. Fluorescence microscopy methods that track the uncoating process in fixed or live cells (*Francis et al., 2016*; *Mamede et al., 2017*) can resolve steps in the uncoating process of individual capsids in the cytoplasm but complementary in vitro methods that allow high throughput measurements and detailed kinetic studies under defined conditions are still missing.

Here we describe an in vitro single-molecule fluorescence imaging assay that allows us to follow the uncoating kinetics of hundreds of individual HIV capsids in a single experiment. This type of single-molecule analysis has the advantage that it can resolve intermediates in the disassembly pathway that are otherwise averaged out in traditional ensemble assays. By observing the properties of many individual capsids, it is possible to classify them according to their uncoating behaviors. This versatile

58

method enables 'bottom-up' approaches to determine the effect of individual host molecules and drugs and is also compatible with 'top-down' studies in which the influence of whole-cell lysates can be observed. Using this method, we are able to classify virions into three categories based on their uncoating behavior. We have also been able to define two discrete uncoating events that we term 'capsid opening' and 'lattice disassembly' and show that known cofactors and drugs have different effects on these two processes. This observation has allowed us to resolve the ambiguity as to what is meant by 'uncoating' and how it can be influenced by external factors.

Results

Single-particle fluorescence imaging of capsid opening

Fusion of the viral particle with the plasma membrane marks the point in time when the viral core is first exposed to the cytoplasm, but the effects of cellular proteins and small molecules on the stability of the capsid lattice are largely unknown. Here, we designed a fluorescence imaging assay to pinpoint the time of capsid opening at the single-particle level after exposing capsids to biochemically different environments in vitro. We produced viral particles containing GFP as a solution phase marker using a proviral construct with Gag-internal GFP (*Figure 1A*) (*Aggarwal et al., 2012*; *Hübner et al., 2007*). GFP is expressed as part of the Gag polyprotein and released by proteolysis during maturation, whereby a fraction of GFP molecules are compartmentalized within the viral capsid, with the remainder enclosed outside the viral capsid but within the viral membrane (*Mamede et al., 2017*; *Yu et al., 2013*). As a control we also used constructs containing a mutation in the late domain of Gag that leads to a block in the abscission of viral particles from the producer cell. The number of GFP-positive particles in the cell supernatant decreased by 99.7% when viral release was blocked (*Figure 1B*), confirming that essentially all GFP-positive particles released in the absence of the block represent viral particles. The fluorescent viral particles were biotinylated, purified by gel filtration and captured via streptavidin onto the surface of a coverslip modified with an inert polymer layer that prevents non-specific adsorption of viral particles and proteins (*Figure 1B*). Using microfluidics, we then delivered a solution containing the bacterial pore-forming protein perfringolysin O (PFO). PFO efficiently permeabilized the viral membrane by assembling into characteristic ring-shaped membrane pores with a mean pore diameter of about 35 nm (*Figure 1D and E*), consistent with its activity on cholesterol-containing membranes (*Dang et al., 2005*). These pores are sufficiently large to permit the passage of proteins while the viral core is retained within the perforated viral membrane allowing the core to be observed over time while it can undergo disassembly.

In our assay, we detected viral membrane permeabilization and capsid opening using time-lapse total internal reflection fluorescence (TIRF) microscopy to monitor the release of GFP molecules trapped in these compartments. GFP-loaded viral particles captured onto the coverslip appeared as bright diffraction-limited spots in the fluorescence image (*Figure 1F*), whereby a typical field of view contained several hundred to a thousand particles with a broad distribution of GFP intensities (*Figure 1G*). We extracted GFP intensity traces for each particle by summing the total fluorescence intensity above background of the diffraction limited spot in each frame of the TIRF movie (see *Figure 1H* for selected traces and for snapshots of the corresponding particles over time). A common feature of the vast majority of traces was a large drop in the GFP signal that occurred from one frame to the next at a variable time point after addition of PFO to the flow channel. We attributed this sudden drop in signal to the release of the pool of GFP molecules enclosed by the viral membrane as a result of PFO-mediated permeabilization. This process was not synchronized and typically occurred at random times for individual particles over a period of several minutes, as expected for the stochastic process underlying assembly of PFO into membrane pores. The precise time of permeabilization could, nevertheless, be determined from the large drop in the GFP fluorescence intensity traces (indicated by 'P' in *Figure 1H*) obtained by single-particle analysis.

Tracking of the residual GFP signal after permeabilization then permitted us to distinguish between three different classes of particles with 'leaky', 'opening' or 'closed' capsids. The majority of traces was characterized by a complete loss of GFP fluorescence upon membrane permeabilization (*Figure 1H*, left panel, see also *Figure 2A*). These particles were classified as containing leaky capsids with a defective and/or unstable CA lattice that did not retain the pool of GFP inside the

59
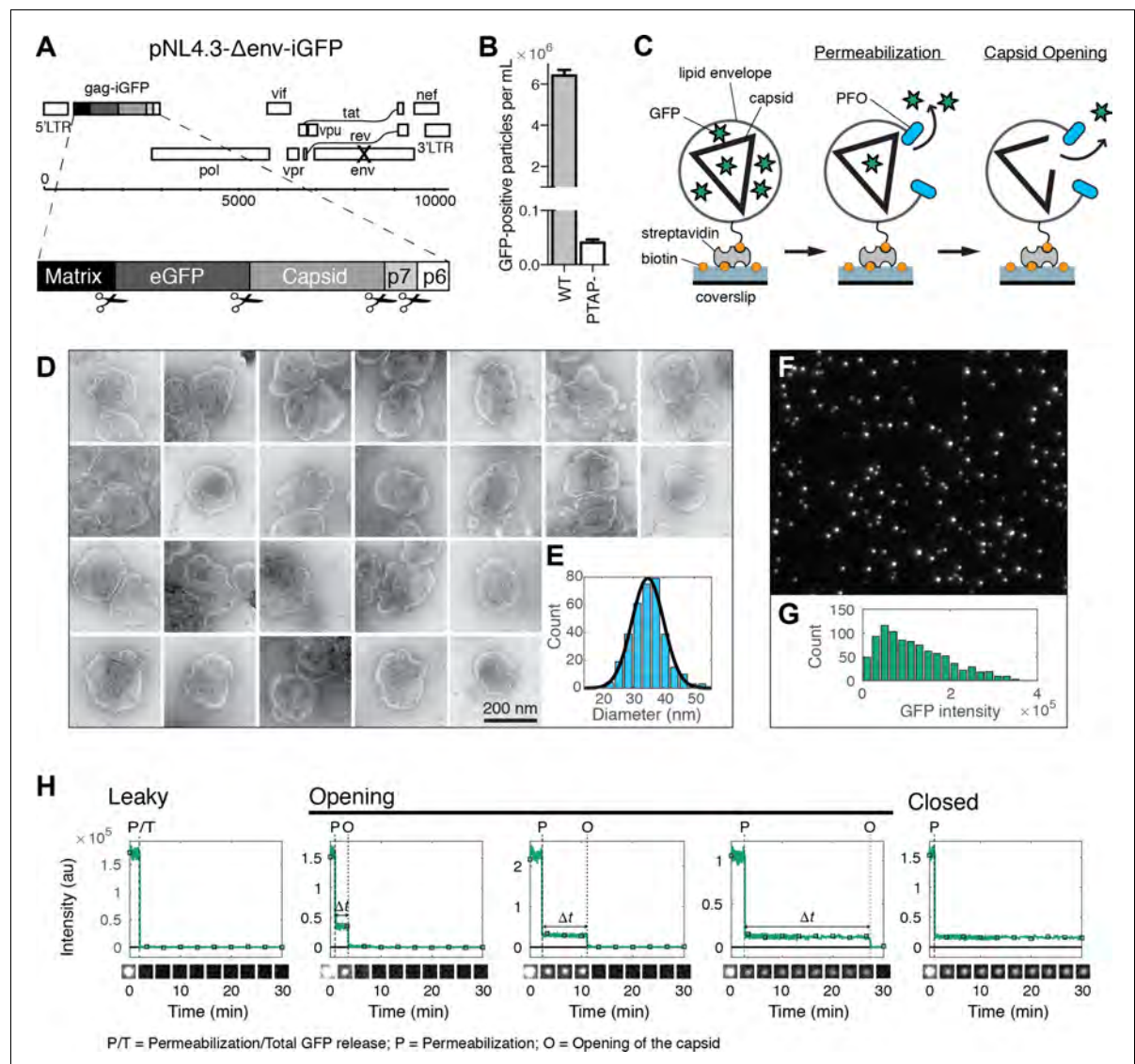
Figure 1. HIV capsid opening assay. (**A**) Map of the proviral DNA contained in the vector pNL4.3-iGFP-ΔEnv. Viral particles with Gag-internal GFP (released as a solution phase marker by proteolysis during maturation) were generated by transfection of HEK293T cells with pNL4.3-iGFP-ΔEnv and psPAX2 in a molar ratio of 1.4:1. (**B**) GFP-positive particles released from HEK293T cells transfected with either wild type or PTAP motif mutants of pNL4.3-iGFP-ΔEnv and psPAX2. (**C**) Schematic diagram of the TIRF assay to measure capsid opening. (**D**) Gallery of negative staining TEM images of viral particles incubated with the pore-forming protein PFO. (**E**) Distribution of PFO pore diameters (34.8 ± 5.2 nm, mean ±standard deviation, N = 347). (**F**) TIRF image of immobilized viral particles in a 450 × 370 pixel region of the field of view. (**G**) Distribution of GFP intensity for each particle in the field of view. (**H**) Fluorescence intensity traces of viral particles with leaky, opening and closed capsids showing the release of GFP contained by the envelope at the point of envelope permeabilization ('P') with PFO and release of encapsidated GFP after spontaneous opening ('O') of the HIV capsid. The capsid opening time (Δt) is the time from permeabilization to capsid opening. The black squares indicate the frames at which the snapshots shown below each trace were taken. The TIRF movie was recorded with an imaging frequency of 1 frame s^{-1}.

The following figure supplement is available for figure 1:

60

capsid (*Welker et al., 2000*; *Yu et al., 2013*). The remainder of traces showed a residual GFP signal after membrane permeabilization that constituted on average 13% of the total GFP signal prior to permeabilization (*Figure 1—figure supplement 1*). This fraction was consistent with the amount of GFP expected to be randomly trapped inside the volume of the capsid (relative to the volume of the viral particle) during maturation. Loss of this residual GFP signal to background levels at a later point in time was attributed to the spontaneous opening of the capsid lattice to create a hole sufficiently large to permit the passage of GFP (indicated by 'O' in *Figure 1H*, middle panels). We then calculated the capsid opening time (denoted as Δt in *Figure 1H*) for each trace as the difference between the time of membrane permeabilization and the time of capsid opening. In a fraction of traces the residual GFP signal remained constant until the end of the TIRF movie and the corresponding particles were classified as having closed capsids that retain GFP for the duration of the experiment (*Figure 1H*, right panel). We conclude that monitoring the steps of GFP release from viral particles at the single-particle level reveals differences in capsid opening times.

Effect of capsid-binding molecules on capsid opening kinetics

We used the capsid opening assay to characterize the intrinsic stability of the HIV capsid in the absence and presence of molecules known to affect the stability of the CA lattice. *Figure 2A* shows the fraction of capsids that are leaky, undergo opening or remain closed within 30 min of adding PFO to the immobilized particles. Leaky capsids constituted the largest fraction of particles (60–80%), irrespective of which type of capsid-binding molecules were present in the solution. Even in the absence of capsid-binding molecules, we observed variability in the fraction of leaky capsids in this range for different batches of particles. These observations suggest that leaky particles result from assembly defects during maturation, which are unaffected by modulators of CA lattice stability that the capsid encounters at a later stage (e.g. after entry into the cell).

To obtain an estimate of the half-life of the opening process, we analyzed the distribution of capsid opening times determined for hundreds of particles that undergo opening (*Figure 2B, C*). The survival curve of intact capsids (i.e. those that remain positive for encapsidated GFP) exposed to buffer without additives could be approximated with an exponential decay function (*Figure 2B*, black lines and *Figure 2—source data 1*) yielding an estimate for the capsid half-life of 8 min (*Figure 2C*), which is similar to a previous estimate of 10 min for the half-life of capsid uncoating in vitro (*Francis et al., 2016*). Fitting a bi-exponential decay made it possible to quantify a sub-population of capsids (~20%) that were substantially less stable and opened with a half-life of less than 1 min (*Figure 2B*, dashed grey line and *Figure 2—source data 2*).

To validate that the GFP release kinetics depend on capsid stability, we assessed the effect of the E45A mutation in CA on capsid opening. This mutation is known to yield hyperstable capsids (*Forshey et al., 2002*; *Yang et al., 2012*), which was also apparent in our capsid opening assay with a 4.5-fold increase in half-life compared to capsids assembled from wild-type CA (*Figure 2C*).

The ability to identify different subpopulations of capsids and to extract a half-life for capsid opening allowed us to quantitatively compare the effect of known capsid-binding proteins and small molecules on capsid stability. Cyclophilin A (CypA) is a host cell protein that binds to the cyclophilin binding loop of CA exposed on the exterior of the capsid (*Gamble et al., 1996*), and this interaction is thought to control capsid stability after cell entry (*Shah et al., 2013*). In our assay, CypA had no effect on capsid half-life when added at a concentration of 1 µM and lead to an approximately two-fold increase in half-life at 20 µM (*Figure 2C*).

The small molecules PF74 and BI2 bind to hexameric CA and inhibit HIV infection at an early post-fusion event (*Bhattacharya et al., 2014*; *Blair et al., 2010*; *Lamorte et al., 2013*; *Price et al., 2014*). Addition of these inhibitors to the capsid opening assay at high concentrations within the range typically used in cellular and biochemical assays revealed an increase in the ratio of opening to closed particles after 30 min (*Figure 2A*) and a pronounced acceleration of capsid opening with half-lives of 41 s and 2.4 min, respectively (*Figure 2C*). In contrast, the small molecule
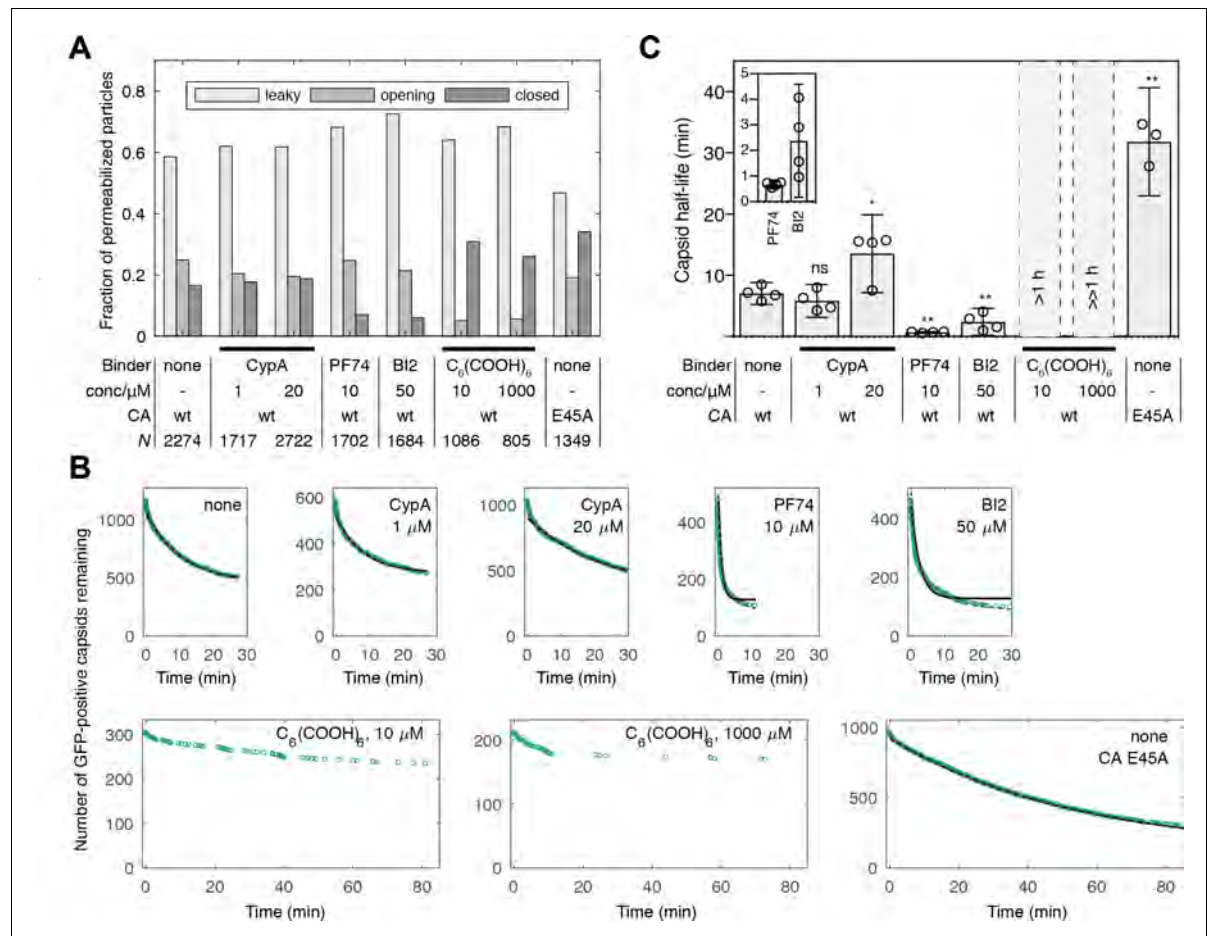
Figure 2. Kinetics of capsid opening. (**A**) Bar chart showing the fraction of capsids classified as 'leaky', 'opening' and 'closed' that are present 30 min after addition of PFO to permeabilize the envelope, recorded in the absence and presence of capsid binders. (**B**) Survival curves of capsids with encapsidated GFP after permeabilization with mono- (black line) and bi-exponential (dotted grey line) fit. The parameter values of the fits are provided in *Figure 2—source data 1* and *2*. The data in panels A and B was combined from multiple measurements (total number of repeats/number of viral preparations): No binder (3/2); CypA - 1 µM (4/2); CypA - 20 µM (5/2); PF74 - 10 µM (4/2); BI2 - 50 µM (5/3); hexacarboxybenzene - 10 µM (3/2); hexacarboxybenzene - 1000 µM (2/1); CA E45A (5/3). (**C**) Half-lives of intact capsids determined by fitting survival curves from individual repeats with a mono-exponential decay function. The error bars represent 95% confidence intervals; unpaired t-test with Welch's correction, p=0.2797 (1 µM CypA), p=0.0403 (20 µM CypA), p=0.0403 (20 µM CypA), p=0.0014 (10 µM PF74), p=0.0022 (50 µM BI2), p=0.0043 (CA E45A). The half-lives of capsids in the presence of hexacarboxybenze ($C_6(COOH)_6$) could not be determined with certainty and were estimated to be >1 hr.
DOI: https://doi.org/10.7554/eLife.34772.005

The following source data is available for figure 2:

Source data 1. Table of coefficient values from a mono-exponential fit of the survival curves in *Figure 2B*.
DOI: https://doi.org/10.7554/eLife.34772.006
Source data 2. Table of coefficient values from a bi-exponential fit of the survival curves in *Figure 2B*.
DOI: https://doi.org/10.7554/eLife.34772.007

hexacarboxybenzene ($C_6(COOH)_6$), which binds to hexameric CA (*Jacques et al., 2016*), showed the opposite effect by strongly inhibiting capsid opening (*Figure 2A*). There was an insufficient number of opening events to allow a robust fit of the survival curves but we estimated that the half-lives in the presence of 10 and 1000 µM hexacarboxybenzene were in the order of 1 hr and 10 hr, respectively. Taken together, our observations show that measuring GFP release from authentic viral capsids at the single-particle level is suitable to reveal the heterogeneity of capsid assembly states and quantify the effect of capsid binders on the opening kinetics of intact capsids.

Kinetics of protein binding to intact HIV capsids

The half-life of the HIV capsid is sufficiently long to use PFO-permeabilized viral particles as a platform to quantify the binding of labeled proteins to authentic viral capsids at the single-particle level as shown in *Figure 3A*. To demonstrate this approach, we added CypA labeled with Alexa Fluor 568 (AF568) at the same time as PFO to the flow channel and followed the fluorescence signals of GFP packaged into the virion and AF568-CypA using dual-color TIRF microscopy. For binding analysis, we selected particles with capsids that remained intact (GFP-positive) for a sufficient period of time to obtain a binding equilibrium. Using a calibration value obtained by single-molecule photobleaching, we converted the AF568 intensity to obtain the number of CypA molecules bound at each location corresponding to a closed capsid.

Representative traces of CypA binding to closed capsids are shown in *Figure 3B*. As before, PFO-mediated permeabilization of each individual particle was evident from the large drop in GFP intensity to a level corresponding to the pool of GFP trapped inside the closed capsid. Coincident with GFP signal loss, we observed a rapid increase in the CypA signal up to an equilibrium binding level. We then obtained the CypA binding kinetics for the entire population of closed capsids in the field by aligning all single-particle traces at the time of membrane permeabilization. The aligned traces recorded in the presence of 1 µM CypA are shown as a heatmap in *Figure 3C*. The median binding trace showed that binding equilibrium was rapidly established, suggesting that the PFO-permeabilized membrane does not present a significant barrier for diffusion of proteins to and from the capsid. The number of molecules bound at equilibrium in the experiment shown in *Figure 3C* had a median of 73 molecules per capsid. Across 12 independent experiments, we measured 58 ± 8 molecules per capsid in the presence of 1 µM CypA (*Figure 3—figure supplement 1*). When imaged for longer periods of time, the plateau level increased slowly, suggesting that a low level of irreversible or non-specific binding may occur over time. However, binding of CypA was completely abolished in the presence of the competitive inhibitor cyclosporin A, which binds to the binding pocket on CypA (*Figure 3C*, bottom panels) (*Mikol et al., 1993*). This observation indicates that the interaction with the permeabilized viral particle is largely driven by an interaction with sites recognized by its binding pocket.

Next, we used the binding assay to obtain an estimate of the dissociation constant (K_D) for the CypA-capsid interaction and the number of binding sites that can be occupied simultaneously on the assembled capsid. Mean binding curves were obtained from aligned single-particle traces recorded at concentrations ranging from 0.1 to 20 µM (*Figure 3D*). Analysis of the equilibrium binding levels gave an estimate of the K_D of 10–12 µM with an estimated 500–1000 molecules bound per capsid at saturation (*Figure 3E* and *Figure 3—figure supplement 2*). This number of sites represents roughly half of the number of CA proteins in an assembled capsid (*Briggs et al., 2003*). The expected CypA:CA ratio at saturation is also 1:2, because binding to both cyclophilin loops of CA molecules connecting neighboring hexamers in the lattice would lead to steric clashes (*Liu et al., 2016*). This observation suggests that the lattice is completely coated with CypA at saturation, and that binding sites on different locations of the capsid are equivalent.

Finally, we obtained the rate of CypA dissociation by measuring the decay of the mean fluorescence intensity associated with closed capsids after removing CypA from solution by flushing the flow channel with buffer (*Figure 3F*). The majority of the fluorescence signal (85%) disappeared rapidly with a rate of 1.5 s^{-1}. This rate was close to the rate of solution exchange achievable in our microfluidic set-up, such that the off-rate of CypA measured here may be limited by mass transport. The residual CypA signal associated with the particles, possibly representing irreversibly bound CypA, decayed with a rate consistent with photobleaching. For comparison, we also measured the binding and dissociation of unlabeled CypA to CA and cross-linked CA hexamers using surface plasmon resonance. Equilibrium binding analysis of the SPR data gave a K_D of 21.8 µM and 19 µM for
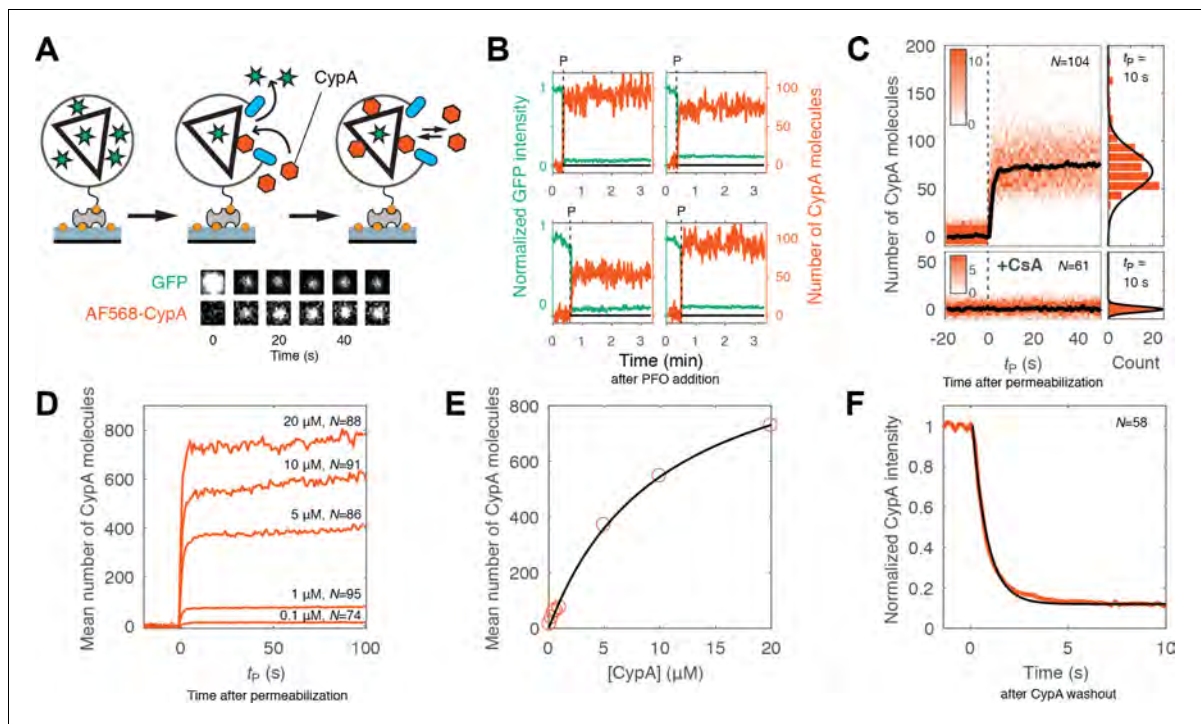
63

Figure 3. Kinetics of CypA binding to the intact capsid. (A) Schematic diagram of the TIRF assay for measuring protein binding to the intact capsid and snapshots of the GFP signal and AF568-CypA signal of a selected viral particle at different times. (B) Example traces of CypA binding (vermillion) to individual closed capsids that retain GFP (green) after permeabilization of the viral envelope (note the residual GFP signal after the large drop). The concentration of CypA was 1 µM. (C) CypA binding traces (vermillion) to all closed capsids in the field of view aligned with respect to the time of envelope permeabilization (t_P = 0). The bold black line represents the median binding trace. CypA binding was recorded in the absence (top) and presence (bottom) of cyclosporine A (CsA). The histograms at the right show the distribution of intensities after binding equilibrium is reached (at t_P = 10 s). Gaussian fitting gave a mean ±standard deviation of 73 ± 20 and 1.6 ± 2.9 in the presence and absence of CsA, respectively. Representative data from four (−CsA) and two (+CsA) independent experiments using different viral preparations. (D) Median CypA binding traces recorded at CypA concentrations ranging from 0.1 to 20 µM as indicated above the corresponding trace. Binding experiments with concentrations above 1 uM were carried out with a mixture of unlabeled and labeled CypA, whereby the concentration of the labeled CypA was kept at 1 µM. (E) Median number of CypA molecules bound at equilibrium as a function of CypA concentration (vermillion circles) and fit of an equilibrium binding model (black line). The fit gave the following estimates for the interaction: KD = 10 µM; number of CypA-binding sites on the intact capsid ~1000. See *Figure 3—figure supplement 2* for an independent repeat experiment. (F) Mean CypA intensity measured at closed capsids after wash-out of CypA from the flow channel at t = 0. The black line represents a fit of the data with an exponential decay function.

DOI: https://doi.org/10.7554/eLife.34772.008

The following figure supplements are available for figure 3:

Figure supplement 1. Variation in the median number of molecules bound at equilibrium per closed capsid measured in independent experiments at different CypA concentrations.
DOI: https://doi.org/10.7554/eLife.34772.009
Figure supplement 2. Equilibrium binding analysis of CypA binding to capsid.
DOI: https://doi.org/10.7554/eLife.34772.010
Figure supplement 3. SPR measurements of the CypA-CA interaction.
DOI: https://doi.org/10.7554/eLife.34772.011

interaction with immobilized CA (consistent with previous data [*Yoo et al., 1997*]) and CA hexamer (*Figure 3—figure supplement 3*), respectively, while the off-rates determined after removal of CypA from solution were 4 ± 0.3 s^{-1} and 3.5 ± 0.4 s^{-1}, respectively. We conclude that CypA binds with low affinity to the authentic viral capsid lattice shortly after membrane permeabilization in an

64

interaction that is governed by rapid kinetics and not fundamentally different from its interaction with CA that is not part of a lattice.

Visualizing capsid lattice disassembly using CypA paint

The capsid opening assay pinpoints the start of the uncoating reaction. To also measure the kinetics of lattice disassembly beyond the appearance of the first defect, we explored the possibility of using labeled CypA to 'paint' the CA lattice, whereby the signal of bound CypA is proportional to the number of CA molecules that remain at a given point in time during disassembly, similar to a previous approach using CypA-DsRed (*Francis et al., 2016*). Our observations above revealed that CypA fulfils two important requirements for its use as a capsid lattice paint. Firstly, CypA binding does not have a measurable effect on capsid opening when used at concentrations of up to 1 μM (*Figure 2C*). Secondly, CypA binds (and dissociates) with fast rates to binding sites all over the surface of the lattice (*Figure 3*). In the experiments shown here, we added labeled CypA to the buffer at the same time as adding PFO, but in principle it is possible to add (and withdraw) the label at any point in time during the uncoating experiment. We then observed the CypA signal as a function of time for each GFP-positive particle in the field of view, whereby the vast majority of particles showed the appearance of a CypA signal above background shortly after permeabilization. Below we focus on the analysis of leaky and opening capsids, whereby the intensity of the CypA signal was converted into a measure for the integrity of the capsid lattice.

Particles with leaky capsids (complete disappearance of the GFP signal in a single step) showed a spike in the CypA signal upon membrane permeabilization that typically decayed rapidly (within seconds to minutes, see *Figure 4B* for example traces). The median CypA intensity trace obtained by aligning all traces with leaky capsids at the time of membrane permeabilization showed instantaneous accumulation of CypA intensity followed by a short dwell time of 5–7 s and exponential decay characterized by a half-life of 14–25 s (*Figure 4C*). We interpreted this signal as follows: particles with leaky capsids contain a CA lattice that is poised to fall apart and only persists for a short period of time before disassembly. The distribution of CypA molecules bound per capsid at the intensity peak (*Figure 4C*, middle panel) suggested the presence of particles containing almost complete capsids with only minor defects as well as particles with only partially assembled lattices. The distribution of CypA paint intensities measured 5 min after permeabilization (*Figure 4C*, right panel) revealed a small residual signal, suggesting the presence of residual CA.

Single-particle traces of opening capsids (*Figure 4D*) were characterized by the following phases: First, rapid binding of CypA upon membrane permeabilization, reaching a binding equilibrium while the capsid remained closed (*Figure 4E*, left heatmap). Second, the CypA fluorescence signal started to decay within a short dwell time of capsid opening (GFP release) and then reached a stable level above background. We interpret the second phase as the disassembly of most of the CA lattice. The median disassembly kinetics after capsid opening (*Figure 4E*, right heatmap) were governed by a half-life of approximately 70–100 s. The rapid decay of the lattice after initiation of uncoating observed here with labeled monomeric CypA is consistent with previous measurements in vitro and in cells using a tetrameric probe, CypA-dsRed, that binds irreversibly to the capsid lattice (*Francis et al., 2016*). As observed for leaky capsids, we detected residual CypA intensity at the end of the disassembly phase, possibly due to the presence of some CA molecules remaining associated with the viral RNA inside the permeabilized viral particle.

Overall, the disassembly process after capsid opening followed a similar process as observed for leaky capsids, but with slower kinetics. We conclude that capsid opening is the rate-limiting step for capsid uncoating, and lattice disassembly will proceed rapidly once the capsid has developed the first defect.

CypA paint reveals the effects of PF74 and hexacarboxybenzene on capsid lattice disassembly

As shown above, PF74 accelerated capsid opening, while hexacarboxybenzene strongly inhibited this step. A simple explanation of these observations is that binding of these compounds globally affects capsid stability. In this case, we would predict that the rates of lattice disassembly are affected in the same way as capsid opening, that is increased in the presence of PF74 and decreased in the presence of hexacarboxybenzene. To test this prediction, we used CypA paint to determine
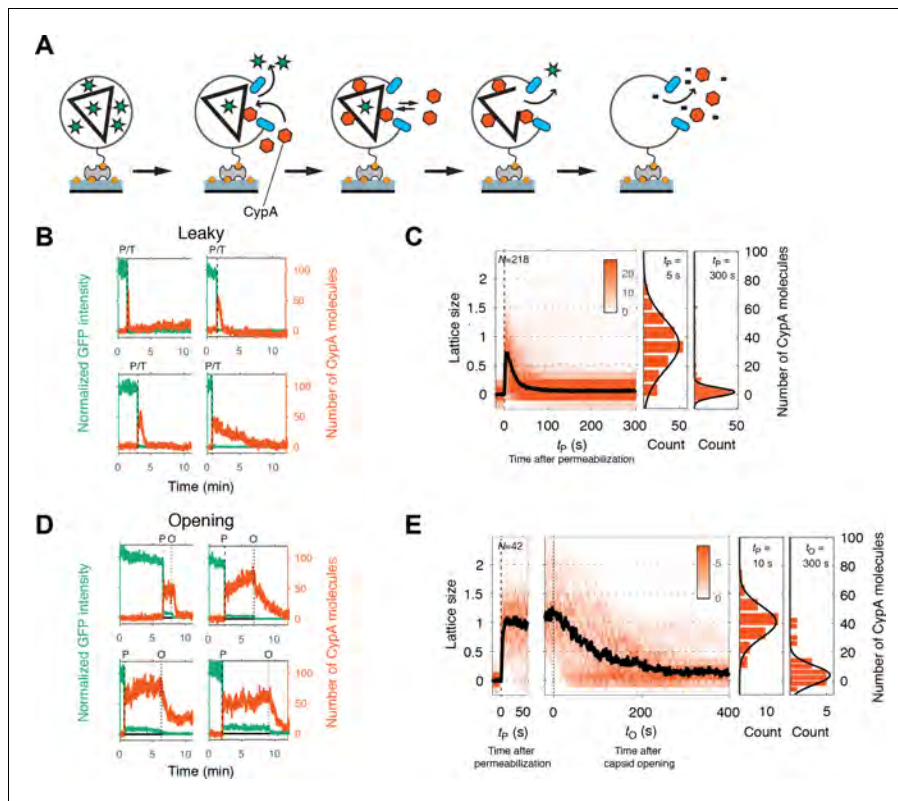
Figure 4. Painting the capsid with CypA to visualize lattice disassembly kinetics. (**A**) Schematic diagram of the TIRF CypA paint assay. (**B**) Example traces of AF568-CypA binding (vermillion) to individual leaky capsids that do not retain GFP (green) after permeabilization of the viral envelope. The concentration of CypA was 0.7 μM. (**C**) Heatmap of CypA binding traces to all leaky capsids in the field of view aligned with respect to the time of envelope permeabilization ($t_P = 0$). The bold black line represents the median CypA trace. The histograms at the right show the distribution of intensities at $t_P = 5$ s and 300 s. (**D**) Example traces of AF568-CypA binding (vermillion) to individual capsids that initially retain a fraction of the GFP signal (green) after permeabilization of the viral envelope, and then open to release this residual GFP signal. The concentration of CypA was 0.7 μM. (**E**) Heatmap of CypA intensity traces of all capsids in the field of view that undergo opening. The traces in the left panel are aligned with respect to the time of envelope permeabilization ($t_P = 0$), while the traces in the right panel are aligned with respect to capsid opening. The bold black line represents the median CypA trace. The histograms at the right show the distribution of intensities after binding equilibrium is reached (at $t_P = 10$ s) and at the end of lattice disassembly. Representative data from three independent experiments using different viral preparations.
DOI: https://doi.org/10.7554/eLife.34772.012

the effect of these compounds on the kinetics of lattice disassembly. CypA binding to the capsid was indistinguishable in the presence and absence of these compounds (*Figure 3—figure supplement 1*), suggesting that binding of either compound does not interfere with CypA binding. Surprisingly, in the presence of PF74, we observed no decrease in the CypA paint signal after capsid opening (*Figure 5B*, right heatmap). This observation suggests that the lattice develops a defect to allow the passage of proteins but is otherwise highly stabilized such that no (further) CA proteins are released from the lattice. The amount of CA protein lost during the opening step was below the limit of detection in our assay (compare the CypA paint intensity histograms before and after capsid opening, *Figure 5B*). This stabilization of the lattice was also observed for leaky capsids (*Figure 5A*). Here, too, the CypA paint signal remained constant for at least 8 min. The observations indicate that the lattice did not release a substantial number of individual CA subunits (or small multimers), but we cannot rule out breakage of the capsid into stable parts that are too large to traverse the PFO pores. In contrast to the strong stabilization observed with PF74, hexacarboxybenzene only had a
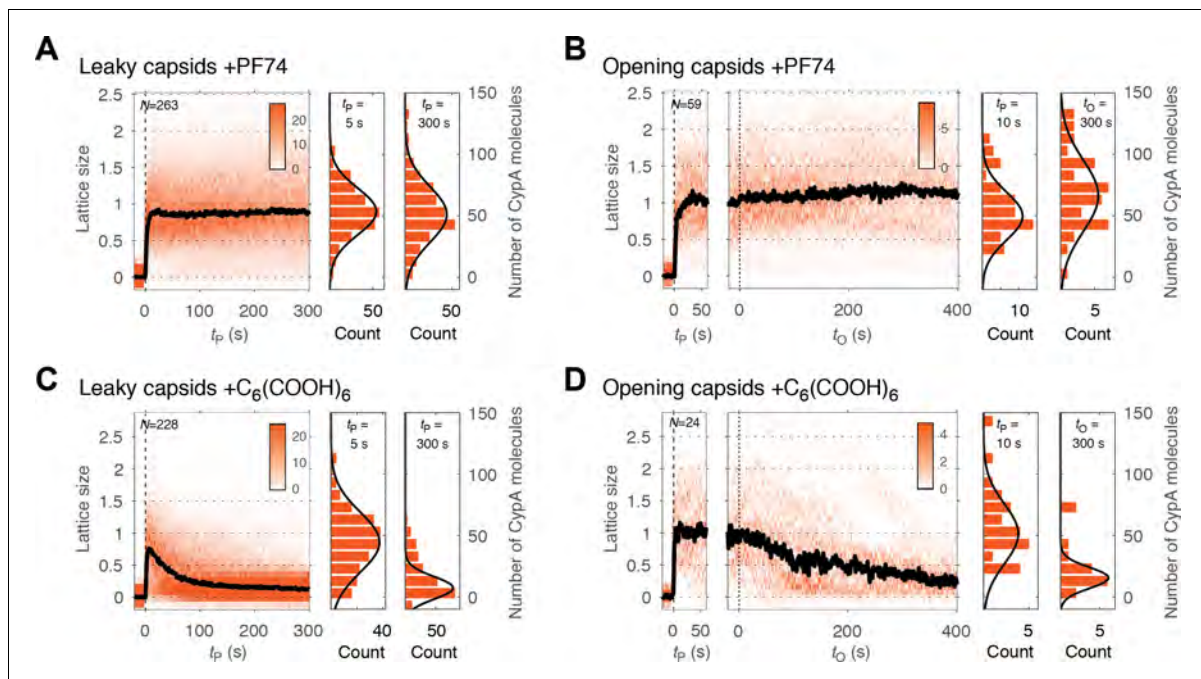
66

Figure 5. PF74 but not hexacarboxybenzene stabilizes the CA lattice after capsid opening. (**A, C**) Heatmaps of CypA binding traces to all leaky capsids in the field of view aligned with respect to the time of envelope permeabilization (t_P = 0) in the presence of PF74 (**A**) or hexacarboxybenzene (**C**). The bold black line represents the median CypA trace. (**B, D**) Heatmaps of CypA intensity traces of all capsids in the field of view that undergo opening in the presence of PF74 (**B**) or hexacarboxybenzene (**D**). The traces in the left panel are aligned with respect to the time of envelope permeabilization (t_P = 0), while the traces in the right panel are aligned with respect to capsid opening (t_O = 0). The bold black line represents the median CypA trace. Heatmaps are representative of data acquired in two independent experiments using different viral preparations.
DOI: https://doi.org/10.7554/eLife.34772.013

modest stabilizing effect on the CA lattice after capsid opening, as seen from the CypA paint signal decay from that point onwards (*Figure 5D*); the inability to prevent collapse of the lattice was also apparent for leaky capsids (*Figure 5C*). We conclude that while PF74 promotes a structural change leading to a defect in the capsid that allows passage of proteins, only little (if any) CA protein is lost during this step, and the remaining lattice is highly stabilized. In contrast, hexacarboxybenzene strongly inhibits capsid opening but has little effect on uncoating once the process has started.

Cell lysate slows capsid opening but not lattice disassembly

Finally, we conducted capsid opening and CypA paint experiments in the presence of cell lysate to test whether it was compatible with our single-particle approaches. PFO-mediated permeabilization was unaffected when HeLa cell lysate was added to the buffer at a final protein concentration of 1 mg mL^{-1}. However, capsid opening was slowed down with a four-fold increase in the half-life of this process (*Figure 6A and B*). CypA bound to the exposed capsid in the same manner as observed in buffer (*Figure 6C*). The number of CypA molecules bound on intact (closed) capsids at equilibrium was comparable to that measured in buffer (*Figure 3—figure supplement 1*), indicating that there was no competition with endogenous CypA due to the high dilution factor used in this experiment. CypA paint revealed that the process of uncoating in diluted cell lysate was in principle the same as is buffer, with the lattice falling apart shortly after it had opened up, albeit with a slightly reduced rate (*Figure 6D and E*). The stabilizing effect exerted by the diluted cell lysate is consistent with previous observations (*Francis et al., 2016*; *Fricke et al., 2013*; *Guth and Sodroski, 2014*), and it may be amplified when components are present at cytosolic concentrations. Identification of components
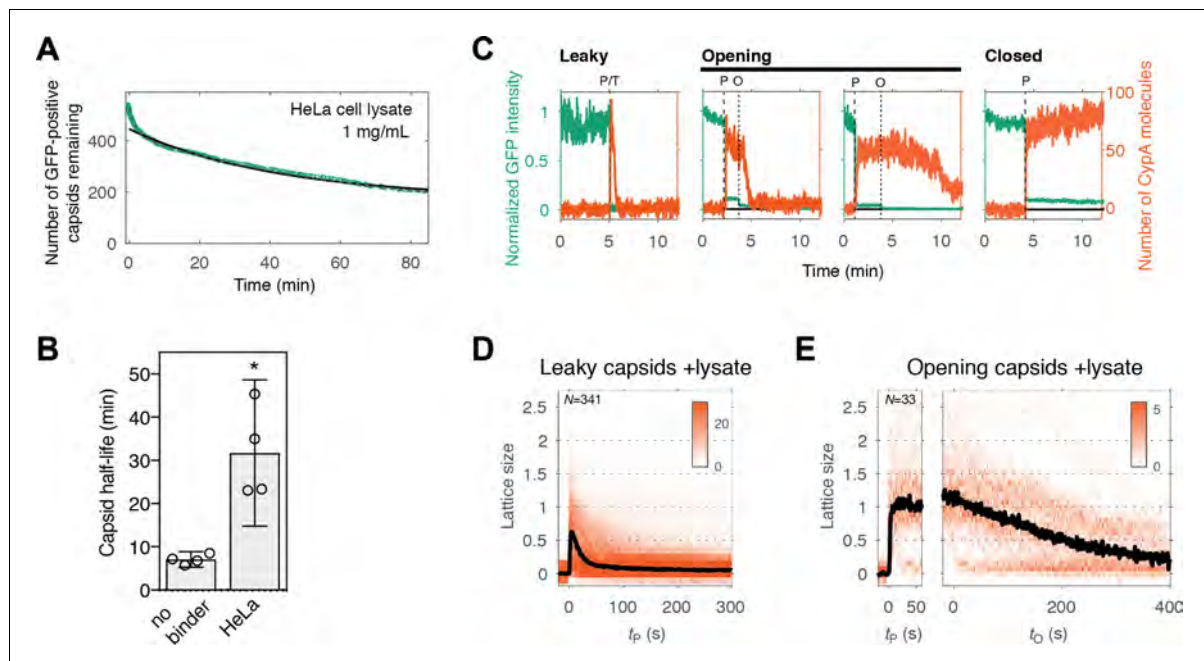
Figure 6. Capsid opening and lattice disassembly measured in the presence of HeLa cell lysate. (A) Survival curve of GFP-positive capsids in the presence of HeLa cell lysate. The half-life determined from the curve is 48 min. Combined data from a total of five repeats using two different viral preparations. (B) Half-life of intact capsids determined by fitting survival curves from individual repeats with a mono-exponential decay function. The error bars represent 95% confidence intervals; unpaired t-test with Welch's correction, p=0.0184. (C) Example traces of AF568-CypA binding (vermillion) in the presence of HeLa cell lysate to individual capsids (green) after permeabilization of the viral envelope. The concentration of CypA was 1 µM. (D) Heatmap of CypA binding traces to all leaky capsids in the field of view aligned with respect to the time of envelope permeabilization. The bold black line represents the median CypA trace. (E) Heatmap of CypA intensity traces of all capsids in the field of view that undergo opening. The traces in the left panel are aligned with respect to the time of envelope permeabilization, while the traces in the right panel are aligned with respect to capsid opening. The bold black line represents the median CypA trace.

DOI: https://doi.org/10.7554/eLife.34772.014

The following source data is available for figure 6:

Source data 1. Table of coefficient values from a mono-exponential fit of the survival curves in *Figure 6A*.
DOI: https://doi.org/10.7554/eLife.34772.015

Source data 2. Table of coefficient values from a bi-exponential fit of the survival curves in *Figure 6A*.
DOI: https://doi.org/10.7554/eLife.34772.016

contributing to this effect is the subject of future investigation, whereby the single-particle methods introduced here are suitable to dissect the effect of specific perturbations in the context of a complex mixture such as cell lysate.

Discussion

Measurement of the single-particle uncoating kinetics of authentic HIV capsids immediately after removing the protective barrier of the viral membrane has allowed us to observe the effects of capsid-binding molecules on discrete steps in the capsid uncoating process. The order of events established with our new assays would have been obscured in ensemble measurements due to dephasing. We observed the following main characteristics of HIV-1 capsid uncoating and its interactions with capsid-binding molecules: (1) The integrity and stability of capsids in a population is highly heterogeneous, whereby the majority of capsids contain defects and/or uncoat immediately after removal of the viral membrane. (2) In the absence of capsid binders, uncoating is an all-or-none

process that proceeds rapidly after the first defect is created. (3) Capsid-binding molecules exhibit differential effects on the steps that control initiation and continuation of uncoating.

The structural heterogeneity of the HIV capsid is well described, with the assembly process yielding a variety of conical, tubular and other shapes that often contain structural defects such as gaps in the CA lattice (*Briggs et al., 2003*; *Frank et al., 2015*; *Mattei et al., 2016*; *Yu et al., 2013*). Here, we identify functionally distinct classes of capsids on the basis of their GFP release kinetics, allowing us to quantify the functional heterogeneity for hundreds of capsids within a population and relate them to different assembly states. By utilizing a pore-former to permeabilize the viral membrane in a controlled manner while recording capsid opening traces, we are able to observe early events that occur upon exposure of the capsid to a change in conditions and thus capture unstable assembly states. This approach circumvents the need for isolating viral cores, a process which exposes cores to experimental buffer conditions for extended periods of time (*Shah and Aiken, 2011*) and would result in a loss of this information. Our results show that the assembly states range from incomplete or imperfect (leaky) lattices to fully assembled (closed) capsids that nevertheless exhibit pronounced differences in uncoating kinetics. Here, we have quantified the fraction of particles of different stability for a viral particle that lacks HIV envelope protein and has GFP inserted into the Gag polyprotein. These features may affect maturation and capsid assembly or lead to misclassification of some particles, for example as a result of incomplete proteolysis. It is therefore important to note that wild type HIV may exhibit a different distribution of capsid stability types. Nevertheless, it is striking that 60–80% of capsids in our experiments are not fully closed and are unable to retain GFP upon membrane permeabilization. This category includes early assembly intermediates but mostly structures that are essentially fully assembled (as judged by our CypA paint method, see below) yet unable to form a closed cone. We assign the latter class of leaky structures to capsids with holes that are also observed in intact viral particles by cryo-electron microscopy (*Mattei et al., 2016*) and by GFP release in vivo (*Yu et al., 2013*). The abundance of these types of particles obtained here using a viral preparation protocol that avoids harsh treatments (such as centrifugation) suggests that capsid assembly frequently becomes trapped at this stage, whereby remodeling of the lattice to allow it to close might be a slow process.

Host cell proteins that interact with the viral capsid after cell entry often recognize assembled CA rather than CA monomers (*Yamashita and Engelman, 2017*). Cross-linked CA hexamers and self-assembled lattices from recombinant CA (*Ganser-Pornillos et al., 2004*; *Pornillos et al., 2010*) or CA-NC protein (*Campbell and Vogt, 1995*) are powerful tools for identification and structural studies of capsid-binding molecules but do not fully recapitulate the structural features (including curvature and flexibility) of the lattice that may be required for binding. In contrast, our assay provides access to the authentic, wild-type capsid lattice for determining interaction kinetics, affinity and stoichiometry, and thus assess structural models for the binding mode of host proteins on the intact lattice. A recent study of self-assembled CA lattices in complex with CypA using cryo-electron microscopy and solid-state NMR spectroscopy suggested that each CypA bridges two hexamers in the lattice by simultaneously contacting the cyclophilin loops on two neighboring CA proteins, one via its canonical binding site and one via a postulated non-canonical binding site located on the opposite side of the CypA molecule (*Liu et al., 2016*). While our binding measurements are consistent with a 1:2 CypA:CA stoichiometry at saturation, we observed that the K_D and off-rate for the CypA-capsid complex were only two-fold lower compared to complex with CA. Further, CypA binding resulted in only modest stabilization of the capsid (two-fold increase in half-life). Our data is consistent with a binding mode that relies primarily on an interaction via the canonical binding site and suggests that binding via the non-canonical binding site is either very weak and/or not immediately accessible for most CypA molecules interacting with the capsid. The fast interaction kinetics imply rapid turn-over of CypA and/or exchange with other host proteins that compete for binding to the capsid lattice.

The observation that CypA binding at low concentrations is neutral with respect to capsid opening provides an added dimension to our single-particle assay. The ability to 'paint' the capsid with fluorescent CypA at sub-stoichiometric ratios (about 1:20 CypA:CA) enables kinetic studies of capsid disassembly. We observed that defective capsids collapsed rapidly after membrane permeabilization suggesting that they are only stable in the presence of the high concentrations of free CA inside the viral membrane (most CA released by proteolysis during maturation is not incorporated into the capsid and remains in solution at a concentration in the low mM range). Similarly, we found that lattice

disassembly of an initially intact capsid is a rapid process that ensues as soon as the first gap in the lattice has appeared, that is uncoating is primarily controlled by the slow rate of removing the first (few) CA subunits.

The ability to simultaneously monitor appearance of the first defect and overall lattice stability allows us to define different stages of 'uncoating' and study how they may be influenced by external factors, as demonstrated here by dissecting the effects of two known capsid-binding molecules, PF74 and hexacarboxybenzene. PF74 is a drug molecule designed to target CA (*Blair et al., 2010*). At high concentration ($\geq$10 μM), it blocks HIV infection at a stage before reverse transcription (*Price et al., 2014*). It has been described as stabilizing self-assembled hexameric CA or CA-NC tubes but destabilizing HIV cores (*Bhattacharya et al., 2014*; *Da Silva Santos et al., 2016*; *Fricke et al., 2013*; *Shi et al., 2011*). In our assay, PF74 uncoupled the step of capsid opening from lattice disassembly. Addition of PF74 led to a pronounced acceleration of capsid opening but the remaining lattice was highly stabilized. This observation reconciles the previous ambiguity regarding the mode of action of PF74. It stabilizes CA lattices, but in a manner that makes it incompatible with a closed structure. Binding rapidly leads to capsid rupture in a manner that releases little CA but removes the barrier for free diffusion of proteins. In contrast, we found that hexacarboxybenzene is a potent inhibitor of capsid opening as seen from the remarkable increase in the half-life of this process. But in the event that the core does open, disassembly proceeds in a manner similar to the untreated capsid.

Taken together our observations suggest that the CA lattice has enhanced stability as long as it forms a closed surface, as predicted from coarse-grained simulations of capsid lattice disassembly (*Grime et al., 2016*). Appearance of a local defect leads to catastrophic failure of the lattice whereby the defect could rapidly propagate via dissociation of CA subunits that are no longer stabilized by dimer and/or trimer interfaces linking neighboring hexamers in the lattice (*Figure 7*). The interactions between subunits in a hexamer (or pentamer) represent a weak link in the CA lattice. Hexacarboxybenzene stabilizes the hexamer by binding in the its central electropositive pore (*Jacques et al., 2016*), leading to an increase in the energy barrier for dissociation of the first CA molecule(s), but only if the surrounding lattice is intact. Progressive loss of hexamer subunits would be expected to destroy the binding site for hexacarboxybenzene, leading to its dissociation and further destabilization of the disassembling part of the lattice. PF74 on the other hand binds in a pocket between CA subunits in a hexamer and stabilizes the hexameric lattice (*Bhattacharya et al., 2014*; *Price et al., 2014*). We speculate that PF74 may stabilize a particular conformation that is incompatible with the highly curved section of the capsid, leading to breakage at those points, whereby the restructured lattice is sufficiently stable to prevent dissociation of CA from hexamers adjacent to the gap.

What are the implications of our findings for uncoating in the cell? Two currently debated, non-mutually exclusive models for uncoating pose that core opening occurs either en route towards the nucleus (cytoplasmic uncoating) or after docking of the core at the nuclear pore complex (*Campbell and Hope, 2015*). In both models, residual CA protein remains associated with the pre-integration complex during and after nuclear import, but to what extent CA protein is lost from the capsid in the cytoplasmic uncoating model remains unclear. The intrinsic instability of the lattice after capsid opening observed here suggests that partially uncoated states with the capsid largely intact do not exist unless stabilized by host cell proteins. Such a stabilizing role has been suggested for CypA (*Liu et al., 2016*; *Shah et al., 2013*); however, the only modest stabilization of the lattice observed here in the presence of physiological concentrations suggests that other factors may be involved in this process. While not naturally present during an infection, the effect of the capsid-binding molecules, PF74 and hexacarboxybenze, offer insight into additional mechanisms that may be at play. PF74 binds at a junction between two neighboring CA proteins within the hexamer. This site can also be occupied by two host proteins: CPSF6 and Nup153 (*Matreyek et al., 2013*; *Price et al., 2014*). The observation that small-molecule binding at this site results in what could be described as a partially uncoated state raises the possibility that these two cofactors may also play roles in regulating the core-opening/uncoating event in vivo. In addition, the inhibition of capsid opening in the presence of hexacarboxybenze suggests that polyanionic species bound at the Arg18 cluster in the central pore of a hexamer could greatly enhance the lifetime of the closed core as it travel through the cytoplasm. Rapid uncoating could then be initiated, for example after docking at the nuclear pore complex, by catalyzing removal of a few CA subunits. In an accompanying paper,
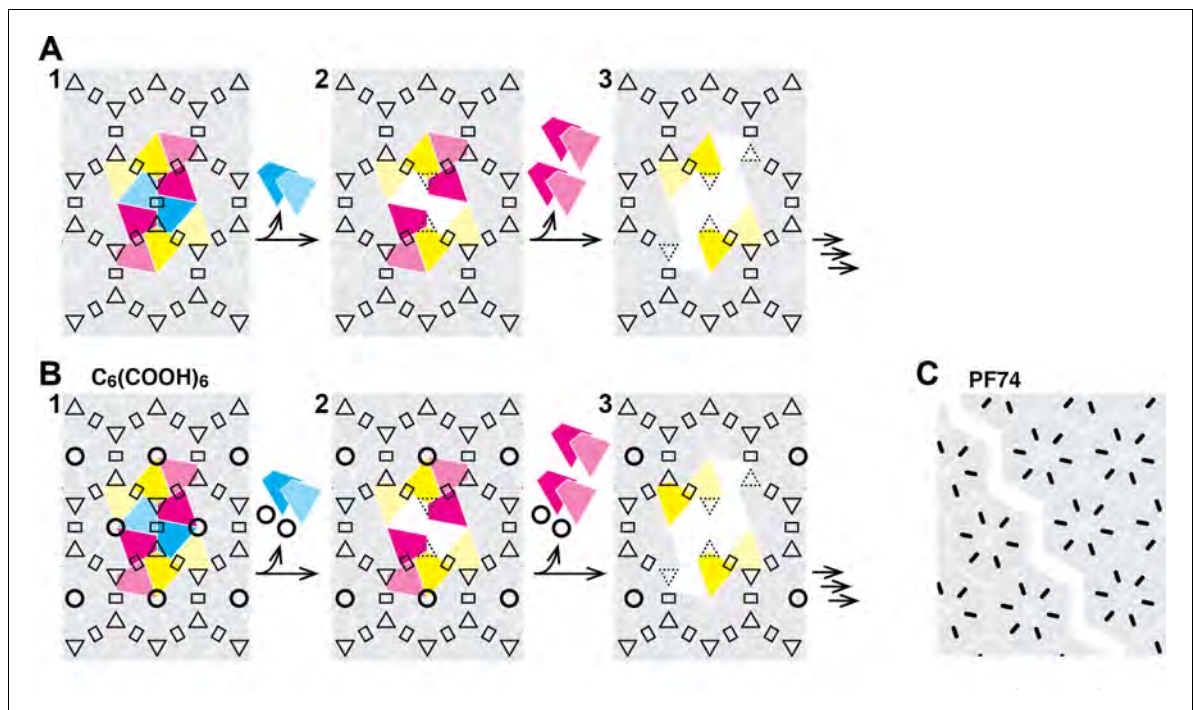
Figure 7. Schematic of the hexameric CA lattice and proposed disassembly pathway. (**A**) Intact CA lattice with dimeric and trimeric interfaces between hexamers highlighted as rectangles and triangles, respectively. Removal of a CA subunit (dark cyan) from a hexamer in the lattice leads to destabilization and dissociation of its dimer partner (light cyan) in the neighboring hexamer; GFP release may occur as early as at this stage. The defect propagates by dissociation of subunits (dark magenta) that have now lost contacts within the hexamer and at the trimer interface, followed by (or concomitant with) loss of their corresponding dimer partners (light magenta). Disassembly continues in all directions from the initial defect with increasing rate while the length of the defect edge grows. (**B**) Binding of hexacarboxybenzene (circles) to the central pore stabilizes the hexamer, reducing the probability of dissociation of the first CA subunit(s). Once the defect is created, the stabilizing effect of hexacarboxybenzene is insufficient to prevent disassembly via the pathway described in A. (**C**) Binding of PF74 (black lines) may lead to capsid rupture instead of loss of CA subunits, whereby PF74 molecules bound at the interfaces between CA subunit act as a glue to prevent dissociation of CA subunits from hexamers adjacent to the defect.

DOI: https://doi.org/10.7554/eLife.34772.017

we show that the naturally occurring polyanion inositol hexakisphosphate is selectively packaged into viral particles and stabilizes the mature lattice against spontaneous opening as observed here for the non-natural compound hexacarboxybenzene.

The competition for binding to the capsid between host molecules that facilitate or restrict infection, and their effect on uncoating remain to be fully determined, but our assay is ideally suited to answering these questions. The advantages of our approach include the ability to extract hundreds of single-particles traces in a single experiment for detailed kinetic analysis under defined conditions and the low requirements for reagents. The compatibility of the assay with lysates should prove powerful to dissect the effect of capsid-binding proteins and small molecules in complex mixtures containing components of different pathways and allows the study of perturbations via knock-down or overexpression of candidate proteins and lysates from different cell types or cells stimulated with different treatments, for example to induce antiviral states. The methods described here could readily be extended to competition binding studies or screening of the effect of small molecules on properties of the viral capsid for drug discovery.

71

Materials and methods

Key resources table

Reagent type (species) or resource	Designation	Source or reference	Identifiers	Additional information
Recombinant DNA reagent	pNL4.3-iGFP-ΔEnv	DOI: 10.1371/journal.ppat.1002762		
Recombinant DNA reagent	pNL4.3-iGFP-CA E45A-ΔEnv	This paper		Proviral construct generated by subcloning a fragment with the CA E45A mutation into pNL4.3-iGFP-ΔEnv using the XbaI-SbfI restriction sites.
Recombinant DNA reagent	psPAX2	NIH AIDS Reagent Program	#11348	
Cell line (human)	HEK293T	ATCC	ATCC CRL-3216	
Cell line (human)	HeLa	ATCC	ATCC CCL-2	
Chemical compound, drug	PF74	Sigma Aldrich	SML0835	
Chemical compound, drug	BI2	Enamine	Z1982491200	

Constructs for production of viral particles

The proviral construct pNL4.3-iGFP-ΔEnv was generated as described previously (*Aggarwal et al., 2012*). It contains the open reading frame for eGFP flanked by protease cleavage sites inserted into the Gag gene between the coding sequences for MA and CA. In addition, it contains the SalI-BamHI fragment from HXB2, in which the start codon of the Env gene is mutated to a stop codon (TGA) to prevent expression of the envelope protein. The proviral construct pNL4.3-iGFP-CA E45A-ΔEnv containing an additional mutation to produce CA E45A was generated by subcloning a fragment with that mutation into pNL4.3-iGFP-ΔEnv using the XbaI-SbfI restriction sites. Constructs with PTAP to LIRL mutation in the late domain of Gag were generated by moving the SphI-SbfI fragment of a pNL4.3 construct with Gag-LIRL (courtesy of Eric Freed) into pNL4.3-iGFP-ΔEnv and into psPAX2. The second-generation lentiviral packaging plasmid psPAX2 (Cat# 11348, from Didier Trono) encoding the Gag, Pol, Rev, and Tat genes was obtained through the NIH AIDS Reagent Program, Division of AIDS, NIAID, NIH.

Cell lines

HEK-293T cells and HeLa cells were obtained from ATCC. Identity testing was carried out by PCR. Cell lines tested negative for mycoplasma.

Production, purification and biotinylation of viral particles

Viral particles were produced by transfecting HEK293T cells with a mixture of pNL4.3-iGFP-ΔEnv and psPAX2 (1.4:1, mol/mol) using polyethylenimine (PEI Max) reagent (Polysciences, 9002-98-6). The virus-containing medium was collected 48 hr post-transfection and centrifuged (2100 x g, 20 min, 4°C) to remove cells. Next, viral membrane proteins were biotinylated to allow immobilization of viral particles on surfaces. The biotinylation reagent EZ-Link Sulfo-NHS-LC-LC-Biotin (Thermo Scientific, 21338) was added to the virus-containing medium (~1 mg per 7 mL of medium) and the mixture was incubated for 90 min at 4°C. Biotinylated viral particles were then purified by size exclusion chromatography using a HiPrep 16/60 Sephacryl S-500 HR column (GE Healthcare) equilibrated with HBS (50 mM HEPES pH 7.5, 100 mM NaCl) and stored at 4°C for use within 7 days.

Counting of GFP-positive viral particles

PTAP mutant virus was produced alongside WT pNL4.3-iGFP-ΔEnv as outlined in the methods above. To enumerate HIV particles per mL, 5 μL of each virus preparation was added to 45 μL of DMEM complete media and spinoculated onto poly-L-lysine-coated glass-bottom (175 μm thickness) 96-well plates (Greiner Sensoplate, Sigma) at 1200 × g for 60 min at 4°C. GFP-positive particles were detected using an inverted Olympus IX-70 microscope equipped with a 60 × oil immersion

72

objective (1.42 NA), microtiter stage (DeltaVision ELITE Image Restoration Microscope, Applied Precision/Olympus) and Evolve 512 EMCCD camera (Photometrics). Four fields of view were acquired per sample and counted using a viral particle count algorithm developed in Cellprofiler (Broad Institute) based on intensity and size cut offs. Viral counts per mL in the initial sample were then calculated from the viral count per μm^2 by taking the surface area of the well bottom and the initial sample volume into account. Means and standard deviations represent three independent viral counts.

Expression and purification of CypA

Human CypA was expressed using a pET expression vector in BL21 (DE3) *E. coli* grown in Luria-Bertani medium at 37°C with shaking. Protein expression was induced by addition of isopropyl β-D-thiogalactopyranoside to a final concentration of 1 mM, and the cells were grown for 3 hr at 37°C with shaking. Cells were harvested by centrifugation, resuspended in cold (4°C) lysis buffer (25 mM HEPES, pH 7.6, 1 mM DTT, 0.02% NaN3, supplemented with 'Complete' protease inhibitor and 1 mg mL^{-1} lysozyme) and lyzed by sonication on ice. The lysate was clarified by centrifugation (Thermo Fisher SS-34 rotor, 19,000 rpm, 30 min, 4°C). The supernatant was passed through a syringe filter (0.22 μm) and purified by anion exchange chromatography using a 10 mL HiTrap Q HP column (GE Healthcare Life Science, 17-1154-01) equilibrated with a buffer containing 25 mM HEPES, pH 7.6, 1 mM DTT, 0.02% NaN3. CypA eluted in the flow-through and fractions containing CypA were pooled and adjusted to a pH of 5.8 with 1% v/v acetic acid. After removal of aggregates by centrifugation (Sorvall SS34 rotor, 19,000 rpm, 1 hr, 4°C), the supernatant was applied to a cation exchange chromatography column (5 mL HiTrap SP HP, GE Healthcare Life Science, 17115201) equilibrated with a buffer containing 25 mM sodium phosphate, pH 5.8, 1 mM DTT, 0.02% NaN3 and CypA was eluted with a linear gradient from 0 to 1 M NaCl over 20 column volumes. Fractions containing purified CypA were dialyzed against CypA storage buffer (25 mM MOPS, pH 6.6, 1 mM DTT, 0.02% NaN3), concentrated using an Amicon-15 Ultra centrifugal filtration device (10 k MWCO, Merck, UFC901024) to a final concentration of 300 μM and frozen in liquid nitrogen for storage at −80°C. The yield was approximately 3 mg/g of cell mass.

Labeling of CypA

CypA was labeled by reaction with a 4-fold molar excess of Alexa-Fluor 568-C5-maleimide (Thermo Fisher Scientific, A10254) in PBS (pH 7.4, 0.1 mM TCEP) for 10 min at room temperature. The reaction was quenched by addition of 1 M DTT to a final concentration of 17 mM. Labeled CypA was separated from unconjugated dye using Zeba desalting spin columns (Thermo Fisher Scientific, 89883) equilibrated with AF568-CypA storage buffer (50 mM Tris, pH 7.9, 20% v/v glycerol, 1 mM DTT). Under these conditions, CypA is quantitatively labeled at residue C51. CypA labeled at C51 binds in surface plasmon resonance measurements to immobilized CA or CA hexamers with the same affinity as unlabeled CypA. Labeled CypA was frozen in liquid nitrogen and stored at −40°C.

Negative staining transmission electron microscopy of viral particles treated with perfringolysin O

Recombinant perfringolysin O was produced as described previously (*Rossjohn et al., 1997*). Viral particles purified by size exclusion chromatography were concentrated by 40-fold using Amicon Ultra-4 centrifugal ultrafiltration devices (Merck, UFC800324) and incubated with PFO at a final concentration of 0.5 μM at 37°C for 10 min in the presence of 0.1 mM inositol hexakisphosphate. A formvar/carbon grid (Ted Pella, 01801) was cleaned in a glow discharge unit and modified with Cell-Tak adhesive (0.05 mg mL^{-1}, Corning, 354240). The grid was then incubated with a sample (5 μL) containing PFO-treated viral particles for 1 min at room temperature, and the solution was wicked away using filter paper. The sample was immediately stained twice with uranyl formate (1% w/v) and excess solution wicked away with filter paper. The grids were dried under a gentle stream of nitrogen gas and allowed to dry further overnight. The samples were imaged using a FEI Tecnai G2 20 Transmission Electron Microscope equipped with a BM Eagle digital camera. Diameters of the PFO pores were measured using ImageJ.

Fabrication and operation of microfluidic flow cells

Glass coverslips were cleaned by sonication in ethanol for 30 min followed by sonication in 1 M NaOH for 30 min, rinsed with ultrapure water and dried. PDMS devices for assembly of microfluidic flow cells (channel height 60 μm, channel width 800 μm) were prepared using standard protocols for soft lithography. After treating the PDMS device and the coverslip with an air plasma inside a plasma cleaner for 3 min, the PDMS device was mounted on the coverslip and the assembled microfluidic flow cell was heated in an oven at 70°C for at least 15 min to improve bonding between the glass and the PDMS. The glass surface at the bottom of the microfluidic channels was then modified by adsorption of a co-polymer composed of poly-L-lysine (PLL) and biotinylated poly(ethylene glycol) (PEG) (Susos AG, PLL(20)-g[3.4]-PEG(2)/PEG(3.4)-biotin (20%)). A solution of PLL-PEG-biotin (1 mg mL^{-1} in PBS) was injected into the flow channels and incubated at room temperature for 30 min followed by flushing the channels with water and drying. The channels were then filled with a solution of streptavidin (Sigma-Aldrich, 0.2 mg mL^{-1} in blocking buffer containing 20 mM Tris pH 7.5, 2 mM EDTA, 50 mM NaCl, 0.03% NaN3, 0.025% Tween 20, 0.2 mg mL^{-1} BSA) for 15 min and rinsed with HBS pH 7.5. The microfluidic flow cell was mounted on the microscope stage and connected to tubing. Solutions were pulled through the channels at a flow rate of 100 μL min^{-1} (unless specified otherwise) using a syringe pump connected to the outlet tubing and operating in 'withdraw' mode.

TIRF microscopy assays

Biotinylated viral particles in HBS (30–100 μL) were flowed through the flow channel and captured on the modified coverslip surface. Unbound viral particles were washed out with 50 μL of HBS pH 7.5. TIRF microscopy assays were carried out with imaging buffer (50 mM HEPES pH 7.0, 100 mM NaCl), which was supplemented with an oxygen quenching system for dual colour experiments to reduce photobleaching (2 mM trolox, 2.5 mM protocatechuic acid, 0.25 U mL^{-1} protocatechuate-3,4-dioxygenase).

Images were collected on a custom built TIRF microscope based around an ASI-RAMM frame (Applied Scientific Instrumentation) with a Nikon 100 × CFI Apochromat TIRF (1.49 NA) oil immersion objective. Lasers were incorporated using the NicoLase system (*Nicovich et al., 2017*). Images were captured on two Andor iXon 888 EMCCD cameras (Andor Technology Ltd). 300 mm tube lenses were used to give a field of view of 88.68 μm × 88.68 μm. Alternatively, images were collected on a TILL Photonics TIRF microscope equipped with a Zeiss 100 × Plan Apochromat (1.46 NA) oil immersion objective, solid state lasers for excitation, a beam splitter for simultaneous dual channel acquisition of fluorescence emission using two Andor iXon 897U EMCCD cameras for detection with a field of view of 46 μm × 46 μm.

Capsid opening assay

Imaging buffer (30 μL) containing PFO (200 nM) was injected into the channel to initiate viral membrane permeabilization and TIRF images were acquired (488 nm laser, 20 ms exposure time) with a frequency of 1 frame s^{-1} for the initial phase of the reaction (typically 300–500 frames) followed by a frequency of 0.1 frame s^{-1}. The total duration of the experiment varied depending on the uncoating kinetics, lasting between 15 and 90 min, whereby the total number of frames was kept at 800–900 frames.

Capsid uncoating assay via painting with CypA

Imaging buffer (30 μL) containing PFO (200 nM) and Alexa Fluor 568-labeled CypA (1 μM) was injected into the flow channel. TIRF images were acquired sequentially for the different fluorophores (488 nm and 561 nm laser, 1–3 W cm^{-2} power density,~200 nm penetration depth, 20 ms exposure time) and a frequency of 1 frame s^{-1}. The following equation was used for model fitting to obtain estimates for the dissociation constant and the number of molecules bound at saturation (*Figure 3E*): N(eq) = [CypA]×N(max) / ([CypA]+K$_D$), where N(eq) is the number of molecules bound at equilibrium for a given CypA concentration, [CypA] is the concentration of CypA, N(max) is the number of molecules bound at saturation and K$_D$ is the dissociation constant.

Protein-capsid interaction assay

Protein binding was imaged (sequential acquisition, 488 nm and 561 nm laser, 20 ms exposure time, one frame s^{-1}) after flowing imaging buffer (30 μL) containing PFO (200 nM) and different concentrations of Alexa Fluor 568-labeled CypA (0.1–20 μM) into the flow channel. Protein dissociation was imaged (561 nm laser, 20 ms exposure time, five frame s^{-1}) after wash-out of labeled protein with imaging buffer.

Image analysis

Images were analyzed with software written in MATLAB (The MathWorks, Inc.) adapted from previous work (*Böcking et al., 2011*). Images in the time series were aligned by cross-correlation to the first frame to correct for x/y-drift (*Guizar-Sicairos et al., 2008*). GFP-loaded viral particles appear as diffraction limited objects and were detected as local maxima in the first frame and their positions determined by Gaussian fitting. Overlapping particles were excluded from analysis. Fluorescence traces were calculated by integrating the fluorescence intensity in a 7 × 7 pixel region for each channel. The fluorescence intensity for each object was corrected for background fluorescence determined from pixels in the vicinity of the object. Fluorescence traces were fitted with step traces to identify the presence and time of steps corresponding to permeabilization and capsid opening. Traces were automatically sorted into four classes on the basis of the following criteria: (1) loss of entire GFP signal in one step; (2) loss of GFP intensity in one large (permeabilization) and one small (capsid opening) step; (3) loss of the majority of the GFP signal in one step with residual GFP signal persisting for the rest of the experiment; (4) no permeabilization or otherwise uninterpretable traces (excluded from analysis). The assignment to classes was verified by visual inspection of traces. Capsid opening times were calculated for traces in class two as the time difference between permeabilization and capsid opening. The time of reagent addition (or reagent wash-out) was detected as an overall increase (or decrease) of the background fluorescence in the reagent channel. The number of bound AF568-CypA molecules was determined from the ratio of the AF568-CypA fluorescence intensity associated with the capsid at equilibrium to the fluorescence intensity of a single AF568-CypA molecule. The fluorescence intensity of the single fluorophore was determined from the quantal photobleaching step in photobleaching traces of AF568-CypA molecules adsorbed sparsely to the coverslip surface and imaged continuously.

Surface Plasmon resonance analysis of CypA binding to CA

Biotinylation of CA

CA K158C was expressed and purified using methods adapted from the literature (*Hung et al., 2013*) and biotinylated at the engineered cysteine residue using the following procedure. CA K158C was first assembled into tubes in high salt buffer (50 mM Tris pH 8, 2.5 M NaCl, 0.1 mM TCEP, 0.02% sodium azide), collected by centrifugation (18,000 g, 5 min) and the pellet was resuspended in high-salt buffer. This centrifugation/resuspension procedure was repeated another two times. Biotin maleimide (Sigma-Aldrich B-1267) was then added in a twofold molar excess to the resuspended CA K158C tubes, allowed to react for one min and quenched by the addition 2-mercaptoethanol to a final concentration of 50 mM. The biotinylated tubes were washed by two cycles of centrifugation and resuspension in high-salt buffer as above. Finally, the tubes were collected by centrifugation, resuspended in buffer without salt to induce disassembly, and biotinylated CA was buffer exchanged into SPR running buffer (10 mM HEPES pH 8, 0.005% Tween 20, 2 mM EDTA, 100 mM NaCl) using a Zeba gel filtration spin column.

Biotinylation of cross-linked CA hexamers

Soluble CA hexamers were assembled from CA A14C/E45C/W184A/M185A using a published protocol (*Pornillos et al., 2010*) and biotinylated using EZ-Link sulfo-NHS-LC-LC-biotin (Thermo Fisher Scientific, 21338). The biotinylation reagent was added at a twofold molar excess to CA hexamers in PBS (pH 7) and incubated at room temperature for 30 min. The reaction was stopped by buffer exchange into SPR running buffer using a Zeba gel filtration spin column.

Surface chemistry and SPR measurements

Streptavidin was immobilized on the surface of a CM5 sensor chip (GE Healthcare, BR100399) using the amine coupling kit (GE Healthcare, BR100050). A solution containing EDC (7.5 mg mL^{-1}) and NHS (11.5 mg mL^{-1}) was injected into the flow cells to activate the carboxyl groups followed by a solution containing streptavidin (0.5 mg mL^{-1}) and finally ethanolamine (1 M) to block remaining activated carboxyl groups. All solutions were flowed through the channels for 7 min at a flow rate of 10 µL min^{-1}. Finally, biotinylated CA K158Cor biotinylated CA hexamer were immobilized on the surface by injection a 2.5 µM solution for 30 s at a flow rate of 30 µL min^{-1}. Flow channels modified with streptavidin were used as reference cells. CypA was buffer exchanged into SPR running buffer using a Zeba gel filtration spin column. CypA solutions at a range of concentrations (3.125–100 µM) were flowed through the cells (20 s at a flow rate of 100 µL min^{-1}) followed by a buffer wash (30 s at a flow rate of 100 µL min^{-1}) while measuring the SPR response at a frequency of 40 Hz.

Preparation of cell lysate

HeLa cells were washed with PBS, resuspended in lysis buffer (10 mM Tris-HCl, pH 8, 10 mM KCl, 1.5 mM MgCl2, protease inhibitor and phosphatase inhibitor), and incubated for 15 min at 4°C. Lysis was achieved by passing the cell suspension through a 30.5 g needle (130 strokes with cooling the sample on ice for 2 min at every 10th stroke). Cell lysis was verified by staining a sample of the lysate with trypan blue (added to a final concentration 0.2% w/v). The lysate was centrifuged (18,000 x g, 30 min, 4°C) to remove cell debris and protein levels in the supernatant were estimated from the absorbance at 280 nm. Lysate was frozen in liquid nitrogen and stored at −40°C.

Acknowledgements

Additional information

Author contributions

Chantal L Márquez, Formal analysis, Investigation, Writing—review and editing; Derrick Lau, Vaibhav Shah, Conall McGuinness, Investigation, Writing—review and editing; James Walsh, Software, Investigation, Writing—review and editing; Andrew Wong, Anupriya Aggarwal, Investigation; Michael W Parker, Resources, Writing—review and editing; David A Jacques, Writing—original draft, Writing—review and editing; Stuart Turville, Conceptualization, Resources, Writing—review and editing; Till Böcking, Conceptualization, Formal analysis, Writing—original draft, Writing—review and editing

Author ORCIDs

Michael W Parker ⓘ http://orcid.org/0000-0002-3101-1138
David A Jacques ⓘ http://orcid.org/0000-0002-6426-4510
Till Böcking ⓘ http://orcid.org/0000-0003-1165-3122

Additional files

Supplementary files

• Transparent reporting form
DOI: https://doi.org/10.7554/eLife.34772.018

Data availability

All data generated or analysed during this study are included in the manuscript and supporting files.

References

Aggarwal A, Iemma TL, Shih I, Newsome TP, McAllery S, Cunningham AL, Turville SG. 2012. Mobilization of HIV spread by diaphanous 2 dependent filopodia in infected dendritic cells. *PLoS Pathogens* **8**:e1002762. DOI: https://doi.org/10.1371/journal.ppat.1002762, PMID: 22685410

Ambrose Z, Aiken C. 2014. HIV-1 uncoating: connection to nuclear entry and regulation by host proteins. *Virology* **454-455**:371–379. DOI: https://doi.org/10.1016/j.virol.2014.02.004, PMID: 24559861

Bhattacharya A, Alam SL, Fricke T, Zadrozny K, Sedzicki J, Taylor AB, Demeler B, Pornillos O, Ganser-Pornillos BK, Diaz-Griffero F, Ivanov DN, Yeager M. 2014. Structural basis of HIV-1 capsid recognition by PF74 and CPSF6. *PNAS* **111**:18625–18630. DOI: https://doi.org/10.1073/pnas.1419945112, PMID: 25518861

Blair WS, Pickford C, Irving SL, Brown DG, Anderson M, Bazin R, Cao J, Ciaramella G, Isaacson J, Jackson L, Hunt R, Kjerrstrom A, Nieman JA, Patick AK, Perros M, Scott AD, Whitby K, Wu H, Butler SL. 2010. HIV capsid is a tractable target for small molecule therapeutic intervention. *PLoS Pathogens* **6**:e1001220. DOI: https://doi.org/10.1371/journal.ppat.1001220, PMID: 21170360

Blumenthal R, Durell S, Viard M. 2012. HIV entry and envelope glycoprotein-mediated fusion. *Journal of Biological Chemistry* **287**:40841–40849. DOI: https://doi.org/10.1074/jbc.R112.406272, PMID: 23043104

Böcking T, Aguet F, Harrison SC, Kirchhausen T. 2011. Single-molecule analysis of a molecular disassemblase reveals the mechanism of Hsc70-driven clathrin uncoating. *Nature Structural & Molecular Biology* **18**:295–301. DOI: https://doi.org/10.1038/nsmb.1985, PMID: 21278753

Briggs JA, Grünewald K, Glass B, Förster F, Kräusslich HG, Fuller SD. 2006. The mechanism of HIV-1 core assembly: insights from three-dimensional reconstructions of authentic virions. *Structure* **14**:15–20. DOI: https://doi.org/10.1016/j.str.2005.09.010, PMID: 16407061

Briggs JA, Simon MN, Gross I, Kräusslich HG, Fuller SD, Vogt VM, Johnson MC. 2004. The stoichiometry of Gag protein in HIV-1. *Nature Structural & Molecular Biology* **11**:672–675. DOI: https://doi.org/10.1038/nsmb785, PMID: 15208690

Briggs JA, Wilk T, Welker R, Kräusslich HG, Fuller SD. 2003. Structural organization of authentic, mature HIV-1 virions and cores. *The EMBO Journal* **22**:1707–1715. DOI: https://doi.org/10.1093/emboj/cdg143, PMID: 12660176

Bukrinsky M. 2004. A hard way to the nucleus. *Molecular Medicine* **10**:1–5. PMID: 15502876

Burdick RC, Delviks-Frankenberry KA, Chen J, Janaka SK, Sastri J, Hu WS, Pathak VK. 2017. Dynamics and regulation of nuclear import and nuclear movements of HIV-1 complexes. *PLoS Pathogens* **13**:e1006570. DOI: https://doi.org/10.1371/journal.ppat.1006570, PMID: 28827840

Campbell EM, Hope TJ. 2015. HIV-1 capsid: the multifaceted key player in HIV-1 infection. *Nature Reviews Microbiology* **13**:471–483. DOI: https://doi.org/10.1038/nrmicro3503, PMID: 26179359

Campbell S, Vogt VM. 1995. Self-assembly in vitro of purified CA-NC proteins from rous sarcoma virus and human immunodeficiency virus type 1. *Journal of Virology* **69**:6487–6497. PMID: 7666550

Da Silva Santos C, Tartour K, Cimarelli A. 2016. A novel entry/Uncoating reveals the presence of at least two species of viral capsids during synchronized HIV-1 infection. *PLoS Pathogens* **12**:e1005897. DOI: https://doi.org/10.1371/journal.ppat.1005897, PMID: 27690375

Dang TX, Hotze EM, Rouiller I, Tweten RK, Wilson-Kubalek EM. 2005. Prepore to pore transition of a cholesterol-dependent cytolysin visualized by electron microscopy. *Journal of Structural Biology* **150**:100–108. DOI: https://doi.org/10.1016/j.jsb.2005.02.003, PMID: 15797734

de Marco A, Heuser AM, Glass B, Kräusslich HG, Müller B, Briggs JA. 2012. Role of the SP2 domain and its proteolytic cleavage in HIV-1 structural maturation and infectivity. *Journal of Virology* **86**:13708–13716. DOI: https://doi.org/10.1128/JVI.01704-12, PMID: 23055560

Dharan A, Talley S, Tripathi A, Mamede JI, Majetschak M, Hope TJ, Campbell EM. 2016. KIF5B and Nup358 Cooperatively Mediate the Nuclear Import of HIV-1 during Infection. *PLoS Pathogens* **12**:e1005700. DOI: https://doi.org/10.1371/journal.ppat.1005700, PMID: 27327622

Forshey BM, von Schwedler U, Sundquist WI, Aiken C. 2002. Formation of a human immunodeficiency virus type 1 core of optimal stability is crucial for viral replication. *Journal of Virology* **76**:5667–5677. DOI: https://doi.org/10.1128/JVI.76.11.5667-5677.2002, PMID: 11991995

Francis AC, Marin M, Shi J, Aiken C, Melikyan GB. 2016. Time-Resolved imaging of single HIV-1 uncoating in vitro and in living cells. *PLoS Pathogens* **12**:e1005709. DOI: https://doi.org/10.1371/journal.ppat.1005709, PMID: 27322072

Frank GA, Narayan K, Bess JW, Del Prete GQ, Wu X, Moran A, Hartnell LM, Earl LA, Lifson JD, Subramaniam S. 2015. Maturation of the HIV-1 core by a non-diffusional phase transition. *Nature Communications* **6**:5854. DOI: https://doi.org/10.1038/ncomms6854, PMID: 25569620

Fricke T, Brandariz-Nuñez A, Wang X, Smith AB, Diaz-Griffero F. 2013. Human cytosolic extracts stabilize the HIV-1 core. *Journal of Virology* **87**:10587–10597. DOI: https://doi.org/10.1128/JVI.01705-13, PMID: 23885082

Gamble TR, Vajdos FF, Yoo S, Worthylake DK, Houseweart M, Sundquist WI, Hill CP. 1996. Crystal structure of human cyclophilin A bound to the amino-terminal domain of HIV-1 capsid. *Cell* **87**:1285–1294. DOI: https://doi.org/10.1016/S0092-8674(00)81823-1, PMID: 8980234

Ganser-Pornillos BK, von Schwedler UK, Stray KM, Aiken C, Sundquist WI. 2004. Assembly properties of the human immunodeficiency virus type 1 CA protein. *Journal of Virology* **78**:2545–2552. DOI: https://doi.org/10.1128/JVI.78.5.2545-2552.2004, PMID: 14963157

Grime JM, Dama JF, Ganser-Pornillos BK, Woodward CL, Jensen GJ, Yeager M, Voth GA. 2016. Coarse-grained simulation reveals key features of HIV-1 capsid self-assembly. *Nature Communications* **7**:11568. DOI: https://doi.org/10.1038/ncomms11568, PMID: 27174390

Guizar-Sicairos M, Thurman ST, Fienup JR. 2008. Efficient subpixel image registration algorithms. *Optics Letters* **33**:156–158. DOI: https://doi.org/10.1364/OL.33.000156, PMID: 18197224

Guth CA, Sodroski J. 2014. Contribution of PDZD8 to stabilization of the human immunodeficiency virus type 1 capsid. *Journal of Virology* **88**:4612–4623. DOI: https://doi.org/10.1128/JVI.02945-13, PMID: 24554657

Hulme AE, Perez O, Hope TJ. 2011. Complementary assays reveal a relationship between HIV-1 uncoating and reverse transcription. *PNAS* **108**:9975–9980. DOI: https://doi.org/10.1073/pnas.1014522108, PMID: 21628558

Hung M, Niedziela-Majka A, Jin D, Wong M, Leavitt S, Brendza KM, Liu X, Sakowicz R. 2013. Large-scale functional purification of recombinant HIV-1 capsid. *PLoS One* **8**:e58035. DOI: https://doi.org/10.1371/journal.pone.0058035, PMID: 23472130

Hübner W, Chen P, Del Portillo A, Liu Y, Gordon RE, Chen BK. 2007. Sequence of human immunodeficiency virus type 1 (HIV-1) Gag localization and oligomerization monitored with live confocal imaging of a replication-competent, fluorescently tagged HIV-1. *Journal of Virology* **81**:12596–12607. DOI: https://doi.org/10.1128/JVI.01088-07, PMID: 17728233

Jacques DA, McEwan WA, Hilditch L, Price AJ, Towers GJ, James LC. 2016. HIV-1 uses dynamic capsid pores to import nucleotides and fuel encapsidated DNA synthesis. *Nature* **536**:349–353. DOI: https://doi.org/10.1038/nature19098, PMID: 27509857

Lahaye X, Satoh T, Gentili M, Cerboni S, Conrad C, Hurbain I, El Marjou A, Lacabaratz C, Lelièvre JD, Manel N. 2013. The capsids of HIV-1 and HIV-2 determine immune detection of the viral cDNA by the innate sensor cGAS in dendritic cells. *Immunity* **39**:1132–1142. DOI: https://doi.org/10.1016/j.immuni.2013.11.002, PMID: 24269171

Lamorte L, Titolo S, Lemke CT, Goudreau N, Mercier JF, Wardrop E, Shah VB, von Schwedler UK, Langelier C, Banik SS, Aiken C, Sundquist WI, Mason SW. 2013. Discovery of novel small-molecule HIV-1 replication inhibitors that stabilize capsid complexes. *Antimicrobial Agents and Chemotherapy* **57**:4622–4631. DOI: https://doi.org/10.1128/AAC.00985-13, PMID: 23817385

Li S, Hill CP, Sundquist WI, Finch JT. 2000. Image reconstructions of helical assemblies of the HIV-1 CA protein. *Nature* **407**:409–413. DOI: https://doi.org/10.1038/35030177, PMID: 11014200

Liu C, Perilla JR, Ning J, Lu M, Hou G, Ramalho R, Himes BA, Zhao G, Bedwell GJ, Byeon IJ, Ahn J, Gronenborn AM, Prevelige PE, Rousso I, Aiken C, Polenova T, Schulten K, Zhang P. 2016. Cyclophilin A stabilizes the HIV-1 capsid through a novel non-canonical binding site. *Nature Communications* **7**:10714. DOI: https://doi.org/10.1038/ncomms10714, PMID: 26940118

Mamede JI, Cianci GC, Anderson MR, Hope TJ. 2017. Early cytoplasmic uncoating is associated with infectivity of HIV-1. *PNAS* **114**:E7169–E7178. DOI: https://doi.org/10.1073/pnas.1706245114, PMID: 28784755

Matreyek KA, Yücel SS, Li X, Engelman A. 2013. Nucleoporin NUP153 phenylalanine-glycine motifs engage a common binding pocket within the HIV-1 capsid protein to mediate lentiviral infectivity. *PLoS Pathogens* **9**:e1003693. DOI: https://doi.org/10.1371/journal.ppat.1003693, PMID: 24130490

Mattei S, Glass B, Hagen WJ, Kräusslich HG, Briggs JA. 2016. The structure and flexibility of conical HIV-1 capsids determined within intact virions. *Science* **354**:1434–1437. DOI: https://doi.org/10.1126/science.aah4972, PMID: 27980210

Mikol V, Kallen J, Pflügl G, Walkinshaw MD. 1993. X-ray structure of a monomeric cyclophilin A-cyclosporin A crystal complex at 2.1 A resolution. *Journal of Molecular Biology* **234**:1119–1130. DOI: https://doi.org/10.1006/jmbi.1993.1664, PMID: 8263916

78

Nicovich PR, Walsh J, Böcking T, Gaus K. 2017. NicoLase-An open-source diode laser combiner, fiber launch, and sequencing controller for fluorescence microscopy. *PLoS One* **12**:e0173879. DOI: https://doi.org/10.1371/journal.pone.0173879, PMID: 28301563

Ocwieja KE, Brady TL, Ronen K, Huegel A, Roth SL, Schaller T, James LC, Towers GJ, Young JA, Chanda SK, König R, Malani N, Berry CC, Bushman FD. 2011. HIV integration targeting: a pathway involving Transportin-3 and the nuclear pore protein RanBP2. *PLoS Pathogens* **7**:e1001313. DOI: https://doi.org/10.1371/journal.ppat.1001313, PMID: 21423673

Pornillos O, Ganser-Pornillos BK, Banumathi S, Hua Y, Yeager M. 2010. Disulfide bond stabilization of the hexameric capsomer of human immunodeficiency virus. *Journal of Molecular Biology* **401**:985–995. DOI: https://doi.org/10.1016/j.jmb.2010.06.042, PMID: 20600115

Pornillos O, Ganser-Pornillos BK, Yeager M. 2011. Atomic-level modelling of the HIV capsid. *Nature* **469**:424–427. DOI: https://doi.org/10.1038/nature09640, PMID: 21248851

Price AJ, Jacques DA, McEwan WA, Fletcher AJ, Essig S, Chin JW, Halambage UD, Aiken C, James LC. 2014. Host cofactors and pharmacologic ligands share an essential interface in HIV-1 capsid that is lost upon disassembly. *PLoS Pathogens* **10**:e1004459. DOI: https://doi.org/10.1371/journal.ppat.1004459, PMID: 25356722

Rasaiyaah J, Tan CP, Fletcher AJ, Price AJ, Blondeau C, Hilditch L, Jacques DA, Selwood DL, James LC, Noursadeghi M, Towers GJ. 2013. HIV-1 evades innate immune recognition through specific cofactor recruitment. *Nature* **503**:402–405. DOI: https://doi.org/10.1038/nature12769, PMID: 24196705

Rossjohn J, Feil SC, McKinstry WJ, Tweten RK, Parker MW. 1997. Structure of a cholesterol-binding, thiol-activated cytolysin and a model of its membrane form. *Cell* **89**:685–692. DOI: https://doi.org/10.1016/S0092-8674(00)80251-2, PMID: 9182756

Schaller T, Ocwieja KE, Rasaiyaah J, Price AJ, Brady TL, Roth SL, Hué S, Fletcher AJ, Lee K, KewalRamani VN, Noursadeghi M, Jenner RG, James LC, Bushman FD, Towers GJ. 2011. HIV-1 capsid-cyclophilin interactions determine nuclear import pathway, integration targeting and replication efficiency. *PLoS Pathogens* **7**:e1002439. DOI: https://doi.org/10.1371/journal.ppat.1002439, PMID: 22174692

Shah VB, Aiken C. 2011. In vitro uncoating of HIV-1 cores. *Journal of Visualized Experiments : JoVE*. DOI: https://doi.org/10.3791/3384, PMID: 22105356

Shah VB, Shi J, Hout DR, Oztop I, Krishnan L, Ahn J, Shotwell MS, Engelman A, Aiken C. 2013. The host proteins transportin SR2/TNPO3 and cyclophilin A exert opposing effects on HIV-1 uncoating. *Journal of Virology* **87**:422–432. DOI: https://doi.org/10.1128/JVI.07177-11, PMID: 23097435

Shi J, Zhou J, Shah VB, Aiken C, Whitby K. 2011. Small-molecule inhibition of human immunodeficiency virus type 1 infection by virus capsid destabilization. *Journal of Virology* **85**:542–549. DOI: https://doi.org/10.1128/JVI.01406-10, PMID: 20962083

Sowd GA, Serrao E, Wang H, Wang W, Fadel HJ, Poeschla EM, Engelman AN. 2016. A critical role for alternative polyadenylation factor CPSF6 in targeting HIV-1 integration to transcriptionally active chromatin. *PNAS* **113**:E1054–E1063. DOI: https://doi.org/10.1073/pnas.1524213113, PMID: 26858452

Stremlau M, Perron M, Lee M, Li Y, Song B, Javanbakht H, Diaz-Griffero F, Anderson DJ, Sundquist WI, Sodroski J. 2006. Specific recognition and accelerated uncoating of retroviral capsids by the TRIM5alpha restriction factor. *PNAS* **103**:5514–5519. DOI: https://doi.org/10.1073/pnas.0509996103, PMID: 16540544

von Schwedler UK, Stray KM, Garrus JE, Sundquist WI. 2003. Functional surfaces of the human immunodeficiency virus type 1 capsid protein. *Journal of Virology* **77**:5439–5450. DOI: https://doi.org/10.1128/JVI.77.9.5439-5450.2003, PMID: 12692245

Welker R, Hohenberg H, Tessmer U, Huckhagel C, Kräusslich HG. 2000. Biochemical and structural analysis of isolated mature cores of human immunodeficiency virus type 1. *Journal of Virology* **74**:1168–1177. DOI: https://doi.org/10.1128/JVI.74.3.1168-1177.2000, PMID: 10627527

Yamashita M, Engelman AN. 2017. Capsid-dependent host factors in HIV-1 infection. *Trends in Microbiology* **25**:741–755. DOI: https://doi.org/10.1016/j.tim.2017.04.004, PMID: 28528781

Yang R, Shi J, Byeon IJ, Ahn J, Sheehan JH, Meiler J, Gronenborn AM, Aiken C. 2012. Second-site suppressors of HIV-1 capsid mutations: restoration of intracellular activities without correction of intrinsic capsid stability defects. *Retrovirology* **9**:30. DOI: https://doi.org/10.1186/1742-4690-9-30, PMID: 22515365

Yang Y, Luban J, Diaz-Griffero F. 2014. The fate of HIV-1 capsid: a biochemical assay for HIV-1 uncoating. *Methods in Molecular Biology* **1087**:29–36. DOI: https://doi.org/10.1007/978-1-62703-670-2_3, PMID: 24158811

Yoo S, Myszka DG, Yeh C, McMurray M, Hill CP, Sundquist WI. 1997. Molecular recognition in the HIV-1 capsid/cyclophilin A complex. *Journal of Molecular Biology* **269**:780–795 . DOI: https://doi.org/10.1006/jmbi.1997.1051, PMID: 9223641

Yu Z, Dobro MJ, Woodward CL, Levandovsky A, Danielson CM, Sandrin V, Shi J, Aiken C, Zandi R, Hope TJ, Jensen GJ. 2013. Unclosed HIV-1 capsids suggest a curled sheet model of assembly. *Journal of Molecular Biology* **425**:112–123. DOI: https://doi.org/10.1016/j.jmb.2012.10.006, PMID: 23079241
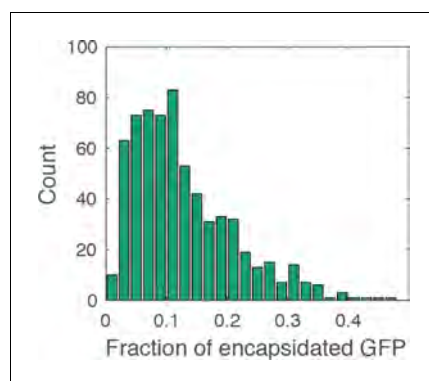
79

Figure 1—figure supplement 1. Histogram of the fraction of encapsidated GFP. The fraction of encapsidated GFP was calculated as the ratio of the GFP intensity associated with the closed capsid (i.e. the mean intensity in the period after membrane permeabilization and before core opening) to the total GFP intensity associated with the viral particle (i.e. the mean intensity before membrane permeabilization). The histogram contains combined data from a total of four repeats using two different viral preparations. The mean fraction of encapsidated GFP is ~13%, similar to the ratio of the volume inside the capsid to the total volume of the viral particle (16%), which was estimated on the basis of the following considerations. Internal volume of the viral particle: The internal virus volume (i.e. excluding the viral membrane and matrix protein layer) has been estimated by cryo-electron tomography (cET) of HIV particles, giving an average value of $V_{particle} = 6.79 \times 10^5$ nm^3 [from **Figure 4**, (**de Marco et al., 2012**)]; this volume corresponds to an internal diameter of 109 nm. Volume of the viral core: The volume of the core was calculated as the volume of an ellipsoid given by $V_{core} = \frac{4}{3} \pi \frac{l}{2} \left(\frac{d_b}{2}\right)^2$, where l is the length of the cone, d_b is the diameter of the broad end. We assumed the following dimensions for the capsid including the CA shell: $l = 109$ nm (i.e. the internal diameter of the virion) and $d_b = 56$ nm (**Briggs et al., 2006**). The internal volume of the capsid was calculated after subtracting twice the thickness of the CA lattice (2×5 nm) from the values for l and d_b, giving $V_{core}^{internal} = 1.10 \times 10^5$ nm^3. The fraction of the internal volume of the capsid relative to the total internal volume of the viral particle is then given by $V_{core}^{internal}/V_{particle} = 16\%$.
DOI: https://doi.org/10.7554/eLife.34772.004
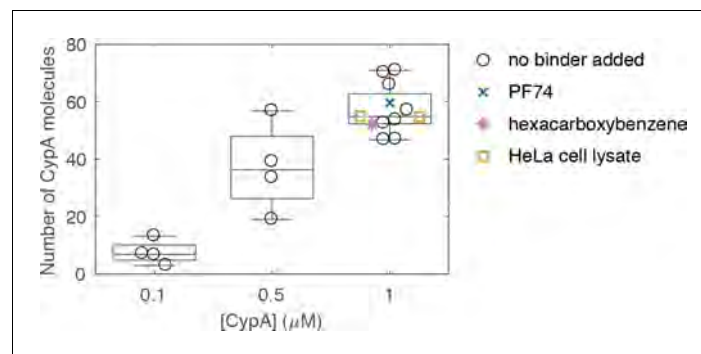
80

Figure 3—figure supplement 1. Variation in the median number of molecules bound at equilibrium per closed capsid measured in independent experiments at different CypA concentrations. Measurements with 1 µM CypA were carried out in the absence and presence of small molecules (PF74 or hexacarboxybenzene) or HeLa cell lysate. Each symbol represents an independent experiment. Experiments were recorded at different times with several different batches of viral particles and on two different TIRF microscopes.

81
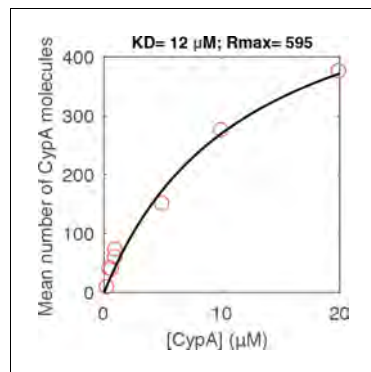
Figure 3—figure supplement 2. Equilibrium binding analysis of CypA binding to capsid. Median number of CypA molecules bound to closed capsids at equilibrium as a function of CypA concentration (vermillion circles) and fit of an equilibrium binding model (black line). The fit gave the following estimates for the interaction: KD = 12 µM; number of CypA-binding sites on the intact capsid ~600. These data were recorded in a repeat experiment for the data shown in *Figure 3E* but with a different batch of viral particles and on a different TIRF microscope.
DOI: https://doi.org/10.7554/eLife.34772.010
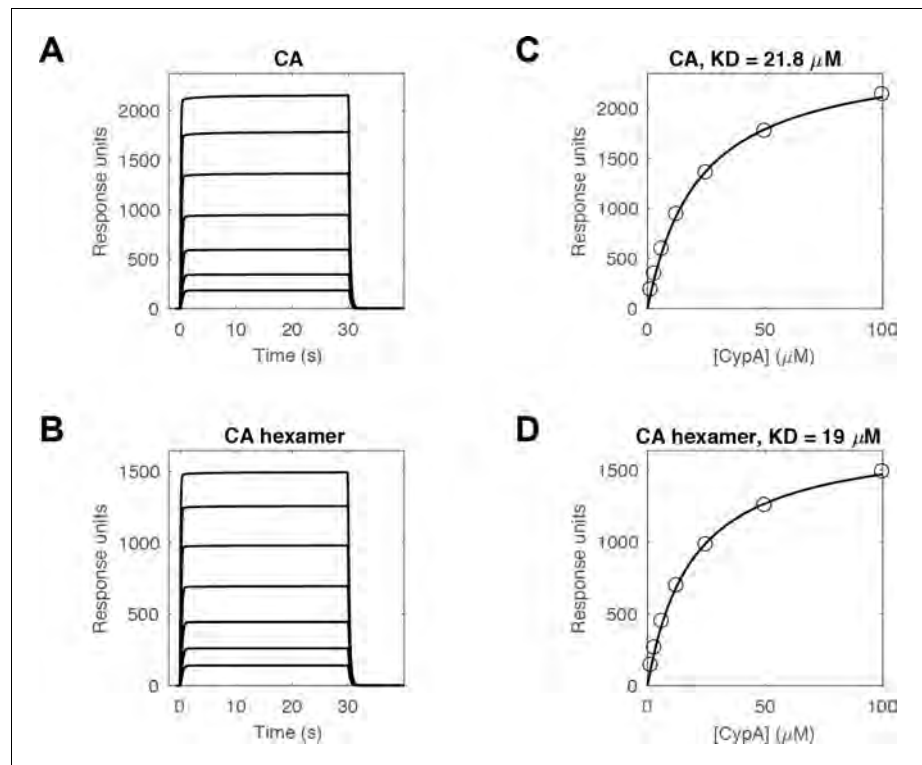
Figure 3—figure supplement 3. SPR measurements of the CypA-CA interaction. (**A**, **B**) SPR traces of CypA binding and dissociation on surfaces modified with (**A**) CA K158C (reacted with a maleimide derivative of biotin) or (**B**) cross-linked CA hexamers (reacted with an NHS ester derivative of biotin) recorded at 1.6, 3.1, 6.3, 12.5, 25, 50 and 100 μM CypA (curves from bottom to top). (**C**, **D**) Response at equilibrium as a function of CypA concentration and fit of a binding model to the data (black line) to obtain the dissociation constant of the CypA interaction with monomeric (C, K_D = 21.8 μM) and hexameric (D, K_D = 19 μM) CA protein.
DOI: https://doi.org/10.7554/eLife.34772.011

83

3.3. Summary

In this chapter, reproduced from the paper "*Kinetics of HIV-1 capsid uncoating revealed by single-molecule analysis*", we described a new method to study HIV capsid uncoating and how capsid disassembly is modulated by different host factors and small molecules. The assay has several advantages:

- Ability to study authentic HIV capsids *in vitro*, utilising small sample volumes in the low µL range
- Hundreds of individual capsids are monitored in a single experiment and analysed as single particles, allowing us to identify intermediates in the disassembly pathway that are averaged out in ensemble experiments
- It allows screening of the effect of several molecules and proteins on capsid stability, as well as the study of their binding kinetics

The new single-particle fluorescence microscopy method allowed us to dissect the uncoating process into two steps, capsid opening and lattice disassembly. We found that spontaneous uncoating is initiated shortly after the viral membrane is compromised and that the first defect in the lattice is the rate-limiting step of uncoating. Once the capsid opens up, the rest of the lattice catastrophically collapses within seconds.

By studying the effect of different host cell factors, small molecules or capsid mutations on capsid stability, we determined that the two uncoating steps can be modulated independently. High concentration of the capsid-binding inhibitor PF74 accelerate capsid opening but strongly stabilise the remaining lattice. Binding of the small molecule hexacarboxybenzene strongly delays initiation of uncoating but do not prevent subsequent lattice disassembly. This same result is obtained with the CA E45A substitution (for lattice disassembly data see supplementary information, **section 8.1**), and with the addition of HeLa cell lysate.

The differential effect produced by the small compounds PF74 and hexacarboxybenzene might reflect how they interact with different surfaces of the viral capsid (**Chapter 3 - Figure 7**), suggesting that different binding pockets modulate the CA lattice stability in different ways. Subsequent chapters present experiments that further dissect how binding of different factors to the $CA_{NTD-CTD}$ hexameric interface (**Chapter 4**) or to the R18 central pore (**Chapter 5**) modulate capsid stability.

Chapter 4

Modulation of HIV-1 capsid stability by binding of factors to the CA_{NTD}-CA_{CTD} hexameric interface

4. Modulation of HIV-1 capsid stability by binding of factors to the CA$_{NTD}$-CA$_{CTD}$ hexameric interface

4.1. Introduction

The CA$_{NTD}$-CA$_{CTD}$ interface has been shown to play an important role in assembly and stabilisation of the HIV-1 capsid [89], [94]. Its flexibility tolerates the curvature in the lattice needed to form the fullerene cone as well as it allows the capsid to accommodate the cellular proteins NUP153 and CPSF6 [75], [95]–[97]. Interaction of these host factors with the capsid is critical for efficient HIV-1 infection. NUP153 depletion reduces 2-LTR circles production and proviral integration, resulting in deficient infectivity [77], [133], [143], [174]. CPSF6 depletion does not interrupt infectivity [143], [147], but decreases viral integration into transcriptionally active genes [78], [184]. Moreover, mislocalisation of CPSF6 to the cytoplasm reduces the translocation of the HIV-1 genetic material into the nucleus inhibiting infection [95], [142], [143], [147]. Interestingly, the small molecule inhibitors PF74 and BI-2 also interact with the CA$_{NTD}$-$_{CTD}$ interface [96], [98], [194]. PF74 modulates HIV-1 infection in a concentration-dependant manner. At high concentrations (>10 µM) reverse transcription is inhibited and infectivity is completely abolished, while at low concentrations (<1.5 µM) infectivity is reduced by ~90% but the production of viral cDNA is not supressed [97], [98], [115], [192]. PF74 has also been shown to block nuclear entry and reduce integration in gene-dense regions [135], [191]. On the other hand, BI-2 greatly decreases HIV-1 infection but it does not disturb the production of early or late RT products at any concentration [137], [194].

How the interaction of these molecules with the CA$_{NTD}$-CA$_{CTD}$ interface relates to defects in different steps of HIV-1 entry is not clear, but understanding their influence on capsid stability could help find the answer. Previous studies have shown that CPSF6 binding promotes stabilisation of authentic cores and *in vitro* assembled CA-NC complexes [108], [142], although a recent investigation found that CPSF6 disrupts CA tubes into small fragments and that its binding to the capsid in the cytoplasm of infected cells induces premature uncoating [183]. Intriguingly, there have also been contradictory observations of the effect of PF74 and BI-2 on CA lattices. They stabilise HIV-1 CA-NC complexes in a concentration dependent manner, but reduce HIV-1 core recovery from infected cells as well as accelerate uncoating of the isolated capsids [96], [108], [115], [160], [192]. While structural information of the specific interaction between CA and CPSF6, PF74 and BI-2 is available, the ambiguity in their mode of

action requires more detailed studies to understand the mechanistic basis of their restriction on HIV-1 infection.

In Chapter 3, we revealed that a high concentration of PF74 accelerates capsid opening and that at the same time stabilises the remaining lattice (**Chapter 3, Figures 2 and 5**). These results may explain the previous conflicting data, since we demonstrated that PF74 stabilises CA lattices but in a manner that makes it incompatible with a closed structure. The aim of this chapter is to further unravel the effect of PF74 over a wide range of concentrations as well as other molecules that bind to the same binding pocket (BI-2 and CPSF6) on capsid stability. Furthermore, we will study the binding kinetics of $CPSF6_p$ to the HIV-1 capsid and determine how CPSF6 and PF74 compete for binding to authentic HIV-1 capsids.

4.2. Low PF74 and high CPSF6$_p$ concentrations mildly accelerate capsid opening

In Chapter 3 we showed that when used in high concentrations of >40-fold of their estimated dissociation constants to CA hexamers, the small drugs PF74 (K_D = 0.26 µM [96], K_D = 0.12 µM [97], K_D = 0.021-0.078 µM [186]) and BI-2 (K_D = 1.2 µM [97]) accelerate the opening of the HIV-1 capsid by 12-fold and 3-fold respectively (**Chapter 3, Figure 2**). Based on the concentration-dependency inhibitory effect shown by PF74 [97], [160], [191], we decided to study how a lower concentration of the antiviral drug affects capsid opening. Additionally, we used the capsid opening assay to assess the effect of the minimal binding epitope for interaction with CA of the host protein cleavage and polyadenylation specificity factor-6 (CPSF6$_{313-327}$ or CPSF6$_p$) [146], since it binds to the same binding surface as PF74 and BI-2. GFP-loaded HIV-1 viral particles captured onto a glass coverslip were permeabilised by injecting a solution containing the pore-forming protein PFO and 1 µM PF74 or 100 µM CPSF6$_p$. The fluorescence intensity of GFP was tracked over 30 minutes by time-lapse total internal reflection fluorescence (TIRF) microscopy. The time of membrane permeabilisation and capsid opening were identified for each viral particle and the capsid opening time was calculated as the difference between them.

Consistent with what was shown in Chapter 3, three different populations of viral particles are detected (**Figure 4.1A**). The fraction of capsids that are leaky and release the GFP molecules in one step varied from 60 to 70% when 1 µM PF74 and 100 µM CPSF6$_p$ are used. These values are comparable to the leaky proportion obtained with untreated viral particles and with particles incubated with 10 µM PF74 and 50 µM BI-2. This observation supports the interpretation that leaky capsids are intrinsically defective cores and that they are not disturbed by the capsid binder used. The other ~30-40% of viral particles contain properly assembled capsids that retain a fraction of the GFP within it, and that can either undergo uncoating or remain closed during the experiment. The fraction of closed capsids observed at 30 min after addition of PFO (~9-25% closed particles for untreated particles) decreased in the presence of molecules that bind to the CA$_{NTD}$-CA$_{CTD}$ binding groove to 3-20% in the presence of PF74 (1 µM) and ~1-8% in the presence of CPSF6$_p$ (100 µM). These results suggest that 1 µM PF74 and 100 µM CPSF6$_p$ promote HIV-1 capsid opening, consistent with the effect produced by high concentrations of PF74 and BI-2.
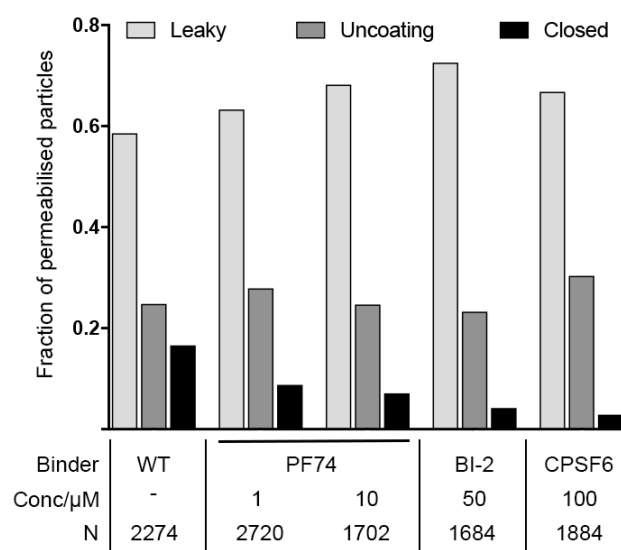
Figure 4.1. Leaky, opening and closed capsids in presence of CA$_{NTD-CTD}$ binders.
Bar chart showing the fraction of capsids classified as 'leaky', 'opening' and 'closed' present 30 min after permeabilisation of the viral membrane of biotinylated HIV-1 viral particles containing free GFP in presence of PF74 (1 and 10 µM), BI-2 (50 µM) and CPSF6$_p$ (100 µM). The data was combined from multiple measurements (total number of repeats/number of viral preparations): No binder (3/2); PF74 - 1 µM (5/4); PF74 - 10 µM (4/2); BI-2 - 50 µM (4/3); CPSF6$_p$ - 100 µM (4/3).

To calculate the capsid opening half-life in the presence of 1 µM PF74 or 100 µM CPSF6$_p$, we fitted the survival curves obtained with the core opening times of capsids that undergo uncoating during the experiment for each condition (**Figure 4.2**). Survival curves of untreated capsids and capsids treated with 10 µM PF74 and 50 µM BI-2 are shown for comparison. Interestingly, the 1 µM PF74 survival curve showed a faster decay than the untreated capsids, but a slower decay than that measured in the presence of 10 µM PF74. The calculated capsid opening half-life in the presence of 1 µM PF74 was 4.04 minutes; just 1.9-fold lower than the control and 6-fold higher than the half-life obtained in the presence of 10 µM PF74, indicating that that the acceleration of capsid opening is concentration dependent.

Capsids incubated with 100 µM CPSF6$_p$ showed a similar capsid opening behaviour to capsids treated with 1 µM PF74. The survival curve showed a slight shift to shorter times compared to untreated capsids (**Figure 4.2**) and the estimated capsid opening half-life was 4.4 minutes. This result indicates that the presence of CPSF6$_p$ at a

concentration in the same range as its K_D for binding to CA hexamers (K_D = 83-100 µM [96], K_D = 50 µM [155], K_D = 12-17 µM [186]) weakly accelerates capsid opening. This effect was similar to the one obtained with 1 µM PF74 (K_D = 0.26 µM [96], K_D = 0.12 µM [97], K_D = 0.021-0.078 µM [186]).
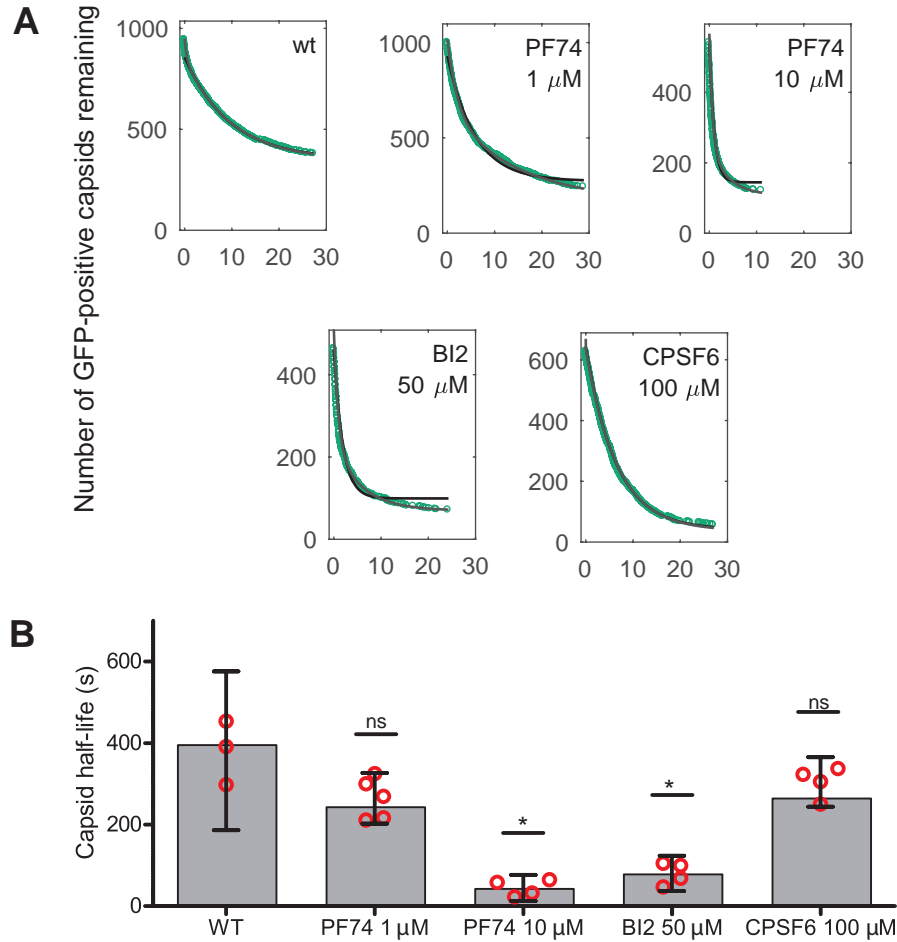
Figure 4.2. Capsid opening in presence of CA$_{NTD-CTD}$ binders. (A) Survival curves obtained from capsids that undergo opening on multiple experiments in presence of PF74 (1 and 10 µM), BI-2 (50 µM) and CPSF6$_p$ (100 µM). Exponential fit (black line) is shown in each graph. **(B)** Half-lives of capsid opening determined by fitting of each survival curve from individual repeats with a mono-exponential decay function. The error bars represent 95% confidence intervals; unpaired t-test with Welch's correction.

In summary, the results obtained with the capsid opening assay indicate that binding of molecules to the CA$_{NTD}$-CA$_{CTD}$ hexameric interface perturbs capsid stability and promotes an acceleration of capsid opening. PF74 alters capsid stability in a concentration-dependant manner. When used at concentration in the range of their

respective K_D, CPSF6$_p$ and PF74 have similarly weak effect on capsid opening. Taken together, these observations suggest that higher concentrations of CPSF6 could potentially lead to a pronounced acceleration of capsid opening.

4.3. PF74 and CPSF6$_p$ stabilise the CA lattice in a concentration-dependent manner

In the previous chapter, we presented that even though the addition of 10 µM PF74 lead to a pronounced acceleration of capsid opening, the remaining lattice was highly stabilised (**Chapter 3, Figure 5**). To delve more deeply into the mechanism of action of PF74, we conducted the CypA paint experiment in the presence of different concentrations of the small drug ranging 0.1-10 µM. We also assessed the effect of 50 µM BI-2 and of varying concentrations of CPSF6$_p$ (1-100 µM) on the kinetics of lattice disassembly. To do so, attached HIV-1 viral particles were permeabilised using microfluidic delivery of a mixture of PFO, the compound of interest and 1 µM 568-CypA to paint the viral capsid. Content (GFP) and the paint (AF568-CypA) markers were followed for ~13 minutes (1 frame per second for 800 frames) by time-lapse TIRFM with alternating fluorescence excitation. Fluorescence intensity traces were extracted for both channels and traces were sorted into disassembly categories (leaky, opening or closed) on the basis of the GFP signal.

A representative data set of leaky capsids for each condition is shown in **Figure 4.3**. In all cases the median CypA binding trace (generated after aligning all traces for particles with leaky capsids at the time of membrane permeabilisation) showed a rapid increase in the CypA paint signal upon membrane permeabilisation, consistent with the presence of an at least partially assembled capsid lattice. The subsequent decay of the CypA paint signal revealed pronounced differences in the kinetics of capsid lattice disassembly (**Figure 4.3, black lines**), whereby the CA lattice was increasingly stabilised (slower disassembly kinetics) with increasing PF74 or CPSF6$_p$ concentrations (**Figure 4.3B-C**).
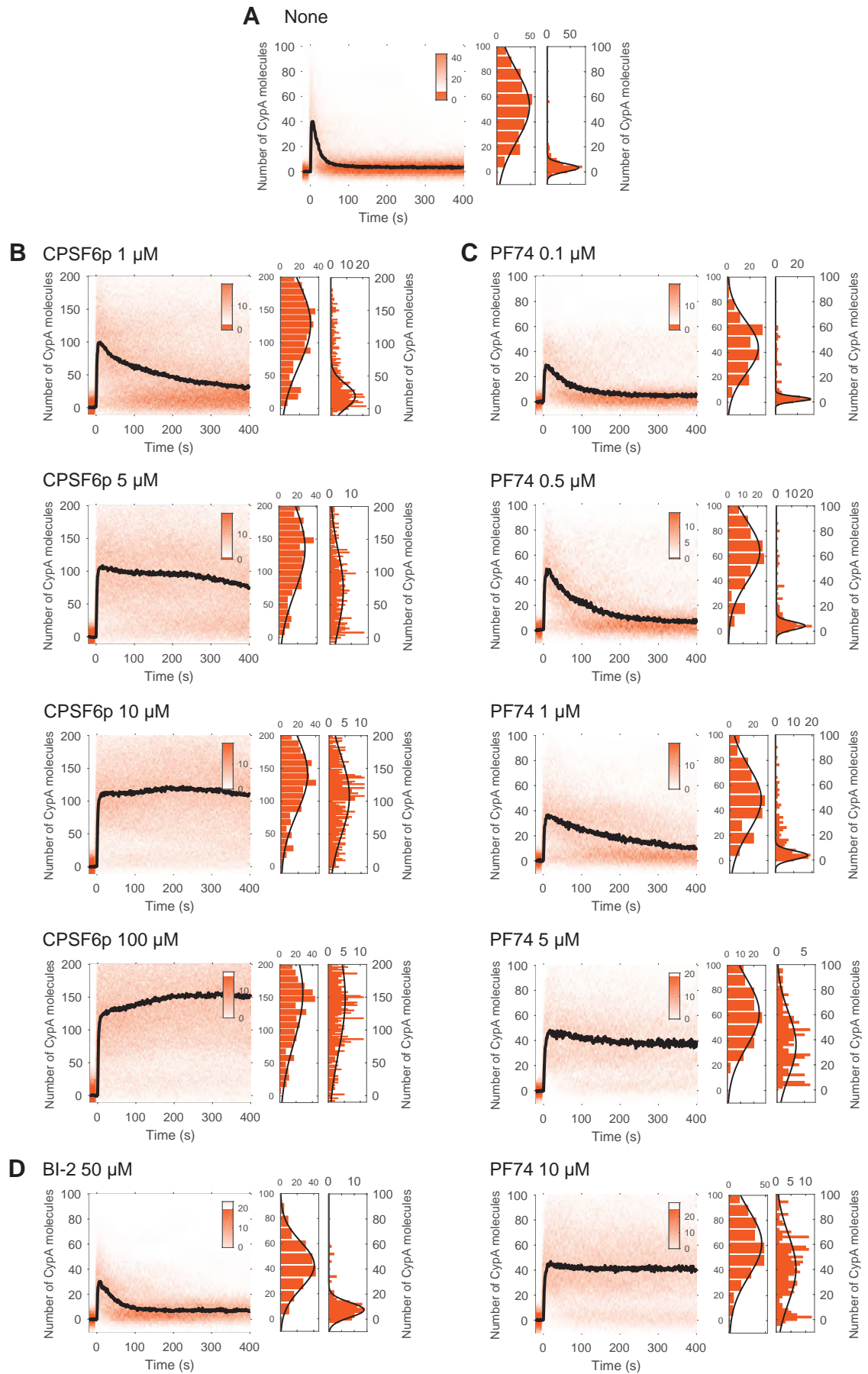
A None

B CPSF6p 1 µM

CPSF6p 5 µM

CPSF6p 10 µM

CPSF6p 100 µM

C PF74 0.1 µM

PF74 0.5 µM

PF74 1 µM

PF74 5 µM

D BI-2 50 µM

PF74 10 µM

Figure 4.3. Lattice disassembly kinetics of leaky capsids in presence of $_{CANTD-CTD}$ binders. Heatmap of AF568-CypA binding traces (vermillion) to all leaky capsids in a field of view aligned with respect to the time of envelope permeabilisation ($t_P = 0$). Each heatmap is a representative data set of **(A)** untreated viral particles, or in presence of different concentrations of **(B)** CPSF6$_p$, **(C)** PF74, and **(D)** BI-2. The bold black line represents the median CypA binding trace. The histograms at the right show the distribution of intensities at t_P = 1-30 s and 380-400 s, respectively.

At the lowest PF74 concentration (0.1 µM) the CypA paint signal reached the background level within 100-200 s after membrane permeabilisation compared to within 50 s in the absence of PF74. Complete stabilisation of the lattice was observed for PF74 concentrations ≥5 µM. In an independent data set (**Supplementary Figure 8.2**) complete stabilisation was observed with 1 µM PF74. The differences between the two data sets could be due to experimental error related to pipetting of small volumes and/or the insolubility of PF74. The concentration dependence of capsid stabilisation with CPSF6$_p$ was similar to that observed with PF74, whereby complete stabilisation of the CA lattice was achieved at 5 µM CPSF6$_p$. An independent data set showing the same outcome is provided in the supplementary section for comparison (**Supplementary Figure 8.3**). Intriguingly, 50 µM BI-2 is unable to prevent the collapse of the leaky capsids, as seen from the CypA paint signal decay (**Figure 4.3D**).

The same effect of molecules binding at CA$_{NTD}$-CA$_{CTD}$ hexameric interface on lattice disassembly kinetics that was observed for leaky capsids was also for capsids that undergo opening during the experiment (**Figure 4.4**). CypA binding traces aligned at the time of membrane permeabilisation (left panel) showed a rapid increase in the CypA paint signal. Comparison of the number of AF568-CypA molecules bound at equilibrium to the closed capsid (i.e. after membrane permeabilisation but before capsid opening) showed that the level of CypA paint was independent of the compound used to modulate capsid stability (**Figure 4.5**). CypA paint traces aligned at the time of capsid opening revealed that CA lattice was stabilised in a concentration-dependant manner. Capsid disassembly was considerably slowed down at 1 µM PF74 and capsids did not disassemble when exposed to 5 µM or 10 µM PF74. Similarly, 1 µM CPSF6$_p$ showed a modest stabilising effect on the CA lattice after capsid opening, which increased with increasing concentrations of the peptide (**Figure 4.4B**). As observed for leaky capsids, BI-2 was unable to stabilise the CA lattice even when it is

used at a high concentration (**Figure 4.4D**). This result may explain why BI-2 has been shown to be a less potent inhibitor than PF74 [192] and could reflect a difference in their binding to the $CA_{NTD-CTD}$ interface.
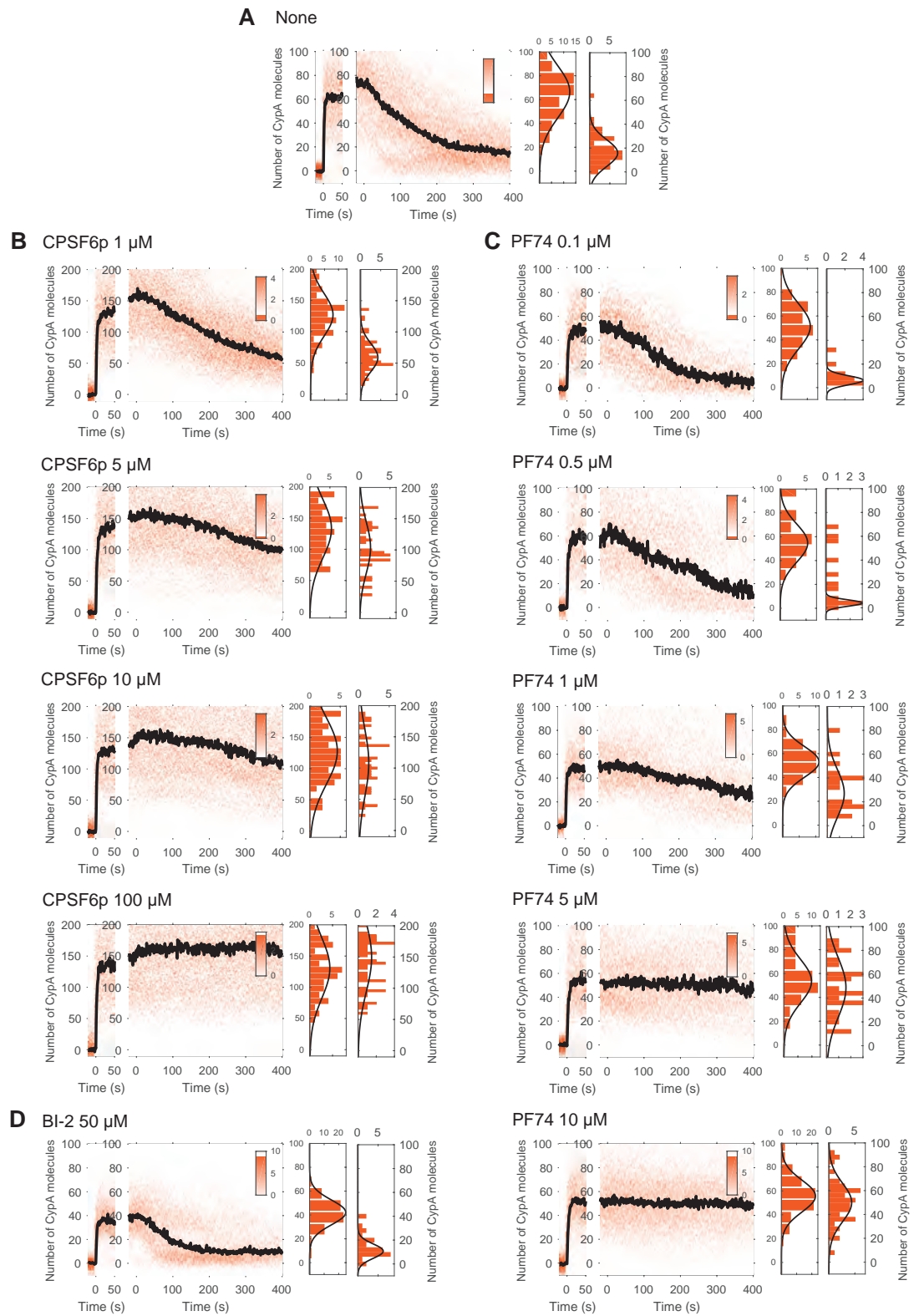
Figure 4.4. Lattice disassembly kinetics of capsids that undergo disassembly in presence of CA$_{NTD-CTD}$ binders. Heatmap of AF568-CypA binding traces (vermillion) to all capsids that undergo disassembly in a field of view aligned with respect to the time of envelope permeabilisation (t_P = 0, left panel) and aligned with respect to capsid opening (right panel). Each heatmap is a representative data set of **(A)** untreated viral particles, or in presence of different concentrations of **(B)** CPSF6$_p$, **(C)** PF74, and **(D)** BI-2. The bold black line represents the median CypA binding trace. The histograms at the right show the distribution of intensities after binding equilibrium is reached (t_P = 10-30 s) and at the end of lattice disassembly (t_O = 380-400 s).

Figure 4.5. Number AF568-CypA bound at equilibrium in presence of CA$_{NTD-CTD}$ binders. Variation in the median number of CypA molecules bound at equilibrium per closed capsid measured in the absence and presence of different concentrations of BI-2, PF74, and CPSF6$_p$. All experiments were carried out using 1 µM AF568-CypA for painting. The error bars represent 95% confidence intervals.

To determine if the stabilising effect produced by the highest concentrations of PF74 and CPSF6$_p$ in the CA lattice is maintained, we repeated the same experiment for a longer period of time. Images were acquired every 6 seconds for a total of 88 minutes to limit the exposure of the sample to excessive laser energy, which may bleach the sample or induce photochemical cross-linking (**Figure 4.6**). 10 µM PF74 and 100 µM CPSF6$_p$ stabilised the CA lattice of both leaky and capsids that undergo uncoating for at least 80 minutes. The CypA paint signal showed only a small decrease for both capsid binders over that period of time (Figure 4.6, compare histograms of the number of CypA molecules shortly after membrane permeabilisation [left] with the

corresponding histograms at the end of the experiment [right]). These data suggest that lattice disassembly is dramatically slowed down in the presence of PF74 or CPSF6. Independent data sets (**Supplementary Figure 8.4**) show a slight decrease on the paint signal over time, although a similar decay is observed for capsids that remain closed during the entire experiment suggesting that bleaching of the fluorescent dye and/or increase of unspecific paint binding to the glass surface are affecting the signal detection.

We conclude that PF74 and CPSF6$_p$ stabilise the CA lattice after the capsid has opened up in a concentration-dependent manner and that the stabilising effect persists for as long as the molecules stay bound to the lattice.
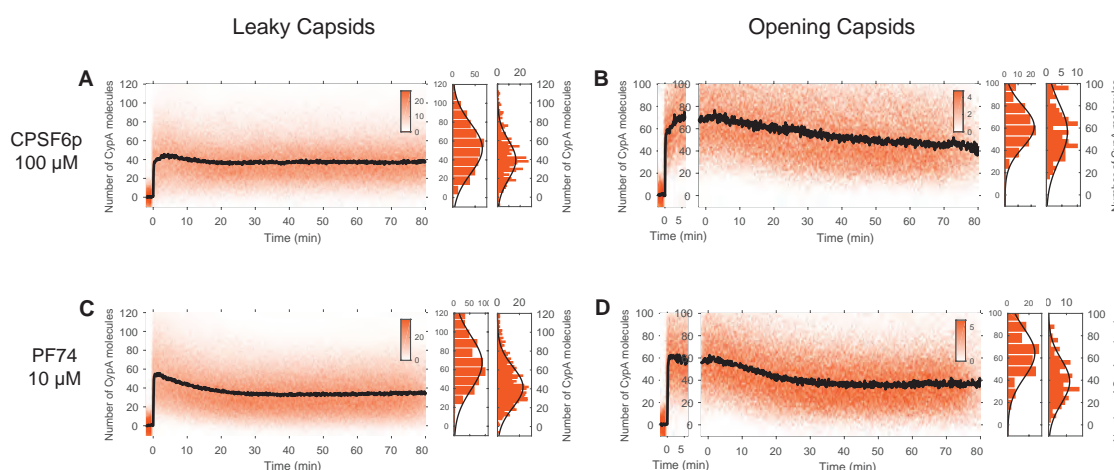
Figure 4.6. Long lattice disassembly kinetics in presence of PF74 and CPSF6$_p$. Heatmap of AF568-CypA binding traces to all leaky capsids (**A** and **C**) and to capsids that undergo disassembly (**B** and **D**) within 80 minutes in presence of 10 µM PF74 and 100 µM CPSF6$_p$. Each histogram at the right show the distribution of intensities after binding equilibrium is reached (t_P = 1-3 min) and at the end of lattice disassembly ($t_{p/O}$ = 78-80 min).
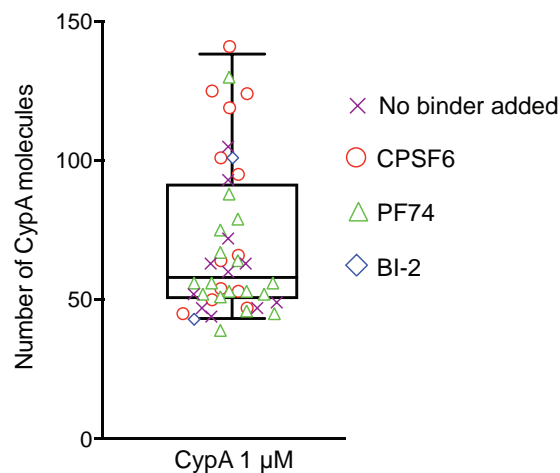
To study whether the stabilising effect on the CA lattice is lost upon dissociation of the CA$_{NTD-CTD}$ binder, we carried out a washout experiment. A solution of PFO plus 10 µM PF74 was injected into a microfluidic channel with attached HIV-1 viral particles. Images were acquired every 5 seconds for ~13 minutes. Next, buffer containing 1 µM AF568-CypA was flushed into the channel in order to dissociate the bound PF74 molecules from the CA lattice and paint it for its visualisation (**Figure 4.7**). AF568-CypA binding to closed capsids reached the same level than on previous experiments (~70

molecules bound at equilibrium), indicating that CypA interact with the fully closed CA lattice as usual. As expected, AF568-CypA also bind to leaky capsids and capsids that opened while they were exposed to PF74, indicating the presence of assembled CA lattice. The extent of lattice present after ~13 minutes of incubation with PF74 corresponds to previous observations using simultaneous painting (compare with **Figure 4.6C-D**). Intriguingly, the CA lattice of both leaky and capsids that undergo uncoating remained stable for at least 250 s after the PF74 washout. This slower rate of CA lattice disassembly than spontaneous uncoating could be due a deficient PF74 dissociation from the assembled CA lattice. Indeed, slower dissociation rate of PF74 from assembled CA hexamers compared to the CA monomer has been observed before [186], although the expected half-life derived from this work is 8-58 seconds (K_{off} = 0.012 - 0.12 s^{-1}).

Figure 4.7. PF74 wash-out. Heatmap of AF568-CypA binding traces algned at the time of paint addition of all **(A)** leaky, **(B)** closed, and **(C)** capsids that undergo disassembly in presence of 10 µM PF74 for ~13 minutes.

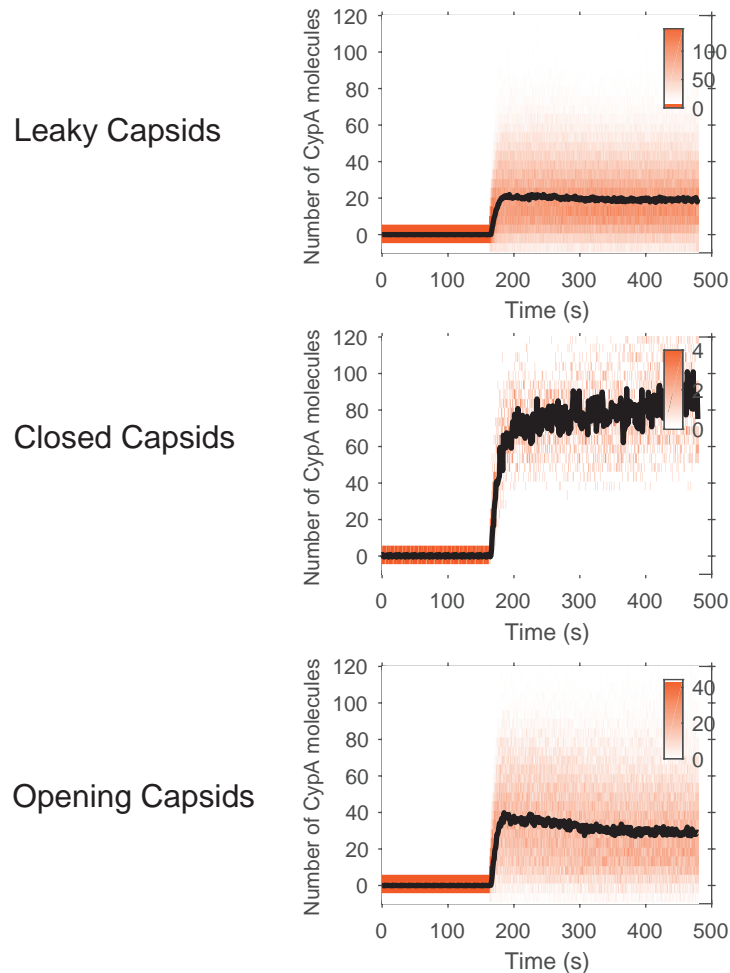## 4.4. CPSF6$_p$ binds to the HIV-1 capsid with higher affinity than previously reported

CPSF6$_p$ has been shown to bind with higher affinity to CA hexamers than to unassembled CA, although the reported value for the K$_D$ of this interaction differ between different experiments, ranging 360-1170 μM to CA$_{NTD}$, 26-436 μM to CA, and 12-100 μM to CA hexamers [95], [96], [155], [185], [186]. The affinity of CPSF6$_p$ for a fully assembled conical HIV-1 CA lattice has not yet been determined. Here, we use our imaging assay with permeabilised viral particles to measure the binding of labelled CPSF6 peptide to intact capsids to determine the dissociation constant of this interaction.

We labelled a version of the CPSF6 peptide that contains an extra cysteine at the C-terminus (CPSF6$_p$-Cys) with Alexa-Fluor 568-C5-maleimide dye. Different concentrations of labelled CPSF6 peptide (CPSF6$_p$-Cys-AF568) were injected together with the pore former protein into a microfluidic channel containing attached HIV-1 viral particles carrying GFP. Binding of the CPSF6$_p$-Cys-AF568 to viral capsids was followed using TIRF microscopy with alternating fluorescence excitation. Images were acquired every second for 800 seconds.

A series of snapshots of CPSF6$_p$-Cys-AF568 binding are shown in **Figure 4.8**. Similar to AF568-CypA binding, upon membrane permeabilisation of the viral particle, a bright diffraction-limited spot appeared in the CPSF6$_p$-Cys-AF568 channel at each location corresponding to viral particle (**Figure 4.8A-B**). Individual traces recorded at these locations (**Figure 4.8C-D**) showed that the CPSF6$_p$-Cys-AF568 signal rapidly increased immediately after release of the GFP contained by the viral membrane. Heatmaps and median traces of CPSF6$_p$-Cys-AF568 binding to leaky capsids and capsids that undergo uncoating are shown in **Figure 4.8E-F**. The number of peptides bound to individual capsids was obtained by calibrating the fluorescence intensity with a value obtained from single-molecule photobleaching experiments. In the case of leaky capsids, the median CPSF6$_p$-Cys-AF568 signal trace decayed rapidly after the initial increase as a result of the lattice disassembly (**Figure 4.8E**). For capsids categorized as "opening" or "closed", the CPSF6$_p$-Cys-AF568 signal stayed constant at an equilibrium level as long as the capsid remained fully intact. Once the capsid opened up, the CPSF6$_p$-Cys-AF568 signal decayed until it reached a stable level above background (**Figure 4.8F**). We conclude that CPSF6$_p$-Cys-AF568 binds to the CA lattice to a level that is proportional to the size of the lattice (i.e. the number of CA subunits in the lattice) similarly to what was observed for AF568-CypA.
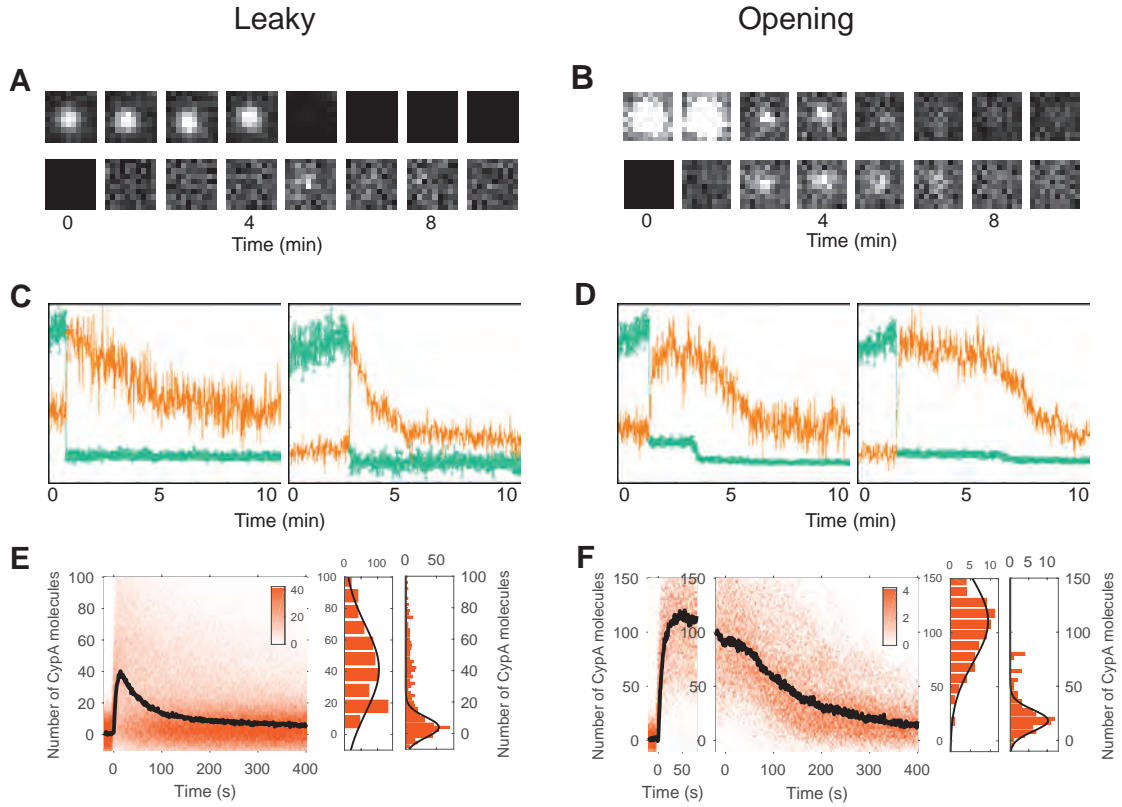
Figure 4.8. Kinetics of CPSF6$_p$ binding. Snapshots of the GFP signal and CPSF6$_p$-Cys-AF568 signal of selected viral particles with **(A)** leaky capsids and **(B)** capsids that undergo uncoating during the experiment at different times. Example traces of CPSF6$_p$ binding (vermillion) to individual **(C)** leaky capsids and **(D)** capsids that undergo uncoating after permeabilisation of the viral envelope. Heatmap of AF568- CPSF6$_p$-Cys binding traces to all **(E)** leaky capsids and **(F)** capsids that undergo uncoating in a field of view aligned with respect to the time of envelope permeabilisation ($t_P = 0$) and to capsid opening ($t_O = 0$). Each heatmap is a representative data set of different repetitions. The bold black line represents the median CypA binding trace. The concentration of CPSF6$_p$-Cys-AF568 was 1 µM in all the experiments. Each histogram at the right show the distribution of intensities after binding equilibrium is reached ($t_P = 1$-30 s) and at the end of lattice disassembly ($t_O = 380$-400 s).

To obtain an estimate of the dissociation constant (K_D) for the CPSF6$_p$-capsid interaction, we extracted CPSF6$_p$-Cys-AF568 binding curves from capsids that remain intact for at least 50 seconds. Different concentrations ranging 0.1 and 10 µM of the peptide were assessed (note that measurements above 1 µM were obtained with a mixture of labelled and unlabelled peptide to avoid excessive background fluorescence

intensities). Traces were aligned at the time of membrane permeabilisation and a representative median CPSF6$_p$-Cys-AF568 binding trace for each concentration is shown in **Figure 4.9A**. Fitting of the median number of CPSF6$_p$ molecules bound at equilibrium as a function of CPSF6$_p$ concentration with an equilibrium binding model (**Figure 4.9B**) gave an estimate of the K$_D$ of 3.4 ± 0.252 µM. This value is 13-fold lower than reported by Zhou *et al.* [155], 25-fold lower than reported by Bhattacharya *et al.* [96], and 4-fold lower than reported by Lad *et al.* [186] for CPSF6$_p$ binding to hexamers. The estimated number of bound peptides at saturation is 450 ± 17, roughly one third of the total CA$_{CTD-NTD}$ binding sites were the peptide could potentially bind. This observation suggests that at saturation the capsid can just accommodate two CPSF6 peptides on each CA hexamer.
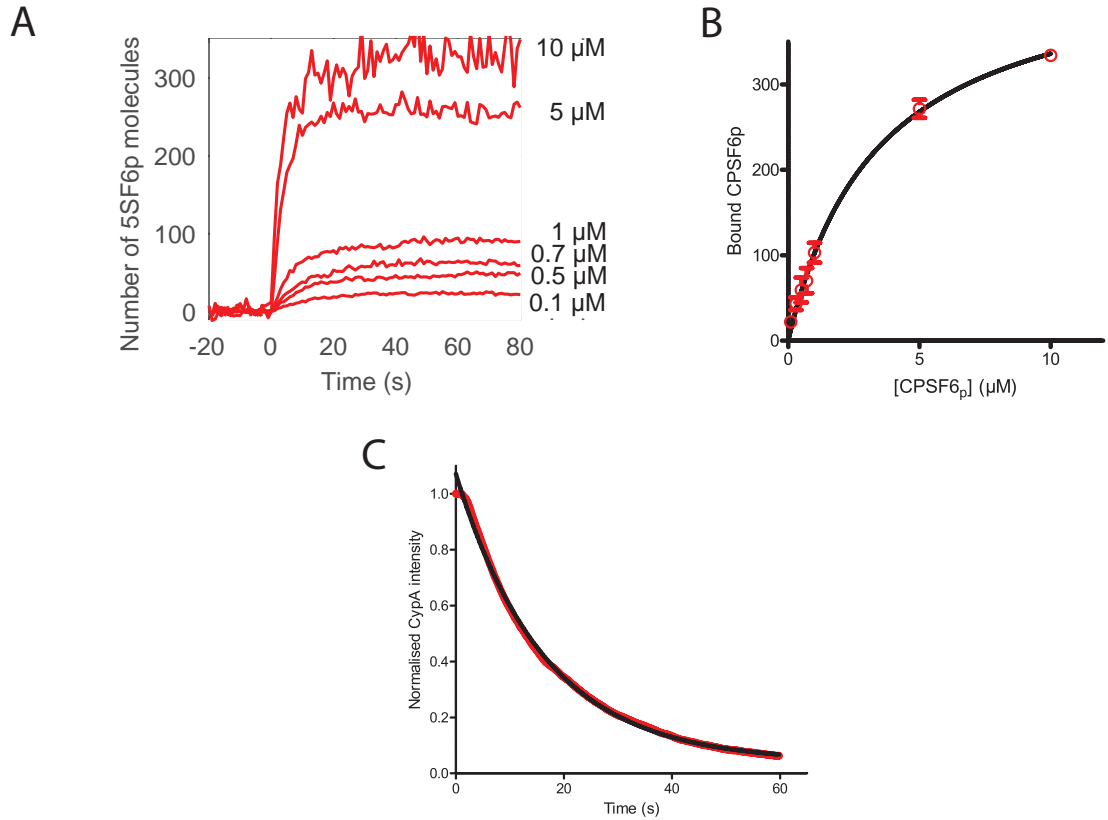
Figure 4.9. Kinetics of CPSF6$_p$ binding to closed capsids. (A) Median CPSF6$_p$-Cys-AF568 binding traces to all closed capsids in the field of view aligned with respect to the time of envelope permeabilisation (t$_P$ = 0) at concentrations ranging from 0.1 to 10 µM as indicated above the corresponding trace. Binding experiments with concentrations above 1 µM were carried out with a mixture of unlabelled and labelled CPSF6$_p$, whereby the concentration of the labelled CypA was kept at 1 µM. **(B)** Median number of CPSF6$_p$-Cys-AF568 molecules bound at equilibrium as a function of CPSF6$_p$ concentration recorded for different experiments. Black line corresponds to the

fit of the data using an equilibrium binding model. **(C)** Mean CPSF6$_p$ intensity measured at closed capsids after wash-out of CPSF6$_p$ from the flow channel at t = 0. The black line represents a fit of the data with an exponential decay function.

A wash-out experiment was performed to measure the kinetics of CPSF6$_p$ dissociation from the CA lattice. HIV-1 viral particles were permeabilised in presence of 1 µM CPSF6$_p$-Cys-AF568 to allow binding and then the fluorescent peptide was removed by rapidly exchanging the solution with buffer. The decay of the mean fluorescence intensity measured on closed capsids at the moment of wash-out is shown in **Figure 4.9C**. The determined off-rate of CPSF6$_p$ is 0.061 s^{-1}, suggesting again an at least 5-fold tighter binding of the peptide to the capsid than previously reported [186].

4.5.   CPSF6$_p$ competes with PF74 for binding to the HIV-1 capsid

PF74 binds to the CA$_{NTD}$-CA$_{CTD}$ interface with high affinity, displaying a K$_D$ to CA hexamers that varies from 0.02 to 0.26 µM [96], [97], [186]. This value is at least 15-fold lower than the dissociation constant obtained with our assay for CPSF6$_p$ (**Figure 4.9B**). To visualise how PF74 competes with CPSF6$_p$ for capsid binding, HIV-1 viral particles were incubated with PFO in presence of 1 µM PF74 and 1 µM CPSF6$_p$-Cys-AF568. TIRF images were acquired and fluorescent traces from the CPSF6$_p$ signal were extracted to analyse its binding (**Figure 4.10**). As expected, CPSF6$_p$-Cys-AF568 binding was decreased in presence of 1 µM PF74. The mean number of bound CPSF6$_p$-Cys-AF568 to closed capsids at equilibrium in presence of 1 µM PF74 is 20.67 (± 5.487, n=3), about ~ 22% of the number of molecules that bind when no binder is added (92.22 ± 7.713, n=9). This result supports the tighter affinity of CPSF6$_p$ to the HIV-1 viral capsid found with our method because otherwise its binding would have been completely abolished by the presence of µM PF74. Indeed, that outcome is observed when the experiment is repeated in presence of 10 µM PF74 (**Figure 4.10C**).
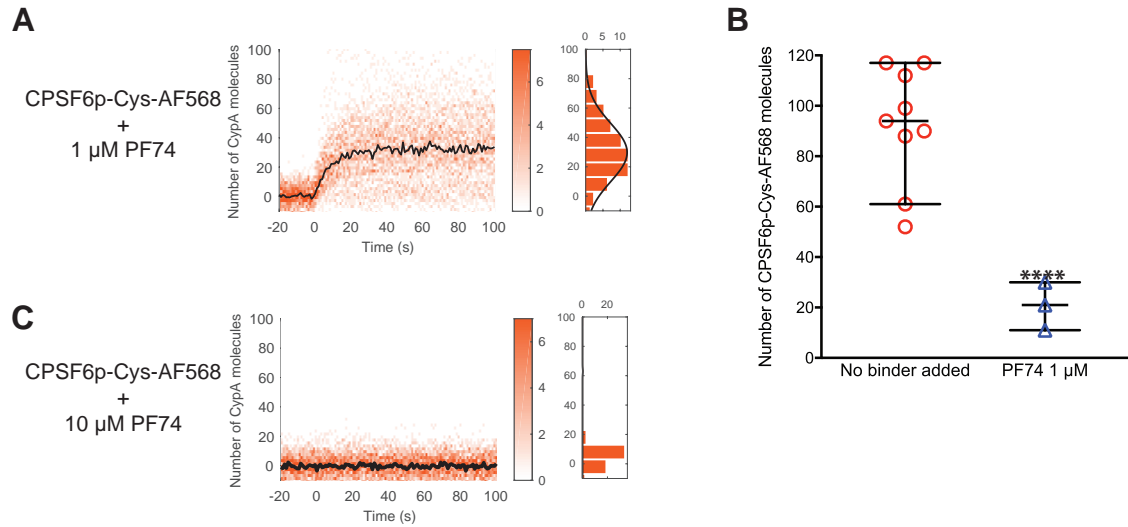
Figure 4.10. Competition between CPSF6$_p$ and PF74 for capsid binding. Heatmap of CPSF6$_p$-Cys-AF568 binding traces to all closed capsids in a field of view aligned with respect to the time of envelope permeabilisation ($t_P = 0$) in presence of **(A)** 1 µM and **(C)** 10 µM PF74. The concentration of CPSF6$_p$-Cys-AF568 used in every experiment was 1 µM. Each histogram at the right show the distribution of intensities after binding equilibrium is reached ($t_P = 30-50$ s). Each heatmap is a representative data set of different repetitions. **(B)** Variation in the median number of CPSF6$_p$-Cys-AF568 molecules bound at equilibrium per closed capsid measured in the absence and presence of 1 µM PF74. The error bars represent 95% confidence intervals; unpaired t-test with Welch's correction, p<0.0001.

4.6.   Discussion

The host cell protein CPSF6, and the small inhibitors PF74 and BI-2 have been shown to interact with the $CA_{NTD\text{-}CTD}$ hexameric interface of the HIV-1 capsid and modulate its stability, although their influence is still puzzling. Previous studies reported that addition of PF74 and BI-2 reduce stability of HIV-1 cores but increase stability of *in vitro* CA assemblies [96], [108], [115], [160], [192]. Similarly, CPSF6 has been shown to accelerate and delay uncoating in infected cells, as well as to stabilise HIV-1 CA-NC complexes [108], [142], [183]. Here, by using our new single-particle fluorescence microscopy method we determined that binding of these molecules modulate the opening of the capsid and the disassembly of the lattice thereafter independently. PF74 accelerates capsid opening and stabilises the remainder of the CA lattice in a concentration-dependant manner. 1 µM PF74 leads to a 2-fold increase in the capsid opening kinetics while 10 µM accelerates it by 12-fold. When used at < 1 µM, PF74 has little effect on the rate of lattice disassembly after the capsid has opened up, but higher concentrations strongly stabilise the CA lattice, preventing completely its collapse at 1-5 µM. Binding of the minimal binding epitope of CPSF6 to the capsid ($CPSF6_p$) also modulates uncoating in a concentration-dependent manner. 100 µM $CPSF6_p$ produce a comparable effect than 1 µM PF74 in the capsid opening, accelerating its kinetics by 2-fold. However, it exerts the same stabilising effect on the CA lattice at just 10 µM. In contrast, 50 µM BI-2 accelerates capsid opening by 3-fold, but fails to stabilise the rest of the CA lattice after the capsid has suffered its first defect.

How do PF74 and CPSF6 exert opposing effects on capsid opening and lattice disassembly? The interface in which they bind could be the key to explain their effect. The interaction between neighbouring CA proteins within the hexamer is weak and flexible, allowing conformational variations within the hexamers and pentamers that tolerate the curvature needed to form the closed capsid [89], [94], [97]. Binding of a molecule to the $CA_{NTD\text{-}CTD}$ interface could strengthen this link. In the absence of binders, the CA lattice disassembles catastrophically once the first defect has opened in the capsid. However, in the presence of PF74 or CPSF6 peptide, no great extent of CA dissociation is observed, possible because the bound molecules reinforce the interaction between neighbouring CA subunits in the hexamer by interacting with both of them (Chapter 3, Figure 7). However, if the capsid is exposed to high concentrations of that molecule, occupancy of many binding pockets at the same time could lead to increased stiffness of the structure, which would in turn limits the flexibility necessary to sustain highly curved sections. Extreme rigidity could lead to a breakage of the

fullerene cone, probably at sections of the capsids with high curvature. Recently published research supports this model. Rankovic *et al.* found that PF74 increases the stiffness of isolated cores in a concentration dependant-manner and that the capsids open at or near the narrow end. However, in their system the fracture happens a few hours after the capsid is exposed to PF74 [212], unlike in our experiments where opening occurs rapidly.

The three CA-binders modulate capsid opening and lattice disassembly to different levels. Their crystal structures in complex with CA hexamers reveal that they occupy the $CA_{NTD-CTD}$ pocket in different ways [96], [97]. BI-2 binds CA with high affinity but interacts exclusively with the NTD of one CA monomer and not with the CTD of its neighbouring CA [97], [194]. BI-2 binding to the $CA_{NTD-CTD}$ pocket may increase the stiffness of the capsid to the point where can cause its failure. However, because it just interacts with one of the CA, BI-2 is unable to prevent their dissociation leading to the disassembly of the lattice after the fracture has happened. Indeed, our observations show that BI-2 does increase the capsid opening kinetics, but once the capsid breaks, it does not prevent the collapse of the remainder of the lattice. In comparison, PF74 and $CPSF6_p$ make contacts with both CA monomers, which explains their stabilising effect.

PF74 inhibits infection at both low and high concentrations, but produces differential effects on reverse transcription. Low concentrations of PF74 do not inhibit reverse transcription but higher concentrations do [97], [98], [115], [192]. Moreover, it has been shown that the inhibition of infection is completely reversed in washout experiment with low concentrations (1 μM) but not with high concentrations (10-30 μM) of PF74 [97]. The defects in reverse transcription produced by high concentrations of PF74 are also irreversible [97]. These observations could be explained by the differential effect of different concentrations of PF74 on capsid stability. Low concentrations of PF74 exhibit modest effects on capsid stability (such that the capsid remains intact in the cell) but might be sufficient to impede binding of required cofactors that use the same binding pocket, hence inhibiting infection. Wash-out of PF74 would then allow the capsid to resume its normal interaction with host factors. On the other hand, at high concentrations of PF74 the capsid might become so inflexible that it breaks rapidly in the cell. Our results suggest that very little CA is released during the rupture of the capsid, but the defect could be big enough to expose the HIV-1 genetic material to the environment. This will allow the detection or degradation of the viral genome by the host cell. This outcome was indeed observed by Mallery *et al.* using the encapsidated

reverse transcription (ERT) assay [213]. This assay measures RT products synthetised within intact viral cores because nucleases (that are added to this assay) degrade exposed nucleic acids. No cDNA was found in presence of 10 µM PF74, consistent with the idea that viral genome is exposed to external enzymes when the capsid opens up. Fracture of the capsid could also inhibit reverse transcription by diluting the components necessary to allow efficient cDNA synthesis. Because the fracture of the capsid happens rapidly after it is exposed to the antiviral drug, the defect cannot be reversed by wash-out.

PF74 has also been shown to affect a later stage of the HIV-1 entry. It reduces infection even when is added 10 hours post-infection [97], [137], [191], interrupts docking of the cores at the nuclear envelope [135], and alters integration site distribution [191]. These observations support the idea that PF74 disturbs binding of host factors involved in nuclear translocation and integration, such as CPSF6 and NUP153 [75], [95]–[97]. The precise role of CPSF6 on HIV-1 infection is still not clear. Its localisation is mainly nuclear but it shuttles between the cytoplasm and the nucleus [181]. Its depletion does not inhibit HIV-1 infection, but decreases proviral integration into transcriptionally active genes [143], [147]. This suggest that binding of CPSF6 to CA is required for a late stage of virus entry and not during the transport of the capsid through the cytoplasm. Our results showed that $CPSF6_p$ stabilises CA lattices in a concentration-dependant manner, even when they are not intact. In the cell CPSF6 may stabilise the capsid in the proximity of the nucleus or right at the nuclear membrane, such that some CA may remain associated with the PICs to facilitate nuclear import and efficient proviral integration. Indeed, CA has been found at high levels at the nuclear membrane and even inside the nucleus [133]–[135].

Several groups have shown that overexpression of a truncated form of a mouse version of CPSF6 (mCPSF6-358) and full length mCPSF6 tagged with a nuclear export signal (mCPSF6-NES) inhibit HIV-1 infection by blocking the entry of the PICs into the nucleus [95], [142], [143], [147]. This inhibition has been has been attributed to competition with other host factors implicated in nuclear translocation, such as NUP153 [77], [133], [143], [174]. mCPSF6-358 has also been shown to stabilise authentic cores [108], [142]. This observation is consistent with our observations that CPSF6 peptide stabilises the lattice against disassembly. Hyper-stabilisation of the capsid lattice in the cytoplasm could contribute to the block of nuclear import because intact capsids have a larger diameter than the nuclear pore complex [138], and are thus though to be unable to enter the nucleus.

In contrast to the stabilising effect of mCPSF6-358, a C-terminally truncated form of human CPSF6 that also lacks the 36 residues encoded by exon 6 (hCPSF6-375) promotes destabilisation of the viral cores and prevents reverse transcription [182]. The phenotype shown by hCPSF6-375 resembles the effect of a high concentration of PF74. Taken together, it could be speculated that subtle changes in the way that CPSF6 peptide interacts with the binding pocket on the CA hexamer (e.g. by removal of the CPSF6 residues encoded by exon 6) could switch between a binding mode that predominantly stabilises the lattice against dissociation and a binding mode that also leads to breakage of the lattice as observed for PF74.

A deletion mutagenesis study determined that the residues 313–327 of CPSF6 constitute the minimal binding epitope for interaction with CA [146]. This peptide, $CPSF6_p$, binds with low affinity to monomeric CA, but its binding is improved when assembled CA hexamers are used, displaying a K_D of 12 to 100 µM [96], [155], [186]. Our data using labelled $CPSF6_p$ indicates that the peptide interacts with higher affinity with authentic viral capsids, showing a K_D of 3.4-4 µM. Our results are consistent with a recent publication using recombinant CPSF6-358 [183] reporting that the protein interacts more strongly with assembled CA tubes than with CA hexamers. Stabilisation of the CA lattice was already observed in our assay at concentrations that lead to partial occupancy of the binding sites available on the lattice. Intriguingly, crystal structures of $CPSF6_p$ in complex CA hexamers have shown that all six possible binding pockets can be occupied at the same time [96], [97]. The fact that binding of fewer CPSF6 peptides to each hexamer is enough to stabilise the entire lattice suggests that binding at one or a few sites may be sufficient to alter the structure of the entire hexamer. Additionally, in a mature fullerene capsid, the assembled CA subunits can adopt different conformations. CypA has been shown to bind to a specific curvature within the lattice [157], and CPSF6 might have a binding preferences for specific conformations of the $CA_{NTD-CTD}$ surface such that CPSF6 binding might concentrate at specific region of the capsid. Finally binding of the full-length protein (e.g. with respect to occupancy) is likely to differ considerably from binding of the full-length protein because of steric requirements.

Currently there is no labelled version of PF74 available, so we cannot determine how many PF74 molecules bind to authentic viral capsids and compare it with CPSF6. This would be interesting to know as the mode of action of PF74 in cells has been suggested to be concentration-dependant: at low concentration, it is thought to compete with host factors for capsid binding, while at high concentrations is believed to

cause irreversible changes to the capsid structure [97], [160], [191]. Our competition experiments revealed that when high concentration of PF74 is used (10 µM PF74 vs 1 µM CPSF6$_p$), binding of fluorescent CPSF6 is completely abolished. This suggests that all the binding pockets on the capsid are being occupied by PF74. However, when they are used at the same concentration (1 µM each), CPSF6 does bind to the lattice but not to the same extent. This reduction may be enough to abolish HIV-1 infection.

Chapter 5

Modulation of HIV-1 capsid stability by binding of polyanions to the central capsid pore

5. Modulation of HIV-1 capsid stability by binding of polyanions to the central capsid pore

5.1. Introduction

Little is known about the recently reported electropositive pore located at the centre of the HIV CA hexamer [72]. The size-selective pore is formed by six arginine residues (R18), one from each CA monomer. It forms the bottom of a chamber-like space, which can be closed or open to the exterior depending on the position of the CA_{NTD} β-hairpins. The R18 ring was shown to be essential for reverse transcription and infection, as chimeric viruses with progressive removal of the arginines display decreased rates of infectivity and reverse transcription. Deoxynucleoside triphosphates (dNTPs) bind avidly to the pore, with extremely rapid association and dissociation kinetics. Furthermore, binding of dNTPs has a stabilising effect on CA hexamers and their binding can be prevented by addition of the competitor hexacarboxybenzene. This 6-fold symmetric polyanion also interacts with the R18 hexamer ring and promotes stabilisation of CA hexameric assemblies. The stabilisation effect is minimally affected when pentacarboxybenzene is used, but decreases drastically when tetra- or tricarboxybenzene molecules are used, indicating that co-ordination of the six R18 positions supports improved binding [72].

These observations suggest that HIV regulates capsid stability through binding of negatively charged molecules to the R18 charged pore. However, the extent of the stabilising effect on authentic viral capsids has not been studied until now. In Chapter 3 of this thesis we showed that binding of hexacarboxybenzene strongly stabilises the viral capsid, allowing it to remain fully closed for hours. However, the binding of the polyanionic molecule does not prevent the catastrophic lattice disassembly that occurs once the capsid has suffered its first defect. This observation suggests that indeed, the electropositive R18 pore in the viral capsid is a critical surface and could be used for the virus as a binding pocket to modulate the stability of the capsid during infection.

Several polyanionic molecules, apart from the dNTPs, are present in the cell. For instance, the structure of ATP is almost identical to dATP and it is present in much higher concentrations in the cell. Moreover, inositol hexakisphosphate (IP6) is also highly abundant in the cell and has a similar structure to hexacarboxybenzene. It has six phosphates instead of carboxylic groups, and it has been shown to interact with

immature CA lattices [187], [189]. Thus, it is reasonable to consider ATP and IP6 as potential capsid binders that could regulate capsid stability during infection.

The main aim of this chapter is to investigate the influence of the polyanionic molecules ATP and IP6 on capsid stability. For that, the molecules were assessed with the capsid opening and lattice disassembly assay developed on this thesis.

5.2.   ATP and IP6 delay capsid opening similarly to hexacarboxybenzene

As shown in Chapter 3 for hexacarboxybenzene, we used the capsid opening assay to investigate the effect of the potential capsid binders ATP and IP6 on capsid stability. Biotinylated HIV-1 viral particles containing free GFP were captured onto a glass surface to then be permeabilised with the pore-forming protein PFO. Three different concentrations of IP6 were tested (1, 10 and 100 µM), while 100 µM of ATP was examined. Membrane permeabilisation and capsid opening were detected by observing the release of the GFP molecules using time-lapse TIRF microscopy.

The fractions of capsids that are leaky, undergo opening or remain closed after ~30 minutes of adding PFO with the different polyanionic molecules are shown in **Figure 5.1** (data obtained with hexacarboxybenzene is included for comparison). In all cases, the majority of the particles (65-80%) contained leaky capsids, presumably as a result of assembly defects which are not affected by the addition of molecules. The rest of the particles (20-35%) contained cores that undergo uncoating or remain closed during the experiment, suggesting that they were properly assembled capsids that retained the encapsidated GFP molecules after membrane permeabilisation. In the control sample without any molecules, around 40% of the properly assembled cores remain closed during the experiment while the rest open up. Interestingly, the ratio between closed and uncoating capsids increased in presence of all polyanions tested (**Figure 5.1**, **dark grey and black bar for each condition**). These observations suggest that polyanions exert a stabilising effect on the closed capsid.
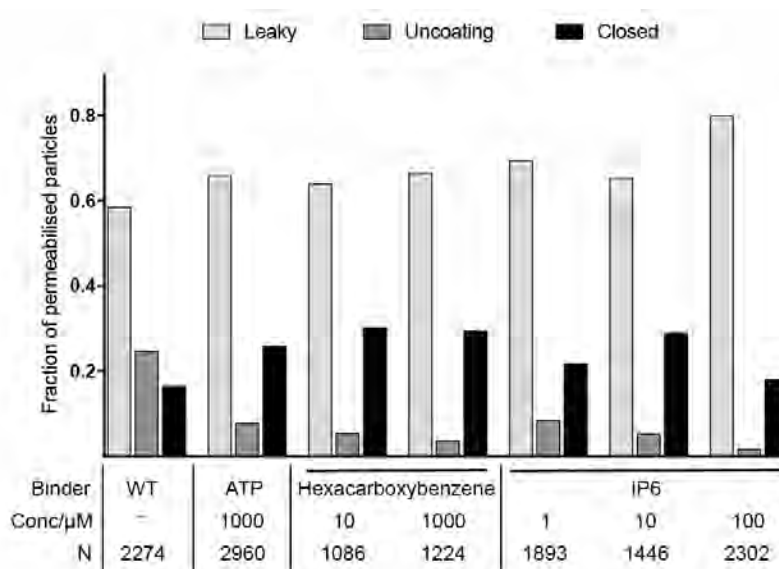

Figure 5.1. Leaky, undergo opening or closed capsids in presence of polyanionic molecules. Bar chart showing the fraction of capsids classified as 'leaky', 'opening'

and 'closed' present 30 min after permeabilisation of the viral membrane of biotinylated HIV-1 viral particles containing free GFP in presence of hexacarboxybenzene (10 and 1000 µM), ATP (1000 µM) and IP6 (1, 10 and 100 µM). The data was combined from multiple measurements (total number of repeats/number of viral preparations): No binder (3/2); ATP - 1000 µM (5/2); hexacarboxybenzene - 10 µM (3/2); hexacarboxybenzene - 1000 µM (3/1); IP6 - 1 µM (4/3); IP6 - 10 µM (2/2); IP6 – 100 µM (3/2).

In order to calculate the half-life of capsid opening in presence of ATP and IP6, we analysed the distribution of the core opening times obtained from the cores that undergo opening during the experiment. **Figure 5.2** shows the survival curves obtained for capsids in the presence of ATP or IP6 as well as for capsid in the presence of hexacarboxybenzene or in the absence of molecules (control).
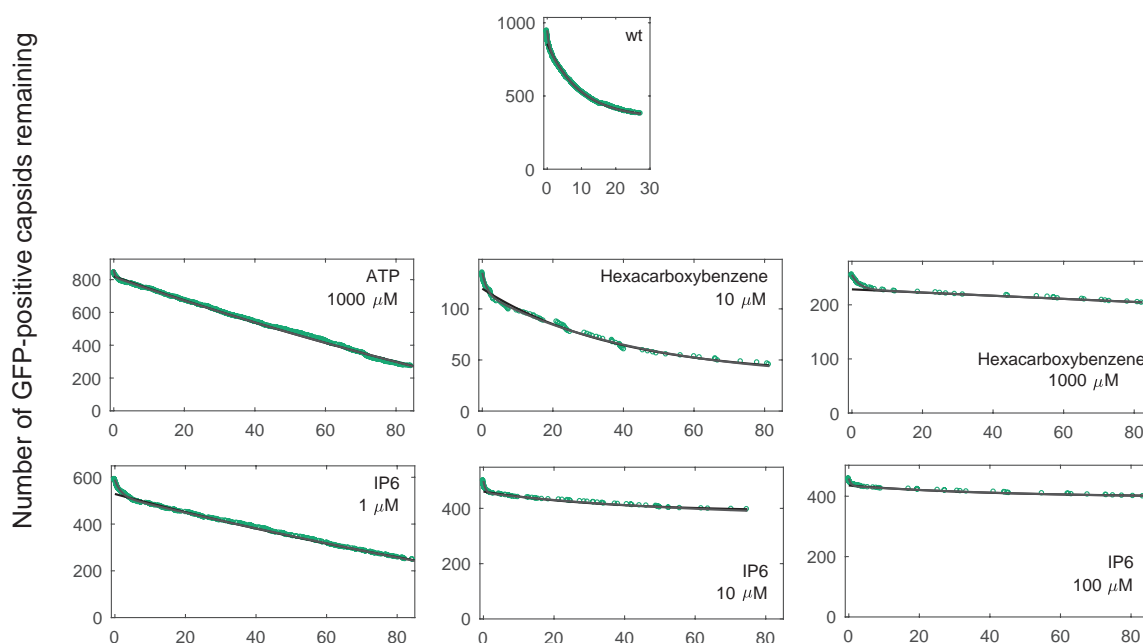
Figure 5.2. Capsid opening in presence of polyanionic molecules. (A) Survival curves obtained from capsids that undergo opening on multiple experiments in presence hexacarboxybenzene (10 and 1000 µM), ATP (1000 µM) and IP6 (1, 10 and 100 µM). Exponential fit (black line) is shown in each graph.

As observed, most of the properly assembled capsids remain closed in all the conditions were polyanion molecules were added. Due to the scarce number of core

opening events observed during the duration of experiment (88 min), the half-lives of capsid opening could not be determined accurately. However, fitting the survival curves with an exponential decay gave an estimate capsid opening hald-life of 1 hour in the case of ATP, similar to the obtained with 10 µM hexacarboxybenzene. Addition of IP6, even at just 1 µM dramatically slowed down the core opening process from a few minutes to hours.

Taken together, these data indicate that the polyanions hexacarboxybenzene, IP6 and ATP strongly inhibit capsid opening.

5.3.   ATP and IP6, like hexacarboxybenzene, do not stabilise the CA lattice after the formation of the first defect

To further investigate the effect of ATP and IP6 on capsid stability, we used the CypA paint assay to get an insight into their effect on lattice disassembly kinetics. HIV-1 viral particles were exposed to PFO in the presence of different concentrations of ATP or IP6 as well as 1 µM 568-CypA to paint the viral capsid, whereby the CypA signal was used as an indirect measure of the integrity of the CA lattice.

Changes in the kinetics of CA lattice disassembly are apparent by comparing CypA paint traces of leaky capsids in the presence of absence of stabilising molecules. Representative heatmaps of CypA paint traces for leaky capsids measured under different conditions are shown in **Figure 5.3** and were characterised by rapid binding of CypA to the CA lattice after membrane permeabilisation, followed by an immediate but more gradual decay of the CypA paint signal as the lattice falls disassembled. We observed that the CypA signal decayed within 1-2 minutes regardless of whether the polyanionic molecules were present or not. This result indicates that similar to hexacarboxybenzene, IP6 and ATP are unable to prevent the collapse of capsids that are not intact, suggesting that the mechanism by which they stabilise the CA lattice requires closed capsids.
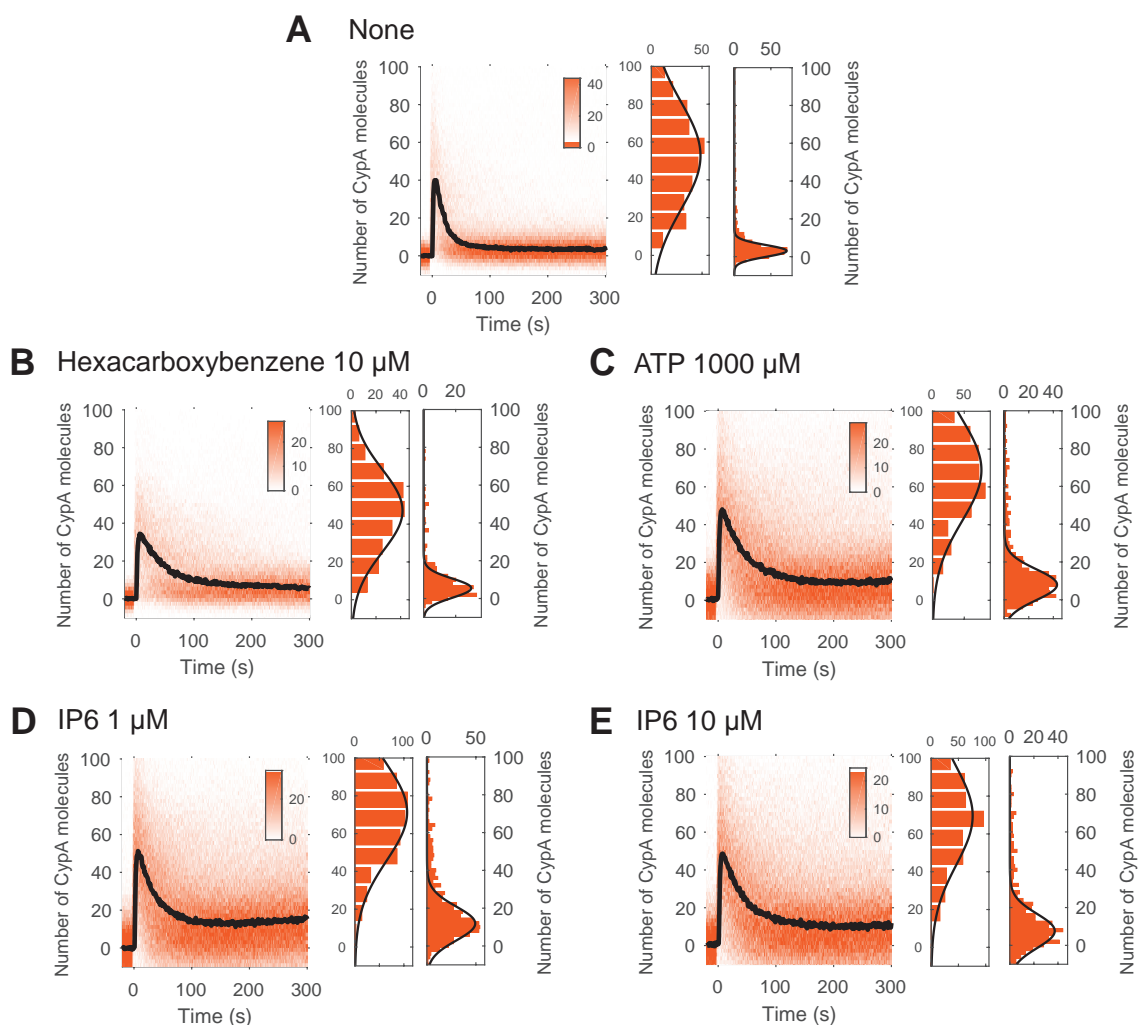
Figure 5.3. Lattice disassembly kinetics of leaky capsids in presence of polyanionic molecules. Heatmap of AF568-CypA binding traces (vermillion) to all leaky capsids in a field of view aligned with respect to the time of envelope permeabilisation ($t_P = 0$). Each heatmap is a representative data set of **(A)** untreated viral particles, or in presence of **(B)** hexacarboxybenzene 10 μM, **(C)** ATP 1000 μM, **(D)** IP6 1 μM, and **(E)** IP6 10 μM. The bold black line represents the median CypA binding trace. The histograms at the right show the distribution of intensities at $t_P = 1$-30 s and 280-300 s respectively.

The effect of the three compounds on lattice disassembly kinetics of capsids was apparent by comparing heatmaps of CypA paint traces for capsids that undergo uncoating during the experiment (**Figure 5.4**). In all conditions, CypA bound to an equilibrium level upon membrane permeabilisation, and then the CypA paint signal decayed after capsid opening. The equilibrium CypA binding level was indistinguishable in the presence and absence of the polyanions (**Figure 5.5**). These

results suggest that binding of CypA for lattice painting was not affected by the presence of hexacarboxybenzene, IP6 and ATP.

Lattice paint traces aligned at the time of capsid opening (**Figure 5.4, right panel**) revealed that IP6 and ATP did not prevent CA lattice disassembly after uncoating was initiated. The median CypA signal trace recorded in the presence of 1000 µM ATP reached the background level after ~300 seconds, the same time that takes spontaneous uncoating to happen. Identical effect was observed for 1 µM and 10 µM IP6, indicating that even higher concentrations of the molecule did not stabilise the CA lattice after core opening. This result agrees with what was observed on leaky capsids, supporting the idea that the polyanions only stabilise fully closed capsids.
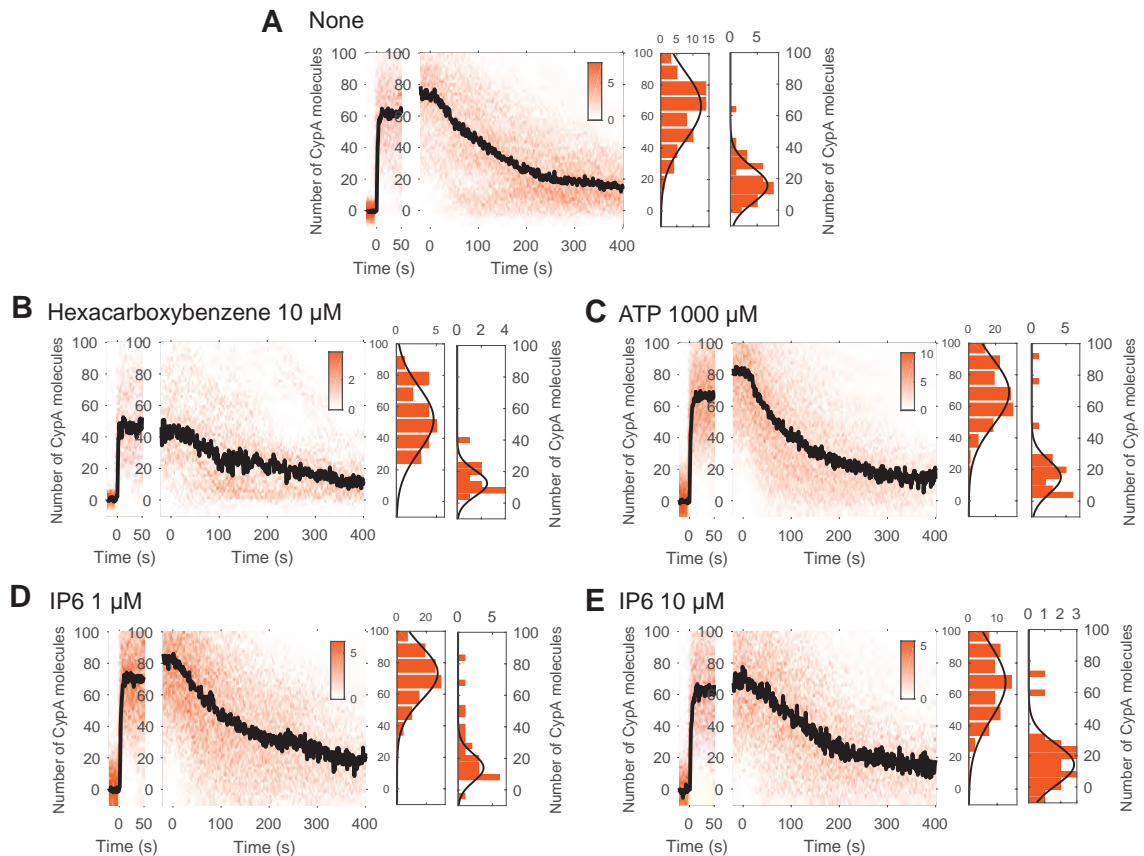
Figure 5.4. Lattice disassembly kinetics of capsids that undergo disassembly in presence of polyanionic molecules. Heatmap of AF568-CypA binding traces (vermillion) to all capsids that undergo disassembly in a field of view aligned with respect to the time of envelope permeabilisation ($t_P = 0$, left panel) and aligned with respect to capsid opening (right panel). Each heatmap is a representative data set of **(A)** untreated viral particles, or in presence of **(B)** hexacarboxybenzene 10 µM, **(C)** ATP 1000 µM, **(D)** IP6 1 µM, and, **(E)** IP6 10 µM. The bold black line represents the

median CypA binding trace. Heatmap each condition. The histograms at the right show the distribution of intensities after binding equilibrium is reached (t_P = 10-30 s) and at the end of lattice disassembly (t_O = 380-400 s).
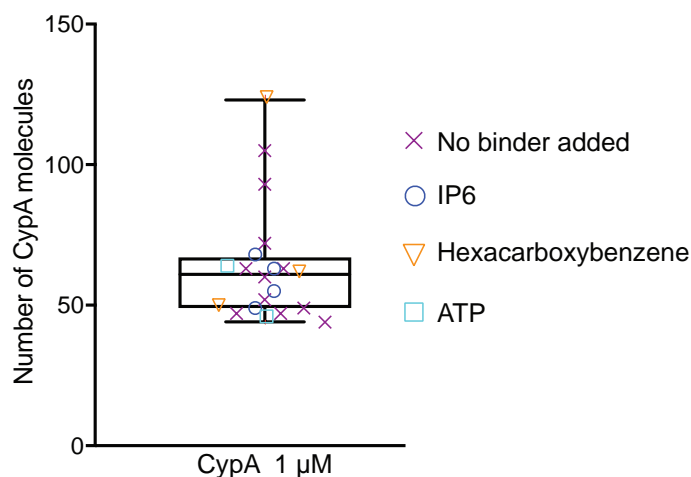
Figure 5.5. Number AF568-CypA bound at equilibrium in presence of polyanionic molecules. Variation in the median number of CypA molecules bound at equilibrium per closed capsid measured in the absence and presence of different concentrations of hexacarboxybenzene, ATP and IP6. All independent experiments were carried out using 1 µM AF568-CypA for lattice painting. The error bars represent 95% confidence intervals.

In conclusion, we observed that ATP and IP6 strongly prevent capsid opening but they do not inhibit lattice disassembly once the process has started as observed for hexacarboxybenzene, pointing to a shared mechanism for capsid stabilisation.

5.4. Discussion

In this chapter, we studied the effect on HIV-1 capsid uncoating kinetics of two new potential capsid binders, adenosine triphosphate (ATP) and inositol hexakisphosphate (IP6). We found that the two polyanionic molecules potently inhibit capsid opening as seen from the remarkable increase in the core opening half-life and the increased number of assembled cores that remain closed. However, none of them prevent the disassembly of the CA lattice once the core has opened up. A similar effect on capsid stability is produced by hexacarboxybenzene, as shown in Chapter 3.

The CA hexamer, the main building block of the HIV capsid, contains an electropositive pore in its centre that is formed by highly conserved arginine residues at position 18 (R18) [72]. This feature has a strongly destabilising effect on the hexamer, yet it is maintained because it is strictly required for infectivity and may serve as an import channel for nucleotides to fuel reverse transcription inside the closed capsid. Hexacarboxybenzene binds to this electropositive pore and stabilises cross-linked CA [72]. The compound also strongly inhibits capsid uncoating as shown in Chapter 3. Hexacarboxybenzene is not a natural compound found in cells and therefore cannot play a role in the viral life cycle. However, the polyanions ATP and IP6 are present at high concentrations in the cell. ATP can be found at millimolar concentrations [214], while IP6 has been reported to be at around 35-50 µM [187], [188]. In collaboration with Leo James and colleagues, we recently evaluated whether these compounds could function in capsid stabilisation [213]. Crystal structures of ATP and IP6 in complex with CA hexamers show that both compounds bind to the centre of the 6-fold axis by coordinating the the R18 ring [213]. In addition, binding of ATP and IP6 leads to stabilisation of the disulphide cross-linked hexamer [213]. Here and in Ref 213 we show using our single-molecule TIRF imaging approach that both compounds exerted a similar effect on capsid stability to hexacarboxybenzene by delaying capsid opening without inhibiting the disassembly of the lattice after the first lattice defect has been formed.

These observations suggest that polyanions affect capsid stability via a shared mechanism, raising the following question: How could polyanions inhibit opening of intact capsids, but be unable to impede lattice disassembly of defective capsids? In the context of an intact capsid, binding of polyanions to the electropositive pore stabilises individual hexameric units, effectively raising the activation energy required to dissociate the first CA subunit(s) from the hexameric building blocks of the lattice. Removal of the first CA subunit from a hexamer in the lattice, would lead to its

destabilisation as a result of lattice contact. In addition, the polyanion would be expected to dissociate because the R18 ring is no longer intact, leading to further destabilisation. Thus, removal of the first subunits will lead to local destabilisation that will propagate across the entire lattice. Notably, the polyanion is not able to prevent dissociation of hexamers that are at the disassembling edge, just as binding of polyanion to cross-linked hexamers are unable to prevent dissociation of the hexamer upon reduction of the disulphide bonds that keep the hexamer together.

The next question arising from these findings is whether the virus exploits polyanions to regulate capsid stability and facilitate infection. Our results presented in Chapter 3 revealed that the HIV-1 capsid is intrinsically unstable, displaying a capsid opening half-life of 8 minutes. In contrast, in the cell the viral capsid has been shown to be more stable, with capsid uncoating times ranging from 30 minutes to ~6 hours [118], [132], [135], [137]. In agreement with this, we demonstrated that the addition of diluted cell lysate increases the core opening half-life to about 50 minutes, suggesting that there are cell-derived molecules that stabilise the HIV-1 capsid. Our results suggest that IP6 and/or ATP could be involved in enhancing the lifetime of the capsid within the host cytoplasm.

Does the capsid have preference for a specific polyanionic molecule? Our results show that capsid stability is enhanced to a greater extent in of the presence of physiological concentrations of IP6 than in the presence of physiological concentrations of ATP. Similarly, endogenous reverse transcription assays revealed that IP6 was more potent in increasing RT product accumulation that ATP [213]. Importantly, radiolabelled IP6 is selectively incorporated into the virions by association with the capsid with a 1:1 stoichiometry (IP6:hexamer) while radiolabelled ATP is not enriched in virions [213]. This raises the question of how IP6 is packaged into the nascent viral particles, since the R18 ring is available just upon formation of the CA hexamers during maturation, which happens after budding from the cell. IP6 has been described previously to interact with immature Gag lattices and promote its assembly *in vitro* [189]. A recent paper now shows that IP6 drives assembly of the immature lattice at the plasma membrane by binding to a six-helix bundle formed by the CA_{CTD} and SP1, via interaction with two lysines (Lys290 and Lys359) [215].

Taken together the recently published structures of IP6 bound to hexamers of the immature and mature lattice [213], [215], the observation that IP6 promotes reverse transcription in the closed capsid [213], and our single-molecule analysis of the effect

of IP6 on capsid uncoating presented here allow us to propose the following model: IP6 serves to drive assembly of the immature lattice in the producer cell and is selectively incorporated into the virion. Upon proteolytic cleavage of the Gag polyprotein, IP6 is released and becomes available to stabilise the mature lattice by binding into the R18 pore. Upon release into the cytoplasm of the target cell, the capsid is stabilised by IP6. Continued association of IP6 with the lattice could be regulated by opening and closing of the molecular iris formed by the N-terminal beta-hairpin of CA. Alternatively, uncoating could be triggered by inducing a local defect in the capsid lattice. Our data suggests that a small defect will be sufficient for lattice disassembly to ensue. In this context, host proteins and/or the formation of dsDNA [119] during RT could provide the trigger for uncoating.

The use of IP6 to modulate capsid assembly and stability has the advantage that the interaction with the capsid is reversible and therefore the disassembly of the CA lattice can be promoted by its dissociation. Molecules with similar roles, called pocket factors, have been described before for picornaviruses [216], [217]. Understanding the exact mechanism by which uncoating of IP6-stabilised capsids is triggered during infection is still to be determined. Furthermore, the interplay between IP6 with the other cellular polyanions, such as dNTPs and ATP, needs to be studied in more detail. The results from this chapter not only helped in the discovery of an HIV pocket factor that controls capsid stability, but may also facilitate the discovery of new antiviral drugs, e.g. exploiting the mechanisms for regulating capsid stability discovered here.

Chapter 6

Conclusions and Future Directions

6. Conclusions and future directions

The HIV-1 capsid has been extensively studied but yet much remains unknown about the uncoating process. Even though it has been known to have a conical topology within the virion for 30 years [218], still most of the research uses monomeric or hexameric CA assemblies as a model to study its role during infection. The fragility of the capsid and its sensitivity to structural manipulation has been a roadblock in the development of an *in vitro* assay to study the properties of authentic capsids, and the complexity of its interactions with host factors such as CypA, CPSF6, NUP153, NUP358, and nucleotides.

The aims of this thesis were to develop an assay to study the disassembly of authentic HIV-1 capsids and to use it to understand how uncoating is modulated by different capsid binders. In Chapter 3 I described the development of our single-particle fluorescence microscopy assay that follows the real-time uncoating kinetics of individual HIV capsids *in vitro*. By permeabilising GFP loaded viral particles with a pore-former protein and painting the lattice with a fluorescent version of CypA, we were able to detect (1) the precise moment at which the capsid develops its first defect, and (2) visualise the disassembly of the CA lattice thereafter. We found that spontaneous uncoating is initiated shortly after the viral membrane is compromised exposing the capsid to a biochemically different environment. Opening of the capsid is the rate-limiting step of uncoating, which is followed by a rapid, catastrophic collapse. Remarkably, these two uncoating phases are modulated differentially by different capsid binders. In Chapter 4 we investigated the effect on capsid stability of molecules that bind to the interface formed between CA_{NTD}-CA_{CTD} of neighbouring subunits in the CA hexamer, while in Chapter 5 we examined polyanionic molecules that bind to the highly positively charged pore formed by the ring of six arginines at the centre of the hexamer. It was found that molecules binding at CA_{NTD}-CA_{CTD} interface could either strongly accelerate capsid opening (PF74) or have little effect on this step (CPSF6) but both molecules strongly stabilise the CA lattice after capsid opening and prevent CA lattice disassembly in a concentration dependant manner. In contrast, binding of the polyanionic molecules hexacarboxybenzene, ATP and the newly discovered CA-binder hexakisphosphate (IP6) strongly delay initiation of uncoating but do not prevent subsequent lattice disassembly.

Dissecting the differential influence of CA binders on capsid opening and lattice disassembly open the door to understanding their role during HIV infection in greater

detail, which could provide essential new understanding on the host-specific effects on uncoating. Even though this thesis examines the effect of individual binders on capsid stability, during infection the HIV-1 capsid interacts with several host factors simultaneously or sequentially, whereby the interplay between different factors provides additional levels of regulation, as observed e.g. for the interplay between TNPO3, CPSF6 and CypA [142], [160], [179]. Further investigation of the relationship between different host factors with the viral capsid in a controlled way at the single molecule level could help dissect their role in cytoplasmic trafficking and nuclear import.

Finally, our system to study uncoating has potential as a medium-throughput assay for screening compounds that target the stability of the capsid lattice and the principle of the approach can readily be applied to other viruses.

Chapter 7

References

7. References

[1]   J. E. Kaplan *et al.*, "Guidelines for prevention and treatment of opportunistic infections in HIV-infected adults and adolescents: recommendations from CDC, the National Institutes of Health, and the HIV Medicine Association of the Infectious Diseases Society of America.," *MMWR. Recomm. reports Morb. Mortal. Wkly. report. Recomm. reports*, vol. 58, no. RR-4, pp. 1–207, 2009.

[2]   UNAIDS, "GLOBAL STATISTICS—2015."

[3]   M. Balter, "Virus From 1959 Sample Marks Early Years of HIV," *Science (80-.).*, vol. 279, no. 5352, p. 801 LP-801, Feb. 1998.

[4]   F. Barre-Sinoussi *et al.*, "Isolation of a T-Lymphotropic Retrovirus from a Patient at Risk for Acquired Immune Deficiency Syndrome (AIDS)," *Science (80-.).*, vol. 220, pp. 868–871, 1983.

[5]   R. C. Gallo, "Frequent Detection and Isolation of Cytopathic Retroviruses," *Science (80-.).*, vol. 224, no. April, pp. 500–503, 1984.

[6]   K. Case, "Nomenclature: Human Immunodeficiency Virus," *Ann Intern Med*, 1986.

[7]   "WHO | HIV/AIDS," World Health Organization, 2016.

[8]   L. Buonaguro, M. L. Tornesello, and F. M. Buonaguro, "Human Immunodeficiency Virus Type 1 Subtype Distribution in the Worldwide Epidemic: Pathogenetic and Therapeutic Implications," *J. Virol.*, vol. 81, no. 19, pp. 10209–10219, 2007.

[9]   G. M. Shaw and E. Hunter, "HIV transmission," *Cold Spring Harb. Perspect. Med.*, vol. 2, no. 11, pp. 1–23, 2012.

[10] D. Klatzmann *et al.*, "Selective Tropism of Lymphadenopathy Associated cin with those stained with Hoechst- Virus (LAV) for Helper-Inducer T Lymphocytes," *Science (80-.).*, vol. 225, pp. 59–63, 1984.

[11] P. U. Cameron *et al.*, "Susceptibility of dendritic cells to HIV-1 infection in vitro," *J. Leukoc. Biol.*, vol. 56, no. 3, pp. 257–265, 1994.

[12] V. Gill *et al.*, "Macrophages are the major target cell for HIV infection in long-term bone marrow culture and demonstrate dual susceptibility to lymphocytotropic and monocytotropic strains of HIV-1," *Br. J. Haematol.*, vol. 93, no. 1, pp. 30–37, 1996.

[13] J. L. Excler, M. L. Robb, and J. H. Kim, "HIV-1 vaccines: Challenges and new perspectives," *Hum. Vaccines Immunother.*, vol. 10, no. 6, pp. 1734–1746, 2014.

[14] U.S. Food and Drug Administration, "Antiretroviral drugs used in the treatment of HIV infection." [Online]. Available: http://www.fda.gov/ForPatients/Illness/HIVAIDS/Treatment/ucm118915.htm.

[15] R. Subbaraman, S. K. Chaguturu, K. H. Mayer, T. P. Flanigan, and N. Kumarasamy, "Adverse effects of highly active antiretroviral therapy in developing countries.," *Clin. Infect. Dis.*, vol. 45, no. 8, pp. 1093–1101, 2007.

[16] T. W. Chun *et al.*, "Presence of an inducible HIV-1 latent reservoir during highly active antiretroviral therapy.," *Proc. Natl. Acad. Sci. U. S. A.*, vol. 94, no. 24, pp. 13193–7, 1997.

[17] F. R. Simonetti, M. F. Kearney, D. R. Program, C. Sciences, and L. Sacco, "Review: influence of ART on HIV genetics," *Curr Opin HIV AIDS*, vol. 10, no. 1, pp. 49–54, 2015.

[18] J. M. Cuevas, R. Geller, R. Garijo, J. López-Aldeguer, and R. Sanjuán, "Extremely High Mutation Rate of HIV-1 In Vivo," *PLoS Biol.*, vol. 13, no. 9, pp. 1–19, 2015.

[19] M. Lusic and R. F. Siliciano, "Nuclear landscape of HIV-1 infection and integration," *Nat. Rev. Microbiol.*, vol. 15, no. 2, pp. 69–82, 2017.

[20] M. Yamashita and M. Emerman, "Retroviral infection of non-dividing cells: Old and new perspectives," *Virology*, vol. 344, no. 1, pp. 88–93, 2006.

[21] J. A. G. Briggs, T. Wilk, R. Welker, H. G. Kräusslich, and S. D. Fuller, "Structural

organization of authentic, mature HIV-1 virions and cores," *EMBO J.*, vol. 22, no. 7, pp. 1707–1715, 2003.

[22] R. Cantin, G. Martin, and M. J. Tremblay, "A novel virus capture assay reveals a differential acquisition of host HLA-DR by clinical isolates of human immunodeficiency virus type 1 expanded in primary human cells depending on the nature of producing cells and the donor source," *J. Gen. Virol.*, vol. 82, no. 12, pp. 2979–2987, 2001.

[23] P. Zhu *et al.*, "Distribution and three-dimensional structure of AIDS virus envelope spikes.," *Nature*, vol. 441, no. 7095, pp. 847–852, 2006.

[24] J. Vlach and J. S. Saad, "Structural and molecular determinants of HIV-1 Gag binding to the plasma membrane," *Front. Microbiol.*, vol. 6, no. MAR, pp. 1–8, 2015.

[25] R. Welker, H. Hohenberg, U. Tessmer, C. Huckhagel, and H. G. Kräusslich, "Biochemical and structural analysis of isolated mature cores of human immunodeficiency virus type 1.," *J Virol*, vol. 74, no. 3, pp. 1168–1177, 2000.

[26] J. Chen *et al.*, "High efficiency of HIV-1 genomic RNA packaging and heterozygote formation revealed by single virion analysis.," *Proc. Natl. Acad. Sci. U. S. A.*, vol. 106, no. 32, pp. 13535–40, 2009.

[27] J. Mak, M. I. N. Jiang, M. A. Wainberg, M. Hammarskjold, D. Rekosh, and L. Kleiman, "Role of Pr160gag-pol in Mediating the Selective Incorporation of tRNALys into Human Immunodeficiency Virus Type 1 Particles," *J. Virol.*, vol. 68, no. 4, pp. 2065–2072, 1994.

[28] J. L. Darlix, M. Lapadat-Tapolsky, H. de Rocquigny, and B. P. Roques, "First glimpses at structure-function relationships of the nucleocapsid protein of retroviruses.," *J. Mol. Biol.*, vol. 254, no. 4, pp. 523–537, 1995.

[29] A. Kotov, J. Zhou, P. Flicker, and C. Aiken, "Association of Nef with the human immunodeficiency virus type 1 core," *J Virol*, vol. 73, no. 10, pp. 8824–8830, 1999.

[30] a Ohagen and D. Gabuzda, "Role of Vif in stability of the human immunodeficiency virus type 1 core.," *J. Virol.*, vol. 74, no. 23, pp. 11055–66, 2000.

[31] H. Wu *et al.*, "Targeting foreign proteins to human immunodeficiency virus particles via fusion with Vpr and Vpx.," *J. Virol.*, vol. 69, no. 6, pp. 3389–3398, 1995.

[32] L. Ratner *et al.*, "Complete nucleotide sequence of the AIDS virus, HTLV-III.," *Nature*, vol. 313, no. 6000, pp. 277–84, 1985.

[33] J. A. G. Briggs *et al.*, "The stoichiometry of Gag protein in HIV-1," *Nat. Struct. Mol. Biol.*, vol. 11, no. 7, pp. 672–675, 2004.

[34] J. S. Saad, J. Miller, J. Tai, A. Kim, R. H. Ghanam, and M. F. Summers, "Structural basis for targeting HIV-1 Gag proteins to the plasma membrane for virus assembly.," *Proc. Natl. Acad. Sci. U. S. A.*, vol. 103, no. 30, pp. 11364–9, 2006.

[35] P. R. Tedbury and E. O. Freed, "The role of matrix in HIV-1 envelope glycoprotein incorporation," *Trends Microbiol.*, vol. 22, no. 7, pp. 372–378, 2014.

[36] B. K. Ganser-Pornillos, M. Yeager, and W. I. Sundquist, "The structural biology of HIV assembly," *Curr. Opin. Struct. Biol.*, vol. 18, no. 2, pp. 203–217, 2008.

[37] D. Muriaux and J.-L. Darlix, "Properties and functions of the nucleocapsid protein in virus assembly," *RNA Biol.*, vol. 7, no. 6, pp. 744–753, 2010.

[38] B. Strack, A. Calistri, S. Craig, E. Popova, and H. G. Göttlinger, "AIP1/ALIX is a binding partner for HIV-1 p6 and EIAV p9 functioning in virus budding.," *Cell*, vol. 114, no. 6, pp. 689–699, 2003.

[39] N. M. Bell and A. M. L. Lever, "HIV Gag polyprotein: Processing and early viral particle assembly," *Trends Microbiol.*, vol. 21, no. 3, pp. 136–144, 2013.

[40] R. Craigie and F. D. Bushman, "HIV DNA integration," *Cold Spring Harb. Perspect. Med.*, vol. 2, no. 7, pp. 1–18, 2012.

[41] W.-S. Hu and S. H. Hughes, "HIV-1 reverse transcription.," *Cold Spring Harb. Perspect. Med.*, vol. 2, no. 10, p. a006882-, 2012.

[42] T. Jacks, M. D. Power, F. R. Masiarz, P. A. Luciw, P. J. Barr, and H. E. Varmus, "Characterization of ribosomal frameshifting in HIV-1 gag-pol expression," *Nature*, vol. 331, 1973.

[43] R. Blumenthal, S. Durell, and M. Viard, "HIV entry and envelope glycoprotein-mediated fusion," *J. Biol. Chem.*, vol. 287, no. 49, pp. 40841–40849, 2012.

[44] C. Brigati, M. Giacca, D. M. Noonan, and A. Albini, "HIV Tat, its TARgets and the control of viral gene expression," *FEMS Microbiol. Lett.*, vol. 220, no. 1, pp. 57–65, 2003.

[45] T. J. Hope, "The Ins and outs of HIV Rev," *Arch. Biochem. Biophys.*, vol. 365, no. 2, pp. 186–191, 1999.

[46] A. Seelamgari *et al.*, "Role of viral regulatory and accessory proteins in HIV-1 replication.," *Front. Biosci.*, vol. 9, no. October, pp. 2388–413, 2004.

[47] B. Klaver and B. Berkhout, "Comparison of 5' and 3' long terminal repeat promoter function in human immunodeficiency virus.," *J. Virol.*, vol. 68, no. 6, pp. 3830–40, 1994.

[48] F. Krebs, T. Hogan, and S. Quiterio, "Lentiviral LTR-directed expression, sequence variation, and disease pathogenesis," *HIV Seq. …*, no. i, pp. 29–70, 2001.

[49] E. O. Freed, "HIV-1 assembly, release and maturation.," *Nat. Rev. Microbiol.*, vol. 13, no. 8, pp. 484–496, 2015.

[50] E. M. Campbell and T. J. Hope, "HIV-1 capsid: the multifaceted key player in HIV-1 infection," *Nat. Rev. Microbiol.*, vol. 13, no. 8, pp. 471–483, 2015.

[51] G. M. Jakobsdottir, M. Iliopoulou, R. Nolan, L. Alvarez, A. A. Compton, and S. Padilla-Parra, "On the Whereabouts of HIV-1 Cellular Entry and Its Fusion Ports," *Trends Mol. Med.*, vol. 23, no. 10, pp. 932–944, 2017.

[52] A. Fassati and S. Goff, "Characterization of Intracellular Reverse Transcription Complexes of Human Immunodeficiency Virus Type 1," *J. Virol.*, vol. 75, no. 8, pp. 3626–3635, 2001.

[53] T. L. Diamond *et al.*, "Macrophage tropism of HIV-1 depends on efficient cellular dNTP utilization by reverse transcriptase," *J. Biol. Chem.*, vol. 279, no. 49, pp. 51545–51553, 2004.

[54] M. D. Miller, C. M. Farnet, and F. D. Bushman, "Human immunodeficiency virus type 1 preintegration complexes: studies of organization and composition.," *J. Virol.*, vol. 71, no. 7, pp. 5382–5390, 1997.

[55] D. McDonald *et al.*, "Visualization of the intracellular behavior of HIV in living cells," *J. Cell Biol.*, vol. 159, no. 3, pp. 441–452, 2002.

[56] A. Bukrinskaya, B. Brichacek, A. Mann, and M. Stevenson, "Establishment of a functional human immunodeficiency virus type 1 (HIV-1) reverse transcription complex involves the cytoskeleton.," *J. Exp. Med.*, vol. 188, no. 11, pp. 2113–2125, 1998.

[57] P. Pawlica and L. Berthoux, "Cytoplasmic Dynein Promotes HIV-1 Uncoating," *Viruses*, vol. 6, pp. 4195–4211, 2014.

[58] Z. Lukic, A. Dharan, T. Fricke, F. Diaz-Griffero, and E. M. Campbell, "HIV-1 Uncoating Is Facilitated by Dynein and Kinesin 1," *J. Virol.*, vol. 88, no. 23, pp. 13613–13625, 2014.

[59] M. Bukrinsky, "A Hard Way to the Nucleus," *Mol. Med.*, vol. 10, no. 1, pp. 1–5, 2004.

[60] A. R. W. Schröder *et al.*, "HIV-1 integration in the human genome favors active genes and local hotspots.," *Cell*, vol. 110, no. 4, pp. 521–9, 2002.

[61] C. M. Farnet and W. A. Haseltine, "Circularization of human immunodeficiency virus type 1 DNA in vitro.," *J. Virol.*, vol. 65, no. 12, pp. 6942–52, 1991.

[62] J. Karn and C. M. Stoltzfus, "Transcriptional and posttranscriptional regulation of HIV-1 gene expression," *Cold Spring Harb. Perspect. Med.*, vol. 2, no. 2, pp. 1–

17, 2012.

[63] S. Stein and G. Engleman, "Intracellular Processing of the gp160 HIV- 1 Envelope Precursor," *J. Biol. Chem.*, vol. 265, no. February, pp. 2640–2649, 1990.

[64] S. Ivanchenko *et al.*, "Dynamics of HIV-1 assembly and release," *PLoS Pathog.*, vol. 5, no. 11, 2009.

[65] H. Wang, A. Ramakrishnan, S. Fletcher, E. V Prochownik, and M. Genetics, "How HIV-1 Gag assembles in cells: putting together pieces of the puzzle," *Virus Res.*, vol. 2, no. 2, pp. 89–107, 2015.

[66] N. E. Kohl *et al.*, "Active human immunodeficiency virus protease is required for viral infectivity.," *Proc. Natl. Acad. Sci. U. S. A.*, vol. 85, no. 13, pp. 4686–90, 1988.

[67] J. Kimpton and M. Emerman, "Detection of replication-competent and pseudotyped human immunodeficiency virus with a sensitive cell line on the basis of activation of an integrated beta-galactosidase gene.," *J. Virol.*, vol. 66, no. 4, pp. 2232–2239, 1992.

[68] J. A. Thomas, D. E. Ott, and R. J. Gorelick, "Efficiency of Human Immunodeficiency Virus Type 1 Postentry Infection Processes: Evidence against Disproportionate Numbers of Defective Virions," *J. Virol.*, vol. 81, no. 8, pp. 4367–4370, 2007.

[69] R. W. Humphrey *et al.*, "Removal of human immunodeficiency virus type 1 (HIV-1) protease inhibitors from preparations of immature HIV-1 virions does not result in an increase in infectivity or the appearance of mature morphology," *Antimicrob. Agents Chemother.*, vol. 41, no. 5, pp. 1017–1023, 1997.

[70] X. Lahaye *et al.*, "The Capsids of HIV-1 and HIV-2 Determine Immune Detection of the Viral cDNA by the Innate Sensor cGAS in Dendritic Cells," *Immunity*, vol. 39, no. 6, pp. 1132–1142, 2013.

[71] J. Rasaiyaah *et al.*, "HIV-1 evades innate immune recognition through specific cofactor recruitment," *Nature*, vol. 503, no. 7476, pp. 402–405, 2013.

[72] D. A. Jacques, W. A. McEwan, L. Hilditch, A. J. Price, G. J. Towers, and L. C. James, "HIV-1 uses dynamic capsid pores to import nucleotides and fuel encapsidated DNA synthesis," *Nature*, vol. 536, no. 7616, pp. 349–353, 2016.

[73] R. C. Burdick *et al.*, *Dynamics and regulation of nuclear import and nuclear movements of HIV-1 complexes*, vol. 13, no. 8. 2017.

[74] A. Dharan *et al.*, "KIF5B and Nup358 Cooperatively Mediate the Nuclear Import of HIV-1 during Infection," *PLoS Pathog.*, vol. 12, no. 6, pp. 1–24, 2016.

[75] K. A. Matreyek, S. S. Yücel, X. Li, and A. Engelman, "Nucleoporin NUP153 Phenylalanine-Glycine Motifs Engage a Common Binding Pocket within the HIV-1 Capsid Protein to Mediate Lentiviral Infectivity," *PLoS Pathog.*, vol. 9, no. 10, 2013.

[76] K. E. Ocwieja *et al.*, "HIV integration targeting: A pathway involving transportin-3 and the nuclear pore protein RanBP2," *PLoS Pathog.*, vol. 7, no. 3, pp. 19–21, 2011.

[77] T. Schaller *et al.*, "HIV-1 capsid-cyclophilin interactions determine nuclear import pathway, integration targeting and replication efficiency," *PLoS Pathog.*, vol. 7, no. 12, 2011.

[78] G. A. Sowd *et al.*, "A critical role for alternative polyadenylation factor CPSF6 in targeting HIV-1 integration to transcriptionally active chromatin," *Proc. Natl. Acad. Sci.*, vol. 113, no. 8, pp. E1054–E1063, 2016.

[79] S. J. Rihn *et al.*, "Extreme Genetic Fragility of the HIV-1 Capsid," *PLoS Pathog.*, vol. 9, no. 6, 2013.

[80] J. C. Magill *et al.*, "Structure and Dynamics of Full Length HIV-1 Capsid Protein in Solution," *J Am Chem Soc*, vol. 3, no. 1, pp. 1–19, 2010.

[81] B. K. Ganser-pornillos, A. Cheng, and M. Yeager, "Structure of Full-Length HIV-1 CA : A Model for the Mature Capsid Lattice," *Cell*, vol. 131, pp. 70–79, 2007.

[82] C. Momany *et al.*, "Crystal structure of dimeric HIV-1 capsid protein.," *Nat. Struct. Biol.*, vol. 3, no. 9, pp. 763–770, 1996.

[83] S. Du *et al.*, "Structure of the HIV-1 full-length capsid protein in a conformationally trapped unassembled state induced by small-molecule binding," *J. Mol. Biol.*, vol. 406, no. 3, pp. 371–386, 2011.

[84] R. K. Gitti, B. M. Lee, J. Walker, M. F. Summers, S. Yoo, and W. I. Sundquist, "Structure of the amino-terminal core domain of the HIV-1 capsid protein.," *Science*, vol. 273, no. 5272, pp. 231–235, 1996.

[85] T. R. Gamble *et al.*, "Crystal structure of human cyclophilin A bound to the amino-terminal domain of HIV-1 capsid," *Cell*, vol. 87, no. 7, pp. 1285–1294, 1996.

[86] T. R. Gamble *et al.*, "Structure of the Carboxyl-Terminal Dimerization Domain of the HIV-1 Capsid Protein," *Science (80-.).*, vol. 278, 1997.

[87] M. Tanaka, B. A. Robinson, K. Chutiraka, C. D. Geary, J. C. Reed, and J. R. Lingappa, "Mutations of conserved residues in the major homology region arrest assembling HIV-1 Gag as a membrane-targeted intermediate containing genomic RNA and cellular proteins," *J. Virol.*, vol. 90, no. 4, p. JVI.02698-15, 2015.

[88] A. T. Gres, K. A. Kirby, V. N. KewalRamani, J. J. Tanner, O. Pornillos, and S. G. Sarafianos, "X-ray crystal structures of native HIV-1 capsid protein reveal conformational variability.," *Science*, vol. 349, no. 6243, pp. 99–104, 2015.

[89] O. Pornillos, B. K. Ganser-pornillos, and M. Yeager, "Atomic-level modelling of the HIV capsid," *Nature*, vol. 469, no. 7330, pp. 424–427, 2011.

[90] D. Morger *et al.*, "The three-fold axis of the HIV-1 capsid lattice is the species-specific binding interface for TRIM5α," *J. Virol.*, p. JVI.01541-17, 2017.

[91] R. Campos-Olivas, J. L. Newman, and M. F. Summers, "Solution structure and dynamics of the Rous sarcoma virus capsid protein and comparison with capsid proteins of other retroviruses," *J Mol Biol*, vol. 296, no. 2, pp. 633–649, 2000.

[92] G. Zhao *et al.*, "Mature HIV-1 capsid structure by cryo-electron microscopy and all-atom molecular dynamics.," *Nature*, vol. 497, no. 7451, pp. 643–6, 2013.

[93] O. Pornillos *et al.*, "X-ray Structures of the Hexameric Building Block of the HIV Capsid," *Cell*, vol. 137, no. 7, pp. 1282–1292, 2009.

[94] E. L. Yufenyuy and C. Aiken, "The NTD-CTD intersubunit interface plays a critical role in assembly and stabilization of the HIV-1 capsid," *Retrovirology*, vol. 10, no. 1, pp. 1–14, 2013.

[95] A. J. Price *et al.*, "CPSF6 Defines a Conserved Capsid Interface that Modulates HIV-1 Replication," *PLoS Pathog.*, vol. 8, no. 8, 2012.

[96] A. Bhattacharya *et al.*, "Structural basis of HIV-1 capsid recognition by PF74 and CPSF6.," *Proc. Natl. Acad. Sci. U. S. A.*, vol. 111, no. 52, pp. 18625–30, 2014.

[97] A. J. Price *et al.*, "Host Cofactors and Pharmacologic Ligands Share an Essential Interface in HIV-1 Capsid That Is Lost upon Disassembly," *PLoS Pathog.*, vol. 10, no. 10, 2014.

[98] W. S. Blair *et al.*, "HIV capsid is a tractable target for small molecule therapeutic intervention," *PLoS Pathog.*, vol. 6, no. 12, 2010.

[99] I. J. L. Byeon *et al.*, "Structural Convergence between Cryo-EM and NMR Reveals Intersubunit Interactions Critical for HIV-1 Capsid Function," *Cell*, vol. 139, no. 4, pp. 780–790, 2009.

[100] B. K. Ganser, "Assembly and Analysis of Conical Models for the HIV-1 Core," *Science (80-.).*, vol. 283, no. 5398, pp. 80–83, 1999.

[101] B. K. Ganser-Pornillos, U. K. von Schwedler, K. M. Stray, C. Aiken, and W. I. Sundquist, "Assembly properties of the human immunodeficiency virus type 1 CA protein.," *J. Virol.*, vol. 78, no. 5, pp. 2545–52, 2004.

[102] Z. Yu *et al.*, "Unclosed HIV-1 Capsids Suggest a Curled Sheet Model of Assembly," *J. Mol. Biol.*, vol. 425, no. 1, pp. 112–123, 2013.

[103] S. Mattei, B. Glass, W. J. H. Hagen, H.-G. Kräusslich, and J. A. G. Briggs, "The

structure and flexibility of conical HIV-1 capsids determined within intact virions," *Science (80-.).*, vol. 354, no. 6318, pp. 1434–1437, 2016.

[104] V. B. Shah and C. Aiken, "In vitro Uncoating of HIV-1 Cores," *J. Vis. Exp.*, no. November, pp. 2–5, 2011.

[105] B. Forshey and U. Von Schwedler, "Formation of a human immunodeficiency virus type 1 core of optimal stability is crucial for viral replication," *J. …*, vol. 76, no. 11, pp. 5667–77, 2002.

[106] L. S. Ehrlich, B. E. Agresta, and C. A. Carter, "Assembly of Recombinant Human Immunodeficiency Virus Type 1 Capsid Protein In Vitro," *J. Virol.*, vol. 66, no. 8, pp. 4874–4883, 1992.

[107] M. Del Álamo, G. Rivas, and M. Mateu, "Effect of macromolecular crowding agents on human immunodeficiency virus type 1 capsid protein assembly in vitro," *J. Virol.*, vol. 79, no. 22, pp. 14271–14281, 2005.

[108] T. Fricke, A. Brandariz-Nuñez, X. Wang, A. B. Smith, and F. Diaz-Griffero, "Human cytosolic extracts stabilize the HIV-1 core.," *J. Virol.*, vol. 87, no. 19, pp. 10587–97, 2013.

[109] M. S. Briones, C. W. Dobard, and S. a Chow, "Role of human immunodeficiency virus type 1 integrase in uncoating of the viral core.," *J. Virol.*, vol. 84, no. 10, pp. 5181–90, 2010.

[110] N. Yan, A. D. Regalado-Magdos, B. Stiggelbout, M. A. Lee-Kirsch, and J. Lieberman, "The cytosolic exonuclease TREX1 inhibits the innate immune response to human immunodeficiency virus type 1," *Nat. Immunol.*, vol. 11, no. 11, pp. 1005–1013, 2010.

[111] V. P. Basu, M. Song, L. Gao, S. T. Rigby, M. N. Hanson, and R. A. Bambara, "Strand transfer events during HIV-1 reverse transcription," *Virus Res.*, vol. 134, no. 1–2, pp. 19–38, 2008.

[112] D. Warrilow, D. Stenzel, and D. Harrich, "Isolated HIV-1 core is active for reverse transcription," *Retrovirology*, vol. 4, pp. 1–5, 2007.

[113] K. Warren *et al.*, "Eukaryotic elongation factor 1 complex subunits are critical HIV-1 reverse transcription cofactors," *Proc. Natl. Acad. Sci.*, vol. 109, no. 24, pp. 9587–9592, 2012.

[114] U. K. von Schwedler and K. M. Stray, "Functional surfaces of the human immunodeficiency virus type 1 capsid protein," *J. …*, vol. 77, no. 9, pp. 5439–5450, 2003.

[115] J. Shi, J. Zhou, V. B. Shah, C. Aiken, and K. Whitby, "Small-molecule inhibition of human immunodeficiency virus type 1 infection by virus capsid destabilization," *J. Virol.*, vol. 85, no. 1, pp. 542–549, 2011.

[116] M. Stremlau *et al.*, "Specific recognition and accelerated uncoating of retroviral capsids by the TRIM5alpha restriction factor.," *Proc. Natl. Acad. Sci. U. S. A.*, vol. 103, pp. 5514–5519, 2006.

[117] Y. Yang, T. Fricke, and F. Diaz-Griffero, "Inhibition of reverse transcriptase activity increases stability of the HIV-1 core.," *J. Virol.*, vol. 87, no. 1, pp. 683–7, 2013.

[118] A. E. Hulme, O. Perez, and T. J. Hope, "Complementary assays reveal a relationship between HIV-1 uncoating and reverse transcription," *Proc Natl Acad Sci U S A*, vol. 108, no. 24, pp. 9975–9980, 2011.

[119] S. Rankovic, J. Varadarajan, R. Ramalho, C. Aiken, and I. Rousso, "Reverse Transcription Mechanically Initiates HIV-1 Capsid Disassembly," *J. Virol.*, vol. 91, no. 12, pp. 1–14, 2017.

[120] M. Yamashita and M. Emerman, "Capsid is a dominant determinant of retrovirus infectivity in nondividing cells.," *J. Virol.*, vol. 78, no. 11, pp. 5670–5678, 2004.

[121] M. Yamashita, O. Perez, T. J. Hope, and M. Emerman, "Evidence for direct involvement of the capsid protein in HIV infection of nondividing cells," *PLoS Pathog.*, vol. 3, no. 10, pp. 1502–1510, 2007.

[122] N. J. Arhel *et al.*, "HIV-1 DNA Flap formation promotes uncoating of the pre-

integration complex at the nuclear pore.," *EMBO J.*, vol. 26, no. 12, pp. 3025–3037, 2007.

[123] D. J. Dismuke and C. Aiken, "Evidence for a Functional Link between Uncoating of the Human Immunodeficiency Virus Type 1 Core and Nuclear Import of the Viral Preintegration Complex Evidence for a Functional Link between Uncoating of the Human Immunodeficiency Virus Type 1 Core and Nu," vol. 80, no. 8, pp. 3712–3720, 2006.

[124] A. Fassati, "HIV infection of non-dividing cells: A divisive problem," *Retrovirology*, vol. 3, pp. 1–15, 2006.

[125] L. Hilditch and G. J. Towers, "A model for cofactor use during HIV-1 reverse transcription and nuclear entry," *Curr. Opin. Virol.*, vol. 4, pp. 32–36, 2014.

[126] Z. Ambrose and C. Aiken, "HIV-1 Uncoating: Connection to Nuclear Entry and Regulation by Host Proteins," *Virology*, pp. 371–379, 2014.

[127] N. Arhel, "Revisiting HIV-1 uncoating," *Retrovirology*, vol. 7, no. 1, p. 96, 2010.

[128] C. Grewe, A. Beck, and H. . Gelderblom, "HIV: Early Virus-Cell interactions." pp. 965–974, 1990.

[129] V. Arfi *et al.*, "Characterization of the Behavior of Functional Viral Genomes during the Early Steps of Human Immunodeficiency Virus Type 1 Infection ," *J. Virol.*, vol. 83, no. 15, pp. 7524–7535, 2009.

[130] A. E. Hulme, Z. Kelley, E. A. Okocha, and T. J. Hope, "Identification of capsid mutations that alter the rate of HIV-1 uncoating in infected cells.," *J. Virol.*, vol. 89, no. 1, pp. 643–51, 2015.

[131] H. Xu *et al.*, "Evidence for biphasic uncoating during HIV-1 infection from a novel imaging assay.," *Retrovirology*, vol. 10, no. 1, p. 70, 2013.

[132] J. I. Mamede, G. C. Cianci, M. R. Anderson, and T. J. Hope, "Early cytoplasmic uncoating is associated with infectivity of HIV-1," *Proc. Natl. Acad. Sci.*, p. 201706245, 2017.

[133] F. Di Nunzio *et al.*, "Human Nucleoporins Promote HIV-1 Docking at the Nuclear Pore, Nuclear Import and Integration," *PLoS One*, vol. 7, no. 9, 2012.

[134] L. Zhou, E. Sokolskaja, C. Jolly, W. James, S. A. Cowley, and A. Fassati, "Transportin 3 promotes a nuclear maturation step required for efficient HIV-1 integration," *PLoS Pathog.*, vol. 7, no. 8, 2011.

[135] A. C. Francis and G. B. Melikyan, "Single HIV-1 Imaging Reveals Progression of Infection through CA-Dependent Steps of Docking at the Nuclear Pore, Uncoating, and Nuclear Transport," *Cell Host Microbe*, vol. 23, no. 4, p. 536–548.e6, 2018.

[136] A. C. Francis, M. Marin, J. Shi, C. Aiken, and G. B. Melikyan, "Time-Resolved Imaging of Single HIV-1 Uncoating In Vitro and in Living Cells," *PLoS Pathog.*, vol. 12, no. 6, pp. 1–28, 2016.

[137] A. E. Hulme, Z. Kelley, D. Foley, and T. J. Hope, "Complementary Assays Reveal a Low Level of CA Associated with Viral Complexes in the Nuclei of HIV-1-Infected Cells.," *J. Virol.*, vol. 89, no. 10, pp. 5350–61, 2015.

[138] N. Pante and M. Kann, "Nuclear Pore Complex Is Able to Transport Macromolecules with Diameters of ~39 nm," *Mol. Biol. Cell*, vol. 13, no. 2, pp. 425–434, 2002.

[139] K. E. Knockenhauer and T. U. Schwartz, "The Nuclear Pore Complex as a Flexible and Dynamic Gate," *Cell*, vol. 164, no. 6, pp. 1162–1171, 2016.

[140] R. Ramalho, S. Rankovic, J. Zhou, C. Aiken, and I. Rousso, "Analysis of the mechanical properties of wild type and hyperstable mutants of the HIV 1 capsid," *Retrovirology*, pp. 1–7, 2016.

[141] R. Yang *et al.*, "Second-site suppressors of HIV-1 capsid mutations: restoration of intracellular activities without correction of intrinsic capsid stability defects," *Retrovirology*, vol. 9, no. 1, p. 30, 2012.

[142] A. De Iaco, F. Santoni, A. Vannier, M. Guipponi, S. Antonarakis, and J. Luban, "TNPO3 protects HIV-1 replication from CPSF6-mediated capsid stabilization in

the host cell cytoplasm.," *Retrovirology*, vol. 10, pp. 1–18, 2013.

[143] K. Lee *et al.*, "Flexible Use of Nuclear Import Pathways by HIV-1," *Cell Host Microbe*, vol. 7, no. 3, pp. 221–233, 2010.

[144] J. Luban, "Absconding with the chaperone: Essential cyclophilin-gag interaction in HIV-1 virions," *Cell*, vol. 87, no. 7, pp. 1157–1159, 1996.

[145] K. A. Matreyek and A. Engelman, "The Requirement for Nucleoporin NUP153 during Human Immunodeficiency Virus Type 1 Infection Is Determined by the Viral Capsid," *J. Virol.*, vol. 85, no. 15, pp. 7818–7827, 2011.

[146] K. Lee *et al.*, "HIV-1 Capsid-Targeting Domain of Cleavage and Polyadenylation Specificity Factor 6," *J. Virol.*, vol. 86, no. 7, pp. 3851–3860, 2012.

[147] T. Fricke *et al.*, "The ability of TNPO3-depleted cells to inhibit HIV-1 infection requires CPSF6.," *Retrovirology*, vol. 10, p. 46, 2013.

[148] Z. Ambrose *et al.*, "Human Immunodeficiency Virus Type 1 Capsid Mutation N74D Alters Cyclophilin A Dependence and Impairs Macrophage Infection," *J. Virol.*, vol. 86, no. 8, pp. 4708–4714, 2012.

[149] M. Yamashita and A. N. Engelman, "Capsid-Dependent Host Factors in HIV-1 Infection," *Trends Microbiol.*, vol. 25, no. 9, pp. 741–755, 2017.

[150] P. Wang and J. Heitman, "The cyclophilins," *Genome Biol.*, vol. 6, no. 7, p. 226, 2005.

[151] K. Wiegers, G. Rutter, U. Schubert, M. Grättinger, and H. G. Kräusslich, "Cyclophilin A incorporation is not required for human immunodeficiency virus type 1 particle maturation and does not destabilize the mature capsid.," *Virology*, vol. 257, no. 1, pp. 261–74, 1999.

[152] E. Sokolskaja, D. M. Sayah, and J. Luban, "Target Cell Cyclophilin A Modulates Human Immunodeficiency Virus Type 1 Infectivity," *J. Virol.*, vol. 78, no. 23, pp. 12800–12808, 2004.

[153] T. Hatziioannou, D. Perez-caballero, P. D. Bieniasz, and S. Cowan, "Cyclophilin Interactions with Incoming Human Immunodeficiency Virus Type 1 Capsids with Opposing Effects on Infectivity in Human Cells Cyclophilin Interactions with Incoming Human Immunodeficiency Virus Type 1 Capsids with Opposing Effects on Infectivity," vol. 79, no. 1e, pp. 176–183, 2005.

[154] S. Yoo, D. G. Myszka, C. Yeh, M. McMurray, C. P. Hill, and W. I. Sundquist, "Molecular recognition in the HIV-1 capsid/cyclophilin A complex.," *J. Mol. Biol.*, vol. 269, no. 5, pp. 780–795, 1997.

[155] J. Zhou, A. J. Price, U. D. Halambage, L. C. James, and C. Aiken, "HIV-1 Resistance to the Capsid-Targeting Inhibitor PF74 Results in Altered Dependence on Host Factors Required for Virus Nuclear Entry," *J. Virol.*, vol. 89, no. 17, pp. 9068–9079, 2015.

[156] E. K. Franke, H. E. Yuan, and J. Luban, "Specific incorporation of cyclophilin A into HIV-1 virions.," *Nature*, vol. 372. pp. 359–362, 1994.

[157] C. Liu *et al.*, "Cyclophilin A stabilizes the HIV-1 capsid through a novel non-canonical binding site," *Nat. Commun.*, vol. 7, p. 10714, 2016.

[158] M. W. Harding, E. Handschumachers, and D. W. Speichersll, "Isolation and Amino Acid Sequence of Cyclophilin*," *J. Biol. Chem.*, vol. 261, no. 18, pp. 8547–8555, 1986.

[159] J. Kallen *et al.*, "Structure of human cyclophilin and its binding site for cyclosporin A determined by X-ray crystallography and NMR spectroscopy," *Nature*, vol. 353, no. 6341, pp. 276–279, 1991.

[160] V. B. Shah *et al.*, "The Host Proteins Transportin SR2/TNPO3 and Cyclophilin A Exert Opposing Effects on HIV-1 Uncoating," *J. Virol.*, vol. 87, no. 1, pp. 422–432, 2012.

[161] Y. Li, A. K. Kar, and J. Sodroski, "Target cell type-dependent modulation of human immunodeficiency virus type 1 capsid disassembly by cyclophilin A.," *J. Virol.*, vol. 83, no. 21, pp. 10951–62, 2009.

[162] S. Li, C. P. Hill, W. I. Sundquist, and J. T. Finch, "Image reconstructions of

helical assemblies of the HIV-1 CA protein," *Nature*, vol. 342, no. 1997, pp. 192–195, 2000.

[163] M. Grättinger, H. Hohenberg, D. Thomas, T. Wilk, B. Müller, and H. G. Kräusslich, "In vitro assembly properties of wild-type and cyclophilin-binding defective human immunodeficiency virus capsid proteins in the presence and absence of cyclophilin A.," *Virology*, vol. 257, no. 1, pp. 247–260, 1999.

[164] D. a Bosco, E. Z. Eisenmesser, S. Pochapsky, W. I. Sundquist, and D. Kern, "Catalysis of cis/trans isomerization in native HIV-1 capsid by human cyclophilin A.," *Proc. Natl. Acad. Sci. U. S. A.*, vol. 99, no. 8, pp. 5247–5252, 2002.

[165] A. De Iaco and J. Luban, "Cyclophilin A promotes HIV-1 reverse transcription but its effect on transduction correlates best with its effect on nuclear entry of viral cDNA," *Retrovirology*, vol. 11, no. 1, pp. 1–15, 2014.

[166] R. Bernad, H. Van Der Velde, M. Fornerod, and H. Pickersgill, "Nup358 / RanBP2 Attaches to the Nuclear Pore Complex via Association with Nup88 and Nup214 / CAN and Plays a Supporting Role in CRM1-Mediated Nuclear Protein Export," *Society*, vol. 24, no. 6, pp. 2373–2384, 2004.

[167] D. H. Lin, S. Zimmermann, T. Stuwe, E. Stuwe, and A. Hoelz, "Structural and functional analysis of the C-terminal domain of Nup358/RanBP2," *J. Mol. Biol.*, vol. 425, no. 8, pp. 1318–1329, 2013.

[168] K. Bichel, A. J. Price, T. Schaller, G. J. Towers, S. M. V Freund, and L. C. James, "HIV-1 capsid undergoes coupled binding and isomerization by the nuclear pore protein NUP358," *Retrovirology*, vol. 10, no. 1, pp. 1–12, 2013.

[169] A. M. Meehan *et al.*, "A Cyclophilin Homology Domain-Independent Role for Nup358 in HIV-1 Infection," *PLoS Pathog.*, vol. 10, no. 2, pp. 1–17, 2014.

[170] R. Zhang, R. Mehla, and A. Chauhan, "Perturbation of host nuclear membrane component RanBP2 impairs the nuclear import of human immunodeficiency virus -1 preintegration complex (DNA)," *PLoS One*, vol. 5, no. 12, 2010.

[171] T. C. Walther, M. Fornerod, H. Pickersgill, M. Goldberg, T. D. Allen, and I. W. Mattaj, "The nucleoporin Nup153 is required for nuclear pore basket formation, nuclear pore complex anchoring and import of a subset of nuclear proteins," *EMBO J.*, vol. 20, no. 20, pp. 5703–5714, 2001.

[172] R. Y. H. Lim *et al.*, "Flexible phenylalanine-glycine nucleoporins as entropic barriers to nucleocytoplasmic transport," *Proc. Natl. Acad. Sci.*, vol. 103, no. 25, pp. 9512–9517, 2006.

[173] B. Fahrenkrog *et al.*, "Domain-specific antibodies reveal multiple-site topology of Nup153 within the nuclear pore complex," *J. Struct. Biol.*, vol. 140, no. 1–3, pp. 254–267, 2002.

[174] Y. Koh *et al.*, "Differential Effects of Human Immunodeficiency Virus Type 1 Capsid and Cellular Factors Nucleoporin 153 and LEDGF/p75 on the Efficiency and Specificity of Viral DNA Integration," *J. Virol.*, vol. 87, no. 1, pp. 648–658, 2013.

[175] M. C. Lai, R. I. Lin, S. Y. Huang, C. W. Tsai, and W. Y. Tarn, "A human importin-β family protein, transportin-SR2, interacts with the phosphorylated RS domain of SR proteins," *J. Biol. Chem.*, vol. 275, no. 11, pp. 7950–7957, 2000.

[176] J. C. Valle-Casuso *et al.*, "TNPO3 Is Required for HIV-1 Replication after Nuclear Import but prior to Integration and Binds the HIV-1 Core," *J. Virol.*, vol. 86, no. 10, pp. 5931–5936, 2012.

[177] L. Krishnan *et al.*, "The requirement for cellular transportin 3 (TNPO3 or TRN-SR2) during infection maps to human immunodeficiency virus type 1 capsid and not integrase.," *J. Virol.*, vol. 84, no. 1, pp. 397–406, 2010.

[178] F. Christ *et al.*, "Transportin-SR2 Imports HIV into the Nucleus," *Curr. Biol.*, vol. 18, no. 16, pp. 1192–1202, 2008.

[179] G. N. Maertens *et al.*, "Structural basis for nuclear import of splicing factors by human Transportin 3," *Proc. Natl. Acad. Sci.*, vol. 111, no. 7, pp. 2728–2733, 2014.

[180] S. Dettwiler, C. Aringhieri, S. Cardinale, W. Keller, and S. M. L. Barabino, "Distinct sequence motifs within the 68-kDa subunit of cleavage factor Im mediate RNA binding, protein-protein interactions, and subcellular localization," *J. Biol. Chem.*, vol. 279, no. 34, pp. 35788–35797, 2004.

[181] S. M. Dudek *et al.*, "Abl tyrosine kinase phosphorylates nonmuscle Myosin light chain kinase to regulate endothelial barrier function.," *Mol. Biol. Cell*, vol. 21, no. 22, pp. 4042–4056, 2010.

[182] T. Hori, H. Takeuchi, H. Saito, R. Sakuma, Y. Inagaki, and S. Yamaoka, "A carboxy-terminally truncated human CPSF6 lacking residues encoded by exon 6 inhibits HIV-1 cDNA synthesis and promotes capsid disassembly.," *J. Virol.*, vol. 87, no. 13, pp. 7726–36, 2013.

[183] J. Ning *et al.*, "Truncated CPSF6 forms higher order complexes that bind and disrupt HIV-1 capsid," *J. Virol.*, no. April, 2018.

[184] S. Rasheedi *et al.*, "The Cleavage and polyadenylation specificity factor 6 (CPSF6) subunit of the capsid-recruited pre-messenger RNA cleavage factor I (CFIm) complex mediates HIV-1 integration into genes," *J. Biol. Chem.*, vol. 291, no. 22, pp. 11809–11819, 2016.

[185] A. Saito *et al.*, "Capsid-CPSF6 Interaction Is Dispensable for HIV-1 Replication in Primary Cells but Is Selected during Virus Passage *In Vivo*," *J. Virol.*, vol. 90, no. 15, pp. 6918–6935, 2016.

[186] L. Lad *et al.*, "Functional Label-Free Assays for Characterizing the in Vitro Mechanism of Action of Small Molecule Modulators of Capsid Assembly," *Biochemistry*, vol. 54, no. 13, pp. 2240–2248, 2015.

[187] N. Veiga *et al.*, "The behaviour of myo-inositol hexakisphosphate in the presence of magnesium(II) and calcium(II): Protein-free soluble InsP6 is limited to 49 μM under cytosolic/nuclear conditions," *J. Inorg. Biochem.*, vol. 100, no. 11, pp. 1800–1810, 2006.

[188] A. J. Letcher, M. J. Schell, and R. F. Irvine, "Do mammals make all their own inositol hexakisphosphate?," *Biochem. J.*, vol. 416, no. 2, pp. 263–270, 2008.

[189] S. Campbell *et al.*, "Modulation of HIV-like particle assembly in vitro by inositol phosphates," *Proc. Natl. Acad. Sci.*, vol. 98, no. 19, pp. 10875–10879, 2001.

[190] S. Thenin-Houssier and S. T. Valente, "HIV-1 Capsid Inhibitors as Antiretroviral Agents," *Curr. HIV Res.*, pp. 270–282, 2016.

[191] A. Saito *et al.*, "Roles of capsid-interacting host factors in multimodal inhibition of HIV-1 by PF74.," *J. Virol.*, vol. 90, no. 12, pp. 5808–5823, 2016.

[192] T. Fricke, C. Buffone, S. Opp, J. Valle-Casuso, and F. Diaz-Griffero, "BI-2 destabilizes HIV-1 cores during infection and Prevents Binding of CPSF6 to the HIV-1 Capsid.," *Retrovirology*, vol. 11, no. 1, p. 120, 2014.

[193] C. Da Silva Santos, K. Tartour, and A. Cimarelli, "A Novel Entry/Uncoating Assay Reveals the Presence of at Least Two Species of Viral Capsids During Synchronized HIV-1 Infection," *PLoS Pathog.*, vol. 12, no. 9, pp. 1–28, 2016.

[194] L. Lamorte *et al.*, "Discovery of novel small-molecule HIV-1 replication inhibitors that stabilize capsid complexes," *Antimicrob. Agents Chemother.*, vol. 57, no. 10, pp. 4622–4631, 2013.

[195] I. Gross, H. Hohenberg, and H. G. Kräusslich, "In vitro assembly properties of purified bacterially expressed capsid proteins of human immunodeficiency virus.," *Eur. J. Biochem.*, vol. 249, no. 2, pp. 592–600, 1997.

[196] C. A. Guth and J. Sodroski, "Contribution of PDZD8 to stabilization of the human immunodeficiency virus type 1 capsid.," *J. Virol.*, vol. 88, no. 9, pp. 4612–23, 2014.

[197] C. C. Douglas, D. Thomas, J. Lanman, and P. E. Prevelige, "Investigation of N-terminal domain charged residues on the assembly and stability of HIV-1 CA," *Biochemistry*, vol. 43, no. 32, pp. 10435–10441, 2004.

[198] O. Pornillos, B. K. Ganser-pornillos, S. Banumathi, Y. Hua, and M. Yeager, "Disulfide bond stabilization of the hexameric capsomer of human

immunodeficiency virus," *J Mol Biol*, no. 401(5), pp. 985–995, 2010.

[199] Y. Yang, J. Luban, and F. Diaz-Griffero, "The Fate of HIV-1 Capsid: A Biochemical Assay for HIV-1 Uncoating," *Methods Mol. Biol.*, vol. 1087, pp. 29–36, 2014.

[200] D. Perez-Caballero, T. Hatziioannou, F. Zhang, S. Cowan, and P. D. Bieniasz, "Restriction of human immunodeficiency virus type 1 by TRIM-CypA occurs with rapid kinetics and independently of cytoplasmic bodies, ubiquitin, and proteasome activity.," *J. Virol.*, vol. 79, no. 24, pp. 15567–72, 2005.

[201] A. E. Hulme and T. J. Hope, "The CsA washout assay to detect HIV-1 uncoating in infected cells," *Methods Mol Biol*, vol. 1087, no. 312, pp. 37–46, 2014.

[202] E. M. Campbell, O. Perez, M. Melar, and T. J. Hope, "Labeling HIV-1 virions with two fluorescent proteins allows identification of virions that have productively entered the target cell," *Virology*, vol. 148, no. 4, pp. 825–832, 2007.

[203] N. Arhel *et al.*, "Quantitative four-dimensional tracking of cytoplasmic and nuclear HIV-1 complexes," *Nat. Methods*, vol. 3, no. 10, pp. 817–824, 2006.

[204] Y. Ma *et al.*, "Real-Time Imaging of Single HIV-1 Disassembly with Multicolor Viral Particles," *ACS Nano*, vol. 10, no. 6, pp. 6273–6282, 2016.

[205] E. M. Campbell, O. Perez, J. L. Anderson, and T. J. Hope, "Visualization of a proteasome-independent intermediate during restriction of HIV-1 by rhesus TRIM5a," *J. Cell Biol.*, vol. 180, no. 3, pp. 549–561, 2008.

[206] C. F. Pereira *et al.*, "Labeling of multiple HIV-1 proteins with the biarsenical-tetracysteine system," *PLoS One*, vol. 6, no. 2, 2011.

[207] W. Hubner *et al.*, "Sequence of Human Immunodeficiency Virus Type 1 (HIV-1) Gag Localization and Oligomerization Monitored with Live Confocal Imaging of a Replication-Competent, Fluorescently Tagged HIV-1," *J. Virol.*, vol. 81, no. 22, pp. 12596–12607, 2007.

[208] A. Aggarwal *et al.*, "Mobilization of HIV spread by diaphanous 2 dependent filopodia in infected dendritic cells," *PLoS Pathog.*, vol. 8, no. 6, 2012.

[209] S. Padilla-Parra, M. Marin, N. Gahlaut, R. Suter, N. Kondo, and G. B. Melikyan, "Fusion of Mature HIV-1 Particles Leads to Complete Release of a Gag-GFP-Based Content Marker and Raises the Intraviral pH," *PLoS One*, vol. 8, no. 8, pp. 1–16, 2013.

[210] P. R. Nicovich, J. Walsh, T. Böcking, and K. Gaus, "NicoLase - An open-source diode laser combiner, fiber launch, and sequencing controller for fluorescence microscopy," *PLoS One*, vol. 12, no. 3, pp. 1–15, 2017.

[211] T. Böcking, F. Aguet, S. C. Harrison, and T. Kirchhausen, "Single-molecule analysis of a molecular disassemblase reveals the mechanism of Hsc70-driven clathrin uncoating," *Nat Struct Mol Biol.*, vol. 18, no. 3, pp. 295–301, 2011.

[212] S. Rankovic, R. Ramalho, C. Aiken, and I. Rousso, "PF74 reinforces the HIV-1 capsid to impair reverse transcription-induced uncoating," *J. Virol.*, no. August, p. JVI.00845-18, 2018.

[213] D. L. Mallery *et al.*, "IP6 is an HIV pocket factor that prevents capsid collapse and promotes DNA synthesis," *Elife*, vol. 7, pp. 1–3, 2018.

[214] T. Yoshida, A. Kakizuka, and H. Imamura, "BTeam, a Novel BRET-based Biosensor for the Accurate Quantification of ATP Concentration within Living Cells," *Sci. Rep.*, vol. 6, no. December, pp. 1–9, 2016.

[215] R. A. Dick *et al.*, "Inositol phosphates are assembly co-factors for HIV-1," *Nature*, 2018.

[216] J. M. Hogle, M. Chow, and D. J. Filman, "Three-dimensional structure of Poliovirus at 2.9A resolution," *Science (80-.).*, vol. 229, pp. 1358–1365, 1985.

[217] M. G. Rossmann *et al.*, "Structure of a human common cold virus and functional relationship to other picornaviruses," *Nature*, vol. 317, no. 6033, pp. 145–153, 1985.

[218] H. R. Gelderblom, M. Ozel, E. H. S. Hausmann, T. Winkel, G. Pauli, and M. a. Koch, "Fine Structure of Human Immunodeficiency Virus (Hiv),

Immunolocalization of Structural Proteins and Virus-Cell Relation," *Micron Microsc.*, vol. 19, no. 1, pp. 41–60, 1988.

Chapter 8

Supplementary Information

8. Supplementary information

8.1. Lattice disassembly kinetics of CA E45A substitution

The effect of the CA E45A substitution on the kinetics of lattice disassembly is shown in **Figure 8.1**. In the case of leaky capsids (**Figure 8.1A**), a rapid CypA binding to the CA E45A lattice after membrane permeabilisation is observed, followed by a decay of the paint signal. This result indicates that the CA E45A substitution does not prevent the disassembly of damaged lattices. A similar result is observed on capsids that undergo uncoating during the experiment. Lattice paint traces aligned at the time of capsid opening (**Figure 8.1B**) revealed that the lattice disassembles in a similar fashion to WT capsids after uncoating is initiated. In conclusion, we observed that the CA E45A substitution delays capsid opening (**Chapter 3, Figure 2**) but does not stop the collapse of the lattice once the capsid has suffered its first defect.
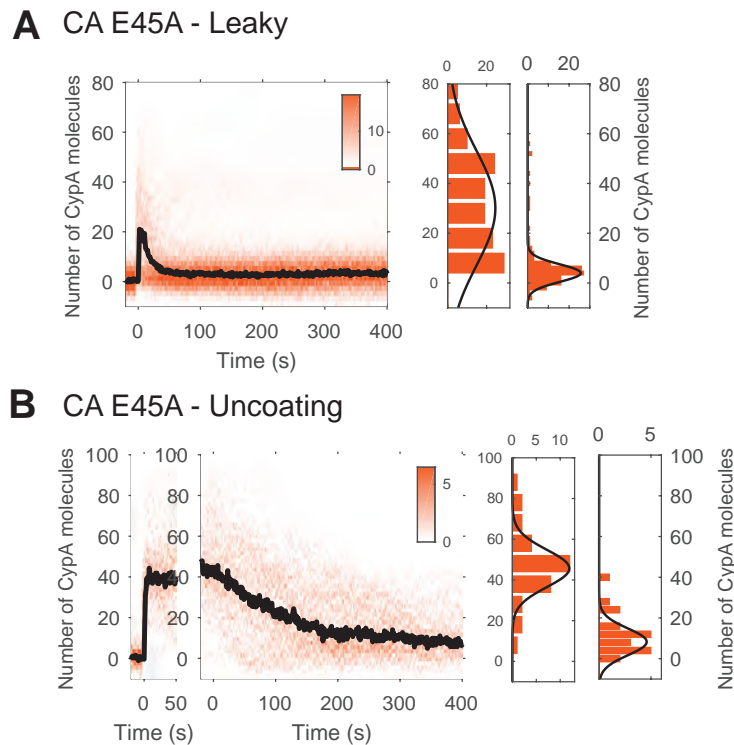

Figure 8.1. Lattice disassembly kinetics of CA E45A substitution. (A) Heatmap of AF568-CypA binding traces to all leaky capsids within 30 minutes for CA E45A viral particles. The histograms at the right show the distribution of intensities at t_P = 1-30 s and 280-300 s respectively. **(B)** Heatmap of AF568-CypA binding traces to all capsids that undergo disassembly within 30 minutes for CA E45A viral particles. The histogram at the right show the distribution of intensities after binding equilibrium is reached (t_P = 10-30 s) and at the end of lattice disassembly (t_O = 380-400 s).

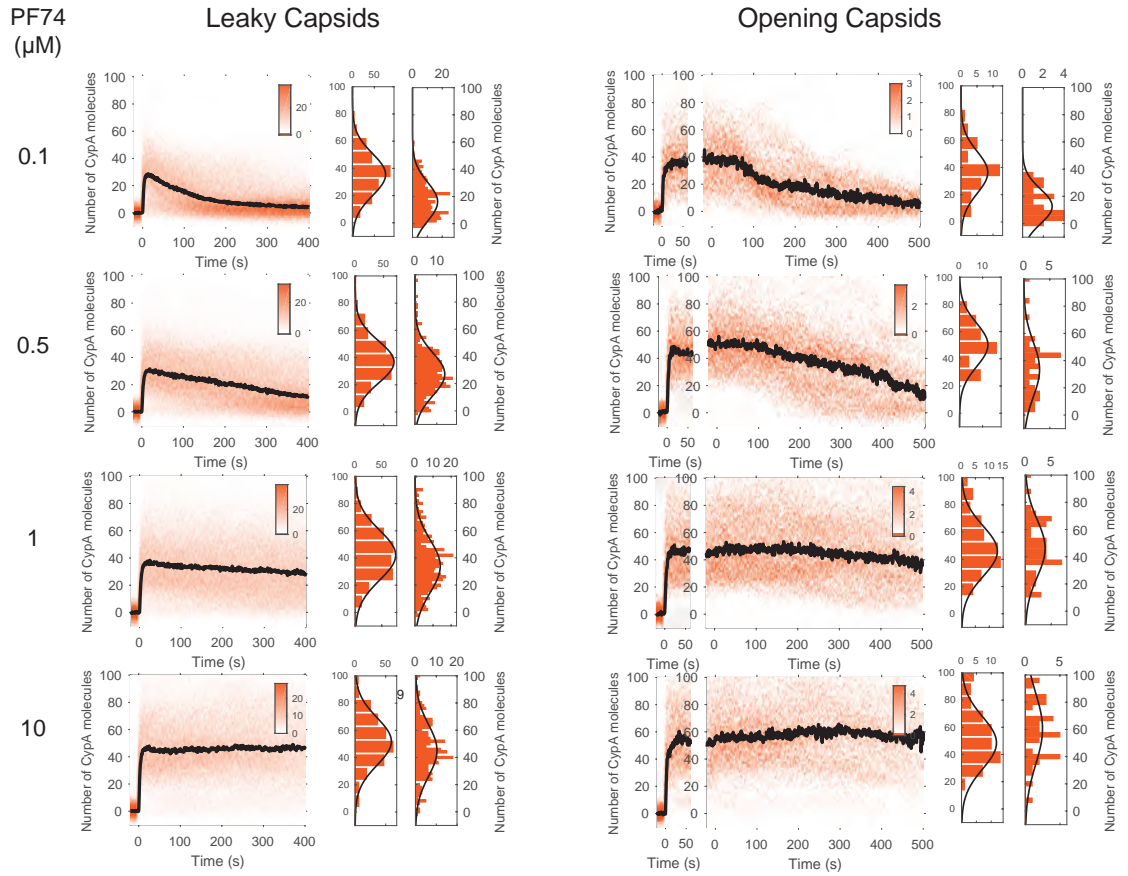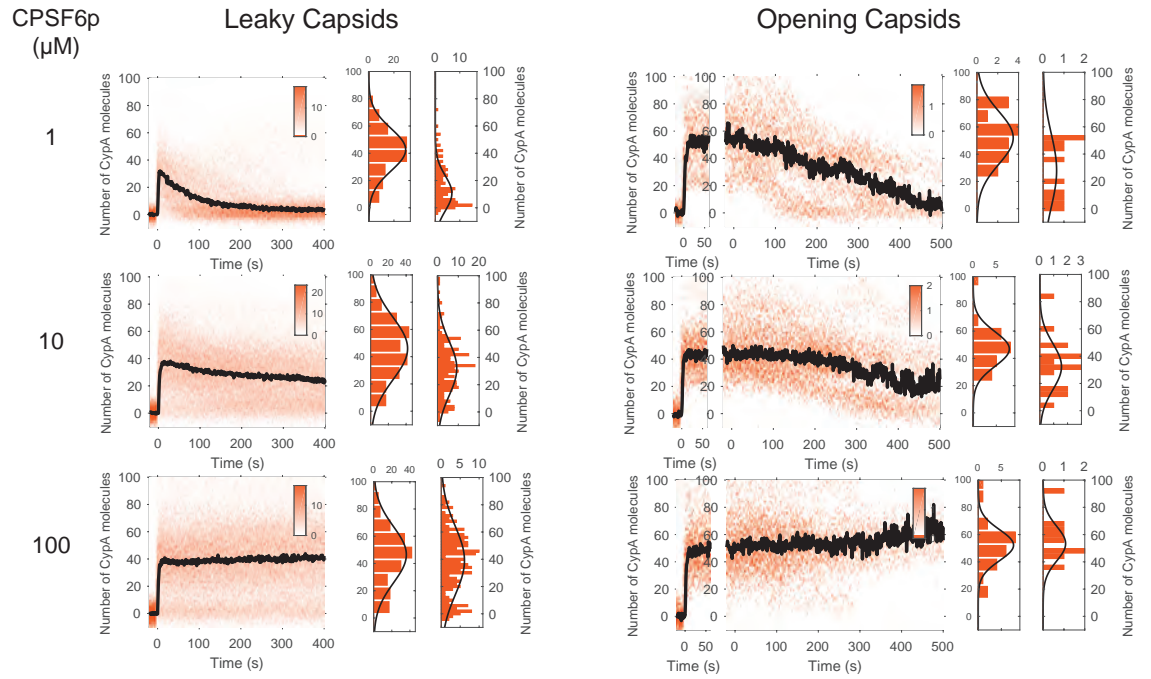## 8.2. Lattice disassembly kinetics in presence of PF74

Figure 8.2. Lattice disassembly kinetics of leaky and uncoating capsids in presence of PF74. Heatmap of AF568-CypA binding traces (vermillion) to all **(A)** leaky capsids and **(B)** capsids that undergo uncoating in presence of different concentrations of PF74. The bold black line represents the median CypA binding trace.

8.3. Lattice disassembly kinetics in presence of CPSF6p

Figure 8.3. Lattice disassembly kinetics of leaky and uncoating capsids in presence of CPSF6p.

Figure 8.3. Lattice disassembly kinetics of leaky and uncoating capsids in presence of CPSF6p. Heatmap of AF568-CypA binding traces (vermillion) to all **(A)** leaky capsids and **(B)** capsids that undergo uncoating in presence of different concentrations of CPSF6p. The bold black line represents the median CypA binding trace.

8.4. Long lattice disassembly kinetics in presence of PF74 and CPSF6p
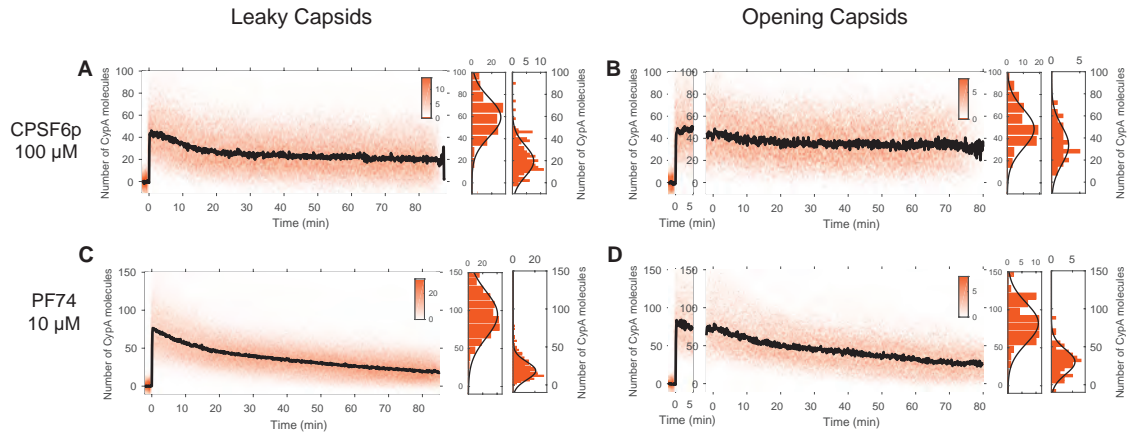

Figure 8.4. Long lattice disassembly kinetics in presence of PF74 and CPSF6p. Heatmap of AF568-CypA binding traces to all leaky capsids (**A** and **C**) and to capsids that undergo disassembly (**B** and **D**) within 80 minutes in presence of 10 µM PF74 and 100 µM CPSF6p. Each histogram at the right show the distribution of intensities after binding equilibrium is reached (t_P = 1-3 min) and at the end of lattice disassembly ($t_{p/O}$ = 78-80 min).